LOW-COMPLEXITY AND POWER-EFFICIENT WIRELESS COOPERATIVE RELAY NETWORKS WITH ENHANCED RELIABILITY

A Thesis
Presented to
The Academic Faculty

by

Gi Wan Choi

In Partial Fulfillment
of the Requirements for the Degree
Doctor of Philosophy in the
School of Electrical and Computer Engineering

Georgia Institute of Technology
May 2013

LOW-COMPLEXITY AND POWER-EFFICIENT WIRELESS COOPERATIVE RELAY NETWORKS WITH ENHANCED RELIABILITY

Approved by:

Professor Xiaoli Ma, Advisor
School of Electrical and Computer Engineering
Georgia Institute of Technology

Professor Emmanouil M. Tentzeris
School of Electrical and Computer Engineering
Georgia Institute of Technology

Professor G. Tong Zhou
School of Electrical and Computer Engineering
Georgia Institute of Technology

Professor William L. Green
School of Mathematics
Georgia Institute of Technology

Professor Faramarz Fekri
School of Electrical and Computer Engineering
Georgia Institute of Technology

Date Approved: November 26, 2012

ACKNOWLEDGEMENTS

The work presented in this dissertation would not have been possible without the influence, support and encouragement of many people. I would like to take this opportunity to express my gratitude for them.

First, I would like to express my sincere gratitude to my advisor, Dr. Xiaoli Ma, for her guidance and constant support during my Ph.D. study. Her thoughtful discussions and careful comments have greatly influenced my Ph.D. work. Her energy and enthusiasm in research really impressed me. I am especially grateful for her best efforts to teach me how to be a good researcher. It was one of the luckiest things in my life to have her as my advisor.

I would also like to thank my dissertation committee members, Dr. G. Tong Zhou, Dr. Faramarz Fekri, Dr. Emmanouil M. Tentzeris, and Dr. William L. Green, for taking the time to serve on my committee and for their suggestions which greatly improved the quality of this dissertation.

My sincere appreciation also goes to my colleagues in my group, Dr. Wei Zhang, Dr. Sungeun Lee, Dr. Qijia Liu, Dr. Yiyin Wang, Qi Zhou, Hayang Kim, Marie Shinotsuka, Malik Muhammad Gul, and Zhenhua Yu, for their helpful discussions and support. I am also thankful to SKBC family who shared their memories with me. Their friendship and encouragement sustained me throughout my Ph.D. study.

Last but not the least, I would like to express my deepest gratitude, love and affection to my wife, Youn Ah Kang, who was always there cheering me up and stood by me through good times and bad times, and to my parents and brother who supported me throughout the long path of my academic endeavor and endured countless sacrifices. To them, I owe all I have ever accomplished.

I'd rather have Jesus

I'd rather have Jesus than silver or gold
I'd rather be His than have riches untold
I'd rather have Jesus than houses or lands
I'd rather be led by His nail-pierced hand
Than to be the king of a vast domain
Or be held in sin's dread sway
I'd rather have Jesus than anything
This world affords today

"For God so loved the world that He gave His one and only Son,
that whoever believes in Him shall not perish but have eternal life." (John 3:16)

TABLE OF CONTENTS

LIST OF TABLES

LIST OF FIGURES

SUMMARY

In recent years, global mobile data traffic has been increasing exponentially as mobile devices pervade our daily lives. To cope with the ever growing demands for higher data rates and seamless connectivity, one solution is to drastically increase the number of macro base stations in the conventional cellular architecture. However, this results in high deployment costs. Deploying low-power nodes such as relays that do not require a wired backhaul connection within a macrocell is one of cost-effective ways to extend high data rate coverage range. Relays are typically deployed to increase signal strength in poor coverage areas or to eliminate dead spots. But more importantly, relays provide a natural diversity, called cooperative diversity. In addition to a direct signal from a base station, extra copies of the same signal are forwarded from relays. Utilizing this diversity at the destination can yield significant performance enhancements. Thus, cooperative relay strategies need to be considered to enable high data rate coverage in a cost-effective manner.

In this dissertation, we consider a simple single-relay network and present low-complexity and power-efficient cooperative relay designs that can achieve low error rate. We first study decode-and-forward (DF) relay networks with a single antenna at each node, where the relay decodes the received signal and forwards the re-encoded information to the destination. In DF relay scheme, decoding at the relay is not perfect and the error-propagation phenomenon is a detrimental problem, preventing the destination from collecting the cooperative diversity. To enable cooperative diversity in DF relay networks, we adopt link-adaptive power-scaling relay strategies where

the relay scales the transmission power of the re-encoded signal based on the reliability of the source-relay link. We generalize power-profile designs and analyze the diversity order enabled by the general power-profile designs. We provide necessary and sufficient conditions for the designs to enable full cooperative diversity at the destination.

In the second part of this dissertation, we extend the power-scaling relay strategy to DF multi-input multi-output (MIMO) relay networks, where multiple antennas are adopted at each node, and show that full cooperative diversity can also be achieved here. To collect spatial diversity provided by multiple antennas without using maximum-likelihood equalizers (MLEs) or near-ML detectors which exhibit high complexity, channel-controlled automatic repeat request (CC-ARQ) scheme is developed for DF MIMO relay networks to enable spatial diversity with linear equalizers (LEs) maintaining low-complexity. We also show that joint cooperative and spatial diversity can be achieved at the destination when the power-scaling strategy and the CC-ARQ with LEs are combined.

Finally, amplify-and-forward (AF) MIMO relay designs, where the relay simply amplifies the received signal and forwards it to the destination, are studied with consideration of peak-power constraints at the relay. One practical concern for AF relaying is that the output signal at the relay may suffer from large peak-to-average power ratio (PAR), which may cause nonlinear distortion and/or saturation in the transmitted signal due to the limited linear range of power amplifiers. Thus, we first investigate peak-power constrained power-scaling strategies and find a sufficient condition to enable joint cooperative and spatial diversity at the destination. Based on this study, we propose simple and practical AF MIMO relay designs with peak-power constraint at the relay. CC-ARQ is also applied to AF MIMO relay networks to reduce the decoding complexity.

CHAPTER I

INTRODUCTION

1.1 Motivations

There have been revolutionary changes in cellular communications systems since the first-generation (1G) analog-based radio networks were introduced in the 1980s [61]. Emerged in the 1990s, the second-generation (2G) systems made the transition from analog to digital signals and provided circuit-switched low-speed data services [70, 97]. The third-generation (3G) systems appeared in the 2000s and introduced packet-switched techniques for high-speed data transmissions [4, 72]. As the mobile broadband traffic grows exponentially, Release 8 of Long-Term Evolution (LTE) standard was frozen in December 2008 by the Third Generation Partnership Project (3GPP) [2]. LTE offers high spectral efficiency, low latency, and high peak data rates using a new air interface technology (orthogonal frequency-division multiple access (OFDMA)/single-carrier FDMA (SC-FDMA)) and advanced antenna techniques [45]. LTE Release 10, referred to as LTE-Advanced, has recently been finalized in March 2011 [1]. LTE-Advanced significantly enhances LTE Release 8 to meet the International Mobile Telecommunications (IMT)-Advanced requirements for the fourth-generation (4G) definition given by the International Telecommunication Union (ITU) [44].

As radio link performance is approaching theoretical limits with 3G and LTE, more fundamental enhancements are sought to improve the network capacity. Heterogeneous networks, where low-power nodes are deployed within macrocell coverage, are receiving significant attention in industry as a cost-effective way to boost the network capacity [15, 18]. In heterogeneous networks, relay nodes can be used to fill

the coverage hole, increase signal strength in poor coverage areas such as cell edge, and extend the coverage, providing a uniform broadband experience to mobile users anywhere in the network.

In addition to extending the network coverage, relay-assisted communications, or cooperative communications, can also be used to combat channel fading effects. To quantify the error performance of wireless transmissions over fading channels, we use diversity order. Diversity order is defined as the negative asymptotic slope of the average error probability versus the average signal-to-noise ratio (SNR) when plotted in a log-log scale [109, 121]. The higher the diversity is, the lower the error probability is when SNR is high. Therefore, diversity-enriched transceivers have well-appreciated merits to cope with the deleterious fading effects [98]. It is well known that the diversity order depends on the degrees of freedom provided by the underlying fading channels using temporal, frequency, polarization, and spatial resources [11, 51, 78, 111]. In cooperative communications, distributed relays, cooperating to transmit/receive their intended signals, form a virtual antenna array to provide a natural diversity. Suppose that a source transmits a message to a destination, but obstacles degrade the source-destination link quality. Thanks to the broadcast nature of the wireless channel, the same message can be heard and forwarded to the destination by relay nodes. The destination may combine the signals received from the source and relays to decode the message. This creates a type of diversity, called cooperative diversity, and designing diversity-enabled relays is important for low error rate.

Multi-input multi-output (MIMO) techniques can be adopted to relay networks to provide higher rates and reliability. With multiple antennas, receive diversity can also be collected by using maximum-likelihood equalizer (MLE) at the receiver. Although MLE enjoys maximum receive diversity, the decoding complexity also increases exponentially as the number of antennas and/or the constellation size increases, which

makes it infeasible for practical systems. To reduce the decoding complexity, low-complexity equalizers, such as linear equalizers (LEs), are often adopted. However, they may not collect the diversity enabled by the channel, showing inferior performance compared to MLE. The error performance of LEs is investigated in [66] to reveal the fundamental condition to achieve full diversity as MLEs do. It is shown that the channels need to be constrained within a certain distance from orthogonality. This condition should be considered at the receiver to collect full diversity with LEs.

It is also important to acknowledge that intrinsic nonlinear characteristics such as peak-power or peak-amplitude constraints exist in many components in communication systems. Since practical power amplifiers (PAs) have limited linear range, the output signal may experience nonlinear distortions and/or saturations. For example, when conventional fixed-gain amplify-and-forward (AF) strategy [48] is adopted, the relay output signal waveform may have high PAR depending on the received signal. Thus, the new AF relay output should be designed with peak-power constraints so that PAs operate solely in the linear region without saturation and without the need of a large back-off.

1.2 Objectives

The objective of this dissertation is to present practical wireless cooperative relay designs that can achieve low error rate, low-complexity, and high power efficiency. More specifically, this dissertation focuses on the following topics:

- Diversity-enabled power profiles at the relay for decode-and-forward (DF) cooperative relay networks;
- Low-complexity DF MIMO relay designs achieving joint diversity;
- AF MIMO relay designs with peak-power constraint.

For DF cooperative relay networks, where the relay decodes the received signal and forwards the re-encoded information to the destination, the decoding errors at the relay may be propagated to the destination, and thus the destination cannot collect the cooperative diversity. To enable cooperative diversity in DF relay networks, we adopt general link-adaptive power-scaling relay strategies. We analyze the diversity enabled by the power profile desgins.

For DF MIMO relay networks, MLE can be adopted at the receiver to collect spatial diversity provided by multiple antennas. However, the high decoding complexity makes MLE infeasible in practical systems. Thus, we propose low-complexity DF MIMO relay designs with LEs for decoding. With low-complexity LEs, we aim to achieve joint cooperative and spatial diversity.

When the AF relaying is adopted for the MIMO relay networks, peak-power constraints from PAs at the relay should be considered to avoid saturation. Significantly scaling down the input signal to the PAs is one solution; however, the cost is a reduced efficiency of the RF-to-DC power conversion. Therefore, we design simple and practical peak-power constrained relay for power efficiency. We also find a sufficient condition to enable joint cooperative and spatial diversity.

1.3 Outline and Notations

The rest of the dissertation is organized as follows:

In Chapter 2, we first present fading channel models widely used in wireless communications. An important parameter, diversity order, which quantifies the error performance in fading channels is introduced. Diversity combining techniques that we use in this dissertation are presented. Then, a literature review on relay networks is presented.

In Chapter 3, we study link-adaptive power-scaling strategies for DF cooperative

systems and the diversity order enabled by general power profiles without any feedback information. We show that the behavior of the power profile near its roots plays an important role in determining the diversity order at the destination. The necessary and sufficient conditions for the power-profile design to enable full cooperative diversity 2 are summarized. We also show that the result can be extended to multi-relay cases.

In Chapter 4, we propose low-complexity DF MIMO relay designs and analyze the diversity order of each design. We first show that the power-scaling design in Chapter 3 can be adopted here to enable cooperative diversity at the destination. To exploit antenna receive diversity, we develop a channel-controlled automatic repeat request (CC-ARQ) scheme with low-complexity LEs. Also, power-scaling strategy combined with the CC-ARQ is proposed to achieve joint cooperative and receive diversity enabled by the network.

In Chapter 5, we present peak-power constrained AF MIMO relay designs and find sufficient conditions on the relay gain to achieve joint cooperative and receive diversity at the destination. Based on the conditions, we propose simple and practical yet diversity enabling relay designs suitable for peak-power limited systems. CC-ARQ is also applied to AF MIMO relay networks to reduce the decoding complexity.

Finally, in Chapter 6, we summarize the main contributions of this dissertation and suggest topics for future research.

Let us introduce the following notations that are used throughout this dissertation unless indicated otherwise:

Upper (lower) bold face letters will be used for matrices (column vectors). Superscript $^{\mathcal{H}}$ denotes Hermitian, * conjugate, and ^{T} transpose. The real and imaginary parts are denoted as $\Re[\cdot]$ and $\Im[\cdot]$. We reserve $|a|$ for the absolute value of scalar a or cardinality of a if a is a set, $\|\boldsymbol{a}\|$ for the 2-norm of vector $\boldsymbol{a}$. $\boldsymbol{I}_N$ and $\mathbf{0}_{\mathrm{N}\times\mathrm{N}}$ denote the $N \times N$ identity matrix and $N \times N$ zero matrix, respectively, and diag$[\boldsymbol{a}]$ stands for

a diagonal matrix with $\boldsymbol{a}$ on its main diagonal. We will denote the $(m,n)^{th}$ element of a matrix $\boldsymbol{X}$ by $X_{m,n}$.

The Gaussian tail function $Q(\cdot)$ is defined as $Q(x) = (1/\sqrt{2\pi}) \int_x^\infty \exp(-t^2/2)dt$. $f(x)$ denotes the probability density function (PDF) of a random variable. We also reserve $E[\cdot]$ as the expectation. $\mathcal{CN}(0, \sigma^2)$ denotes complex Gaussian distribution with zero mean and variance σ^2. The expression $x \to a^+(a^-)$ indicates that x is approaching a from right (left).

CHAPTER II

BACKGROUND

In this chapter, a review of diversity-enabled systems in fading channels is presented. We start with fading channel models and introduce diversity combining techniques to mitigate the effects of fading. Then, we provide a literature research on relay networks.

2.1 Diversity-Enabled Systems in Fading Channels

Wireless communication systems inherently suffer from deleterious channel fading effects. Multipath fading is due to the constructive and destructive combination of randomly delayed, reflected, scattered, and diffracted signal components. Shadow fading is due to shadowing from obstacles affecting the wave propagation [79, 82].

Depending on the nature of the radio propagation environment, there are different models describing the statistical behavior of the multipath fading envelope. The Rayleigh distribution is the most widely used distribution to describe the received envelope [92]. The Rayleigh flat fading channel model assumes that all the components that make up the resultant received signal are reflected or scattered and there is no direct path between the transmitter and the receiver. The PDF of Rayleigh distributed envelope of a randomly received signal is given by [75]

$$f(\beta) = \frac{\beta}{\sigma^2} \exp\left(-\frac{\beta^2}{2\sigma^2}\right), \qquad 0 \leq \beta \leq \infty, \tag{1}$$

where σ^2 is the average power of the received signal. Let $\bar{\rho}$ denoted as the average SNR, then the instantaneous SNR in the Rayleigh fading channel is

$$\rho = \beta^2 \bar{\rho}. \tag{2}$$

For random channel variable β^2, we will use the Rayleigh fading channel model in Eq. (1) throughout this dissertation.

In general, the average error probability in a fading channel is a function of the average SNR $\bar{\rho}$. For example, for point-to-point communications with additive Gaussian channel noise (AWGN), the instantaneous error probability is expressed as a function of ρ as

$$P_{\mathrm{e,inst}}(\rho) = \kappa_1 Q\left(\sqrt{\kappa_2 \rho}\right),$$

where κ_1 and κ_2 are constellation-specific constants [76]. Using Eq. (2) and averaging $P_{\mathrm{e,inst}}(\rho)$ over the random channel variable β^2, the average error probability is now a function of the average SNR $\bar{\rho}$.

To quantify the error performance in fading channels at high SNR, the average error probability P_{e} of an uncoded system is usually approximated at high SNR by

$$P_{\mathrm{e}} \approx (G_c \cdot \bar{\rho})^{-G_d}, \quad \textit{for } \bar{\rho} \to \infty,$$

where G_d and G_c are referred to as diversity order and coding gain, respectively [65, 109]. Especially, we are interested in diversity order of the average error probability, which is defined as follows: [22, 108, 121]

Definition 1 (Diversity order) *Suppose that P_{e} is the average error probability and $\bar{\rho}$ is the average SNR. The diversity order G_d of a given system is defined as:*

$$G_d = \lim_{\bar{\rho}\to\infty} -\frac{\log P_{\mathrm{e}}}{\log \bar{\rho}} \ . \tag{3}$$

Using the symbol "$\dot{=}$" to represent the asymptotic exponential equality, i.e., we use $f(a) \doteq g(a)$ to represent $\lim_{a\to\infty} \frac{f(a)}{\ln a} = \lim_{a\to\infty} \frac{g(a)}{\ln a}$, we can rewrite Eq. (3) as $P_{\mathrm{e}} \doteq \bar{\rho}^{-G_d}$. Similarly, "$\dot{\leq}$" and "$\dot{\geq}$" are defined.

From this definition, the diversity order G_d determines the negative asymptotic slope of the average error probability versus the average SNR when plotted in a log-log scale.

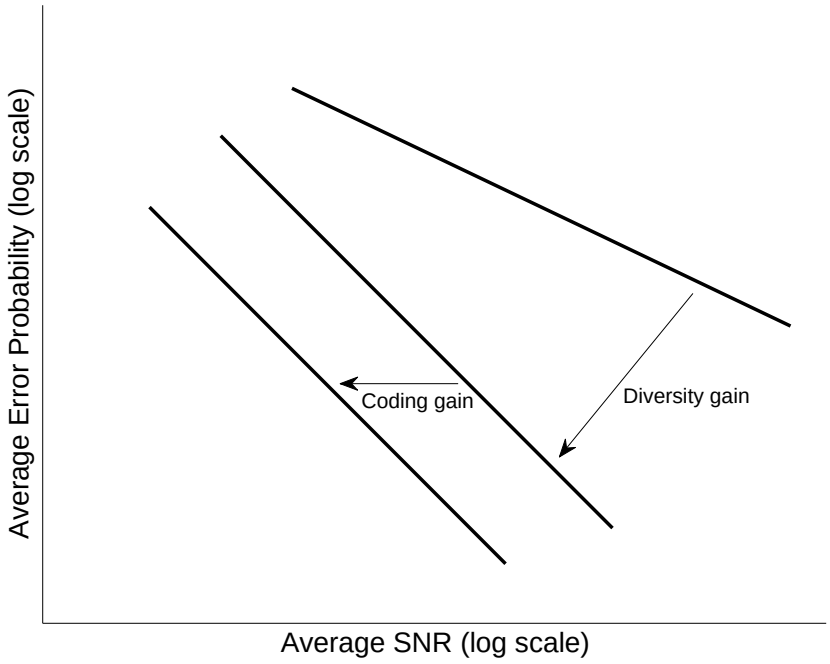

Figure 1: Diversity order and coding gain.

The diversity order is critical in the evaluation of the error performance since the higher the diversity is, the faster the average error probability decreases at high SNR regime. It is well known that the diversity order depends on the degrees of freedom provided by the underlying fading channels. Note, the coding gain G_c measures the shift in SNR of the curve relative to the benchmark curve of $\bar{\rho}^{-G_d}$ (see Figure 1).

One of the most powerful techniques to mitigate the effects of fading is to use diversity combining of signals from independently fading paths. Diversity combining consists of receiving same information over two or more fading channels and combining these multiple replicas at the receiver to increase the overall received SNR. Diversity combining uses the fact that independent signal paths have a low probability of experiencing deep fades simultaneously (see Figure 2).

A variety of diversity techniques for wireless systems are proposed in the literature [50].

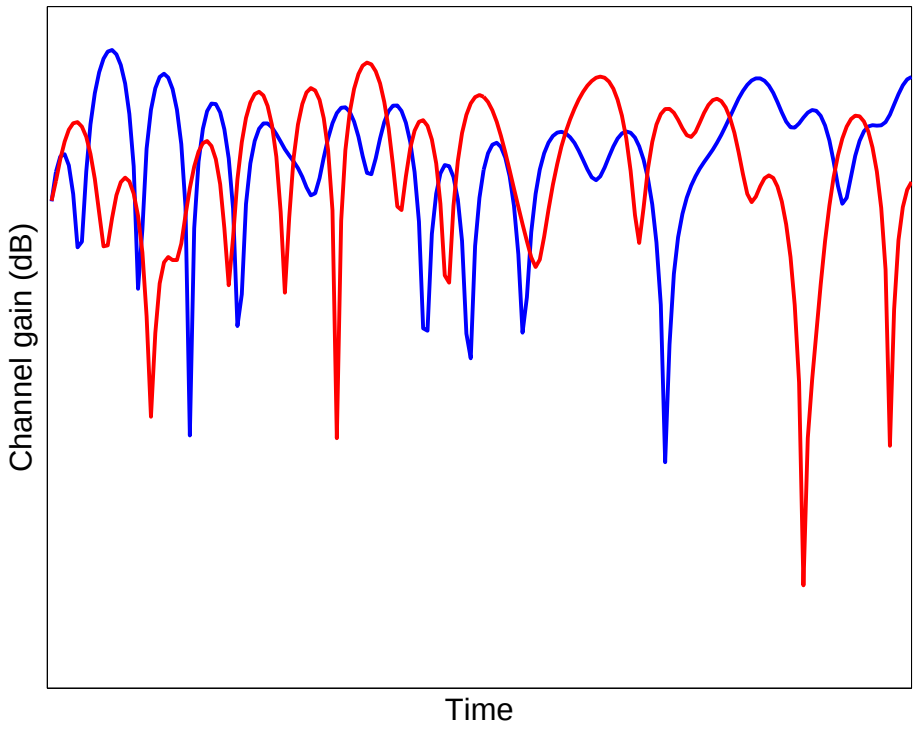

Figure 2: Two independent signal paths.

- Space diversity uses multiple receiver antennas, which is also called an antenna array, where the elements of the array are separated in distance. With receiver space diversity, independent fading paths are realized without an increase in transmit signal power or bandwidth.

- Frequency diversity uses multiple frequency channels which are separated by at least the coherence bandwidth of the channel, e.g., frequency hopping or multicarrier systems.

- Time diversity uses multiple time slots which are separated by at least the coherence time of the channel, e.g., coded systems.

- Multipath diversity resolves multipath components at different delays, e.g., direct sequence spread-spectrum systems with RAKE reception.

- Cooperative diversity is created in cooperative relay networks when the destination receives redundant information from one or more relays in addition to the one from the source directly.

Multiple received copies of a signal can be combined to collect diversity at the receiver. The most commonly used diversity combining techniques are listed below [12, 87]:

- Switched combining - The receiver stays with one of its received copies until its channel gain falls below a threshold, at which time it switches to the next signal.

- Selection combining - The receiver selects the best available signal at any instant. This performs better than switched combining, but it needs to estimate all channel gains simultaneously.

- Equal gain combining (EGC) - The receiver is a simple summation of received signals after the phases of all signals are adjusted so that the contributions add constructively.

- Maximum ratio combining (MRC) - The phases are adjusted as in EGC, but then different gains are scaled (weighed summation) to maximize the received SNR, i.e.,

$$y = \sum_i h_i^* r_i,$$

where h_i is a channel gain for i^{th} signal r_i.

MRC is the optimal combining scheme regardless of fading statistics, and we use MRC in Chapters 3 and 4 for collecting cooperative diversity.

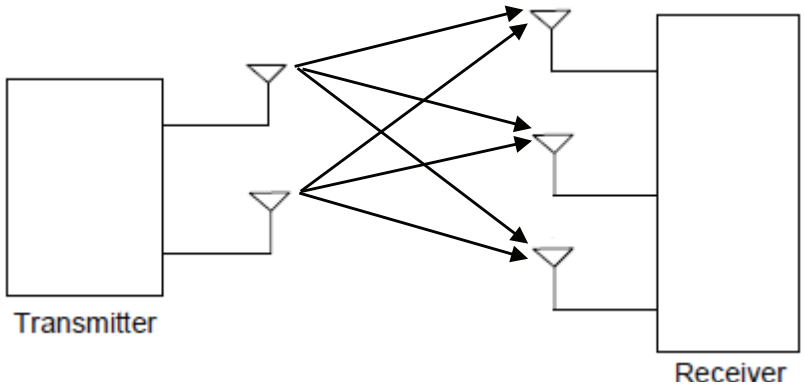

Figure 3: MIMO channel.

2.2 MIMO Systems

MIMO systems are widely adopted in modern wireless communication standards such as IEEE 802.11n (Wi-Fi), Worldwide Interoperability for Microwave Access (WiMAX), HSPA+ and 3GPP LTE/LTE-Advanced. Diversity gains can be achieved by utilizing multiple paths (see Figure 3) enabled by multiple antennas at the transmitter and receiver.

For MIMO systems, spatial multiplexing is often employed, e.g., Vertical-Bell Laboratories Layered Space Time (V-BLAST) transmissions [40, 46], where multiple data streams are transmitted across different spatial domains. Consider MIMO block transmissions [65, 96]

$$\boldsymbol{y} = \boldsymbol{H}\boldsymbol{s} + \boldsymbol{w},$$

where $\boldsymbol{H}$ is the $M \times N$ complex Gaussian channel matrix with zero mean, the $N \times 1$ vector $\boldsymbol{s}$ consists of the information symbols, $\boldsymbol{y}$ is the $M \times 1$ received vector, and $\boldsymbol{w}$ is independent and identically distributed (i.i.d.) complex AWGN. The system has N transmit-antennas and M receive-antennas. For V-BLAST transmissions, a data stream is divided into N sub-streams and transmitted through N antennas.

When MIMO i.i.d. channel is used, different diversity order is achieved at the receiver depending on the equalizer used for detection [66].

The optimal detector is the maximum-likelihood equalizer (MLE), which is based on an exhaustive search among all $N \times 1$ symbol vectors as

$$\hat{\boldsymbol{s}} = \arg\min_{s \in \mathcal{S}^N} \|\boldsymbol{y} - \boldsymbol{H}\tilde{\boldsymbol{s}}\|^2, \tag{4}$$

where $\mathcal{S}$ is the finite alphabet of the symbols. MLE in Eq. (4) provides the optimal error performance with diversity order of M at the receiver. However, the price paid is in high decoding complexity ($\mathcal{O}(|\mathcal{S}|^N)$).

On the other hand, linear equalizers (LEs) are characterized as low-complexity equalizers. Zero-forcing equalizer (ZFE) is often adopted LEs and it is given as

$$\boldsymbol{x} = \boldsymbol{H}^{\dagger}\boldsymbol{y} = \boldsymbol{s} + \boldsymbol{H}^{\dagger}\boldsymbol{w},$$

followed by the quantization step $\mathcal{Q}$ that maps each entry to the nearest symbol in the alphabet $\mathcal{S}$. $\boldsymbol{H}^{\dagger} = (\boldsymbol{H}^{\mathcal{H}}\boldsymbol{H})^{-1}\boldsymbol{H}^{\mathcal{H}}$ denotes the Moore-Penrose pseudo-inverse of the channel matrix $\boldsymbol{H}$. The complexity is dominated by matrix inversion, which requires polynomial complexity $\mathcal{O}(N^3)$ via Gaussian elimination. However, LEs have inferior performance relative to MLEs due to loss of diversity and collect only diversity order of $M - N + 1$ [66].

2.3 Relay Networks

Relay transmission is one of the fastest growing areas of research in wireless networks [74]. To enable effective distribution and collection of signals to and from mobile users, low-power nodes such as picos, femtos, and relays can be deployed to provide cell-splitting gains and to increase the network capacity [28]. Unlike picos and femtos, relays do not require a wired backhaul connection, and thus can be deployed in a cost-effective manner [114].

Relaying is considered as a tool to improve the coverage of high data rates, the cell-edge throughput and/or to provide coverage in new area in cellular systems. Relay technologies have been actively studied and considered in the standardization

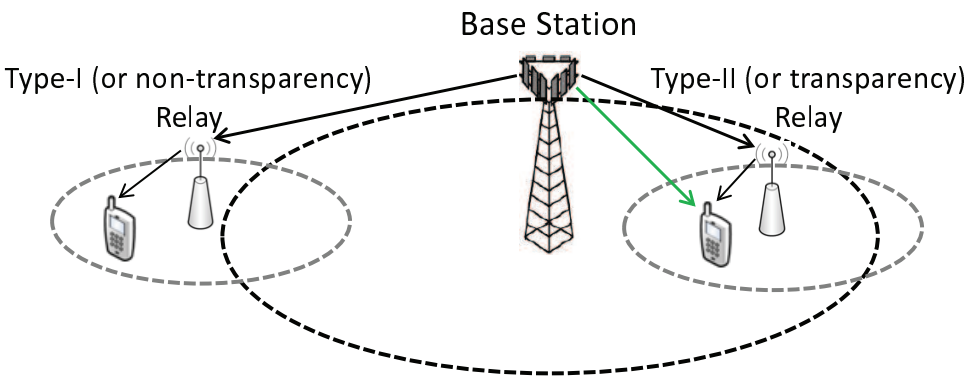

Figure 4: Two types of relay.

process of recent mobile broadband communication systems, such as 3GPP LTE-Advanced [3] and IEEE 802.16j [53]. Two types of relay types have been defined in 3GPP LTE-Advanced (Type-I and Type-II) and IEEE 802.16j (non-transparency and transparency). Specifically, the main objective of a Type-I (or non-transparency) relay is to extend signal and service coverage, as shown in Figure 4. A mobile user which is located far away from a base station (BS), and thus does not have a direct link with the BS, can access the BS through this type of relays. Type-I relays mainly perform IP packet forwarding in the network layer and need to transmit the common reference signal and the control information for the BS.

On the other hand, the main objective of a Type-II (or transparency) relay is to increase the overall system capacity for a mobile user which is located within the coverage of a BS and has a direct communication link with the BS. This type of relays can improve the service quality and link capacity by achieving multipath (or cooperative) diversity and transmission gains through the cooperation with the BS and other relays. So a Type-II relay does not transmit the common reference signal or the control information.

A three-node network, which consists of a source node, a relay node, and a destination node (see e.g., [26, 102]), is a fundamental unit in cooperative communications. Note that we consider direct link between the source and the destination. The model

was originally introduced by Van der Meulen in 1971 [102]. In general, cooperative relaying systems have a source node broadcasting a message to a destination and a number of cooperative relays which in turn forward a processed version to the intended destination node. The destination node combines the source signal and the signals received from the relays. By combining multiple copies, the inherent diversity of the relay channel, cooperative diversity, is usefully exploited, which was briefly introduced in the Section 2.1.

Capacity of three-node relay networks has been studied in [26, 43]. Many cooperation strategies have been proposed to exploit the cooperative diversity and enhance coverage for single-relay systems [59, 62, 83]. Two well-known categories are [59, 62]: *amplify-and-forward* (AF) and *decode-and-forward* (DF) relaying. For the AF strategy, the relay simply amplifies the received signal and forwards it to the destination. The destination combines received signals from the source and the relay using different techniques to collect the cooperative diversity (see [59, 62, 100]). In most AF studies [59, 80, 122], two-hop channel state information (CSI), i.e., the instantaneous CSI of source-relay link, is required for MRC at the destination. In [63], a practical and simple AF strategy is proposed that achieves full cooperative diversity even in the absence of two-hop CSI at both the relay and the destination. However, the AF scheme also amplifies the unwanted noise signal and requires the storage of analog waveforms at the relay, which necessitates expensive radio frequency (RF) storage chains [106].

For the DF scheme, the relay node first decodes the received signal and forwards the re-encoded one to the destination. However, when the relay does not decode the signal correctly, the error may be propagated to the destination and MRC at the destination cannot collect the cooperative diversity [7, 59]. Consequently, much effort has been observed in the literature to improve the performance of the simple and practical DF scheme. Coded cooperation methods were proposed to improve the

error performance [52, 91], where the spatial diversity can be exploited by coding across the source and the relay. The DF-based coding strategies using low-density parity-check (LDPC) codes [35] and turbo codes [120] for the single-relay system have been constructed. In these designs, the source and the relay have to be synchronized well. These techniques rely on the cyclic redundancy check (CRC) at the relay to prevent the forwarding of the erroneous signal. However, this requires additional hardware and time to encode and decode CRC codes at the relay node, which is not desirable for resource-constrained scenarios. Also, they assume that the relay only forwards correct symbols with CRC, but CRC cannot detect all possible errors. Thus, cooperative diversity still cannot be achieved for those designs.

Many other research works have considered cooperative relay networks without CRC codes. For optimal performance, ML decoders at the destination were derived in [13] and [56]. However, the exponential decoding complexity of ML decoder prohibits its usage. Suboptimal techniques performed at the destination were then proposed [19, 84, 106] which require the destination to possess exact knowledge of the instantaneous CSI of the source-relay link. Other techniques focus on the enhancements applied at the relay. Threshold-based relaying strategies were proposed for binary phase-shift keying (BPSK) modulation [73, 88]. The relay selectively forwards symbols based on the reliability of the received signal and thus mitigates error-propagation effects. A link-adaptive relay (LAR) scheme was proposed in [108] to enable cooperative diversity by scaling the transmission power of the re-encoded signal at the relay based on the reliability of the source-relay link. This scheme shows a promising solution to gain diversity while keeping the overhead low (e.g., no feedback, no two-hop information needed at the destination). However, the designs in [108] (e.g., perfect soft limiter) may not be implemented perfectly in hardware due to nonlinear PAs. In practical systems, power profiles can have different shapes which may result in different performances. [77] finds the nonlinear mapping of PA that maximizes the

output signal-to-noise-and-distortion ratio (SNDR). Likewise, general power profiles for LAR should be further analyzed to consider nonlinear characteristics of PA and find the power profiles that enable full cooperative diversity at the destination.

Recently, the idea of using multiple antennas in relay networks is receiving significant interest because MIMO techniques offer higher spectral efficiency and link reliability in point-to-point communications [25, 37]. Capacity bounds for various MIMO relay channels are studied in the literature [14, 39, 86, 104, 105, 112]. Three-dimensional diversity-multiplexing-delay tradeoff [41] in MIMO automatic repeat request (ARQ) relay channels, where ARQ retransmission delay can be exploited as a potential source for diversity [34], is investigated in [57, 93, 113].

Many research works on MIMO relay designs are found in the literature. Linear signal processing schemes at the fixed MIMO relay(s) for multi-user transmission have been considered in [16, 36, 117, 118], where CSI is assumed to be known at the transmitter. The optimization of the relay precoding matrix or joint source-relay precoding matrices was studied in [69, 71, 95] to maximize the information rate. Linear transceiver designs based on the minimum mean square error (MMSE) criterion were proposed in [47, 68, 81, 89, 99]. Antenna selection schemes for MIMO relay were proposed and analyzed in [8, 20, 33, 42]. However, many of the proposed schemes neglect direct source-destination link to simplify the analysis. For transmit diversity, space-time block codes (STBCs) have been applied to MIMO relay networks. Two main approaches have been studied. The first approach is distributed STBC, where STBC is employed with a distributed manner in cooperative relays [10, 55, 115]. In the second approach, the STBC is broadcast to the relay and the destination, and then the relay does amplify-and-forward or uses the same STBC after decoding. With the second approach, the symbol error probability for AF MIMO relay channel [5, 90] and the outage probability for DF MIMO relay channel [17] were analyzed with direct source-destination link and the fixed gain at the relay. However, most

of MIMO relay techniques cannot achieve full receive diversity or they require high complexity receivers, which is impractical and thus may not be suitable for low-complexity communication environments.

CHAPTER III

DIVERSITY-ENABLED DECODE-AND-FORWARD COOPERATIVE RELAY NETWORKS

Wireless cooperative relay networks have caught a lot of attention recently due to their potential to enhance performance by combating fading effects. Numerous strategies have been proposed in the literature to enable cooperative diversity [59, 60, 62, 83]. Among them, decode-and-forward protocol has been well adopted because of its low implementation complexity. The relay node decodes the received signal and forwards the re-encoded information to the destination. However, decoding errors at the relay node cause performance degradation, and thus MRC does not collect the cooperative diversity at the destination [7, 24]. Consequently, much effort has been observed in the literature to improve the performance of the simple and practical DF strategy. However, most decode-and-forward based schemes assume that the relay node has perfect error detection or has feedback information from the destination [35, 52, 64, 91, 120]. In this chapter, we design power profiles at the relay which enable diversity at the destination without any feedback or coding assumptions at the relay and source. Furthermore, the diversity orders enabled by any general power profile are quantified. We then summarize necessary and sufficient conditions on the power profiles to guarantee full diversity at the destination. The theoretical analysis is corroborated with numerical simulations.

3.1 System Model of Cooperative Relay Networks

Consider a simple single-relay network which consists of three nodes: source (S), relay (R), and destination (D) (see e.g., [26, 102]), as depicted in Figure 5. The source

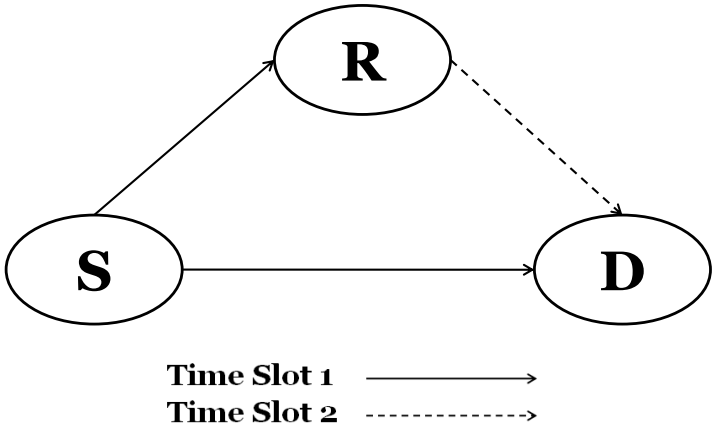

Figure 5: Three-node relay network.

node S broadcasts information symbols to the relay node R and the destination node D in the first time slot. Upon receiving symbols from the source S, the relay R decodes the received signal and forwards re-encoded symbols to D in the second time slot [62]. Suppose that every node is equipped with only one antenna and all channels are mutually independent and subject to flat fading. With subscripts signifying the corresponding link, e.g., y_{sr} denotes the signal from S to R, the mathematical formulation of baseband-equivalent model can be written as

$$\begin{aligned} y_{sr} &= h_{sr}s + w_{sr}, \\ y_{sd} &= h_{sd}s + w_{sd}, \\ y_{rd} &= \sqrt{\alpha}h_{rd}\hat{s} + w_{rd}, \end{aligned} \tag{5}$$

where s is a symbol transmitted by the source S, $\hat{s}$ is the forwarded symbol by the relay R, and y denotes the received signal. The fading channel coefficient h is known at the corresponding receiver side, and w is the additive white Gaussian noise. α is the power scaling factor (PSF) at R. Here we assume Rayleigh fading for all channels, i.e., $h_{ij} \sim \mathcal{CN}(0, \sigma_{ij}^2)$. Noises are independent and $w_{ij} \sim \mathcal{CN}(0, N_0)$. The average

symbol power E[s] is set to 1 and the instantaneous and average SNRs are defined as

$$\begin{aligned} \rho_{ij} &:= |h_{ij}|^2 \bar{\rho}, \\ \bar{\rho}_{ij} &:= E\{\rho_{ij}\} = \sigma_{ij}^2 \bar{\rho}, \\ \bar{\rho} &:= \frac{1}{N_0}. \end{aligned} \tag{6}$$

At the relay, the estimated symbol $\hat{s}$ is obtained through the maximum-likelihood (ML) detector as

$$\hat{s} = \arg\min_{s \in \mathcal{S}} |y_{sr} - h_{sr} s|^2 ,$$

where $\mathcal{S}$ is the constellation of the transmitted symbol. The combining is performed at D as

$$\hat{s}_d = \arg\min_{s \in \mathcal{S}} \left| h_{sd}^* y_{sd} + \sqrt{\alpha} h_{rd}^* y_{rd} - (|h_{sd}|^2 + \alpha |h_{rd}|^2) s \right|^2 .$$

With the estimate at the destination and the average SNR definition in (6), we will use diversity order, defined in Eq. (3), as a performance indicator for cooperative relay networks (Figure 5). Besides the signal directly transmitted from the source, the destination obtains another copy of information transmitted from the relay, and thus, the maximum of cooperative diversity 2 can be obtained for this network setup. To enable the cooperative diversity, [108] has proposed

$$\alpha(\beta) = \frac{\min(\rho_{sr}, \beta \bar{\rho}_{rd})}{\beta \bar{\rho}_{rd}},$$

with $\bar{\rho}_{rd}$ being the feedback information and β being a constant. However, the $\alpha(\beta)$ design in [108] requires feedback from the destination node and only provides a special case of the power profile.

In this chapter, we analyze cooperative diversity order enabled by general power profiles that do not require feedback information and provide sufficient and necessary conditions for full cooperative diversity.

3.2 General Link-Adaptive Relay

Given the system model in (5), in this section, we design a general power profile α at the relay by assuming that α is a nonnegative, continuous function of $\frac{\rho_{sr}}{\bar{\rho}} = |h_{sr}|^2$ in $[0, \infty)$. After deriving some upper and lower bounds on the average symbol-error rate (SER) when the general link-adaptive strategy is applied at the relay, we will analyze the effect of power profiles on the system performance in terms of diversity order.

3.2.1 Average SER Bounds

The instantaneous pairwise error probability at the destination node for the general link-adaptive strategy with BPSK modulation is expressed as [108, Eq. (17)]

$$\begin{aligned} P_b &= \left\{1 - Q\left(\sqrt{2\rho_{sr}}\right)\right\} Q\left(\sqrt{2(\rho_{sd} + \alpha\rho_{rd})}\right) \\ &\quad + Q\left(\sqrt{2\rho_{sr}}\right) Q\left(\frac{\sqrt{2}(\rho_{sd} - \alpha\rho_{rd})}{\sqrt{\rho_{sd} + \alpha\rho_{rd}}}\right) \\ &=: P_{b1} + P_{b2}. \end{aligned} \tag{7}$$

To analyze the diversity, we introduce upper and lower bounds of $E[P_b]$ in the following lemma.

Lemma 1 *Given BPSK modulation, the average SER $E[P_b]$ (over all random channels) can be bounded as*

$$P_{l1} + P_{l2} \leq E[P_b] \leq P_{u1} + P_{u2} + P_{u3},$$

where

$$\begin{aligned}
P_{l1} &= \int_0^\infty \frac{\exp(-\frac{\rho_{sr}}{\bar{\rho}_{sr}})(2-\exp(-\rho_{sr}))}{4\sqrt{\pi}\bar{\rho}_{sr}(2+3\bar{\rho}_{sd})(1+\alpha\bar{\rho}_{rd})}d\rho_{sr},\\
P_{l2} &= \int_0^\infty \frac{\alpha\bar{\rho}_{rd}}{\bar{\rho}_{sd}+\alpha\bar{\rho}_{rd}}\frac{\exp(-\rho_{sr}-\frac{\rho_{sr}}{\bar{\rho}_{sr}})}{4\sqrt{\pi}\bar{\rho}_{sr}\sqrt{\rho_{sr}+2}}d\rho_{sr},\\
P_{u1} &= \frac{1}{2\bar{\rho}_{sd}\bar{\rho}_{sr}}\int_0^\infty \frac{\exp(-\frac{\rho_{sr}}{\bar{\rho}_{sr}})}{1+\alpha\bar{\rho}_{rd}}d\rho_{sr},\\
P_{u2} &= \frac{1}{2\bar{\rho}_{sr}}\int_0^\infty \exp(-\rho_{sr})\\
&\quad \Big\{\frac{1}{2(\alpha\bar{\rho}_{rd}+\bar{\rho}_{sd})}+\frac{\pi\sqrt{\bar{\rho}_{sd}}\sqrt{\alpha\bar{\rho}_{rd}}}{4(\alpha\bar{\rho}_{rd}+\bar{\rho}_{sd})^{\frac{3}{2}}}\Big\}d\rho_{sr},\\
\textit{and}\quad P_{u3} &= \frac{1}{2\bar{\rho}_{sr}}\int_0^\infty \exp(-\rho_{sr})\frac{\alpha\bar{\rho}_{rd}}{\bar{\rho}_{sd}+\alpha\bar{\rho}_{rd}}d\rho_{sr}.
\end{aligned}$$

Proof: The average SER $E[P_b]$ is obtained by taking the expectation of P_b over random channels h_{sr}, h_{rd}, and h_{sd}. The upper bound of $E[P_b]$ is easily found and simplified from [108, Eq. (29)] and the first two equations in Appendix B of [108]. The lower bound of $E[P_b]$ can be obtained as the summation of the lower bounds of $E[P_{b1}]$ and $E[P_{b2}]$. Let us first simplify the lower bound of $E[P_{b1}]$ in [108, Eq. (36)] as

$$\begin{aligned}
E[P_{b1}] &\geq \int_0^\infty \frac{\pi\exp(2+\frac{2}{\alpha\bar{\rho}_{rd}})}{(2+3\bar{\rho}_{sd})\alpha\sqrt{\pi+\frac{\pi}{\alpha\bar{\rho}_{rd}}}}\mathrm{erfc}\left[\sqrt{2+\frac{2}{\alpha\bar{\rho}_{rd}}}\right]\Phi(\rho_{sr})d\rho_{sr}\\
&\geq \int_0^\infty \frac{\pi\exp(2+\frac{2}{\alpha\bar{\rho}_{rd}})}{(2+3\bar{\rho}_{sd})\alpha\sqrt{\pi+\frac{\pi}{\alpha\bar{\rho}_{rd}}}}\frac{\exp[-(2+\frac{2}{\alpha\bar{\rho}_{rd}})]}{\sqrt{\pi}\sqrt{4+\frac{2}{\alpha\bar{\rho}_{rd}}}}\Phi(\rho_{sr})d\rho_{sr}\\
&\geq \int_0^\infty \frac{\Phi(\rho_{sr})}{(2+3\bar{\rho}_{sd})\sqrt{\alpha+\frac{1}{\bar{\rho}_{rd}}}\sqrt{4\alpha+\frac{4}{\bar{\rho}_{rd}}}}d\rho_{sr}\\
&= \int_0^\infty \frac{\exp(-\frac{\rho_{sr}}{\bar{\rho}_{sr}})(2-\exp(-\rho_{sr}))}{4\sqrt{\pi}\bar{\rho}_{sr}(2+3\bar{\rho}_{sd})(1+\alpha\bar{\rho}_{rd})}d\rho_{sr}\\
&=: P_{l1},
\end{aligned}$$

where

$$\Phi(\rho_{sr}) = \frac{1}{2\bar{\rho}_{rd}\bar{\rho}_{sr}\sqrt{\pi}}\left[2\exp\left(-\frac{\rho_{sr}}{\bar{\rho}_{sr}}\right)-\exp\left(-\frac{\rho_{sr}(1+\bar{\rho}_{sr})}{\bar{\rho}_{sr}}\right)\right]$$

and the second inequality is derived from the inequality [110, Eq. (13)]

$$\mathrm{erfc}(x) \geq \frac{2}{\sqrt{\pi}}\frac{\exp(-x^2)}{x+\sqrt{x^2+2}}.$$

For $E[P_{b2}]$, we find the lower bound by limiting the integral interval to $0 < \rho_{sd} < \alpha\rho_{rd}$ for ρ_{sd}. Then, using $Q(x) > \frac{1}{2}$ for $x < 0$,

$$\begin{aligned} E[P_{b2}] &\geq \int_0^\infty \int_0^\infty \int_0^{\alpha\rho_{rd}} \frac{1}{2} Q\left(\sqrt{2\rho_{sr}}\right) f(\rho_{sr}) f(\rho_{rd}) f(\rho_{sd}) d\rho_{sd} d\rho_{rd} d\rho_{sr} \\ &\geq \int_0^\infty \frac{1}{2} Q\left(\sqrt{2\rho_{sr}}\right) \left(1 - \frac{\bar{\rho}_{sd}}{\bar{\rho}_{sd} + \alpha\bar{\rho}_{rd}}\right) \frac{1}{\bar{\rho}_{sr}} \exp\left(-\frac{\rho_{sr}}{\bar{\rho}_{sr}}\right) d\rho_{sr} \\ &\geq \int_0^\infty \frac{\alpha\bar{\rho}_{rd}}{\bar{\rho}_{sd} + \alpha\bar{\rho}_{rd}} \frac{1}{2\bar{\rho}_{sr}} \frac{\exp(-\rho_{sr}) \exp(-\frac{\rho_{sr}}{\bar{\rho}_{sr}})}{2\sqrt{\pi}\sqrt{\rho_{sr} + 2}} d\rho_{sr} \\ &=: P_{l2}, \end{aligned}$$

where a PDF of ρ is

$$f(\rho) = \frac{1}{\bar{\rho}} \exp\left(-\frac{\rho}{\bar{\rho}}\right),$$

and the lower bound

$$Q(x) = \frac{1}{2}\text{erfc}\left(\frac{x}{\sqrt{2}}\right) \geq \frac{\exp\left(-\frac{x^2}{2}\right)}{\sqrt{\pi}\left(\frac{x}{\sqrt{2}} + \sqrt{\frac{x^2}{2} + 2}\right)}$$

is applied to arrive at the third inequality. Therefore, $E[P_b]$ is bounded below by $P_{l1} + P_{l2}$ or by P_{l1} (P_{l2}) alone. ■

As shown in Lemma 1, the upper and lower bounds of the average SER are expressed as the integration with respect to the random SNR ρ_{sr}, since the power profile at the relay is a function of the random SNR ρ_{sr} (or $|h_{sr}|^2 = \frac{\rho_{sr}}{\bar{\rho}}$). Therefore, the diversity of the average SER $E[P_b]$ now only depends on the design of the power profile as a function of $|h_{sr}|^2$.

For general M-ary constellations, the instantaneous pairwise error probability P_s is bounded as [106, Eq. (19)]

$$\begin{aligned} & \frac{1}{2}\, Q\Big(\sqrt{k_c(\rho_{sd} + \alpha\rho_{rd})}\Big) + Q\Big(\sqrt{k_c\rho_{sr}}\Big)\, Q\left(\frac{\sqrt{2}(\rho_{sd} - \alpha\rho_{rd})}{\sqrt{\rho_{sd} + \alpha\rho_{rd}}}\right) \\ \leq\ & P_s = P_{s1} + P_{s2} \\ \leq\ & Q\Big(\sqrt{k_c(\rho_{sd} + \alpha\rho_{rd})}\Big) + \ 4(\log_2 M)\ Q\Big(\sqrt{k_c\rho_{sr}}\Big)\, Q\left(\frac{\sqrt{2}(\rho_{sd} - \phi\alpha\rho_{rd})}{\sqrt{\rho_{sd} + \phi\alpha\rho_{rd}}}\right), \end{aligned} \tag{8}$$

where k_c is a constellation-specific constant, $\phi := \tilde{d}_{\max}/\tilde{d}_{\min}$, $\tilde{d}_{\min} := d_{\min}/2\sqrt{2}$, and $\tilde{d}_{\max} := d_{\max} - \tilde{d}_{\min}$ with $d_{\min}$ ($d_{\max}$) denoting the minimum (maximum) Euclidean distance of the signal constellation. Note that P_{s1} represents the situation that the relay forwards the identical symbols that the source broadcasted, and P_{s2} corresponds to the case that the relay forwards erroneous symbols. P_{s2} is upper (lower) bounded by the worst (best) case, which corresponds to the demodulated symbol at the relay being the farthest (nearest) point in the constellation. Comparing (7) and (8), the upper and lower bounds of P_s have the forms identical to P_b within a scale depending on constants k_c and ϕ. Since diversity order pertains to high SNR behavior, the diversity order is not affected by such constants, and thus, $E[P_s]$ has the same diversity order as $E[P_b]$ as shown in [106, 108]. Therefore, claims on the diversity order for BPSK in this chapter can be extended to any constellations and we have the following corollary.

Corollary 1 *For a general link-adaptive relay network setup in* (5)*, the diversity order at the destination is not affected by the underlying modulation scheme.*

3.2.2 General Link-Adaptive Relay Strategy

A general link-adaptive system defines power profile α as a function of $|h_{sr}|^2$ with certain constraints. Let us make the following descriptions of the behaviors of power profiles $\alpha(|h_{sr}|^2)$ when $|h_{sr}|^2 \to \infty$ and $|h_{sr}|^2 \to r$, where r is the root of $\alpha(|h_{sr}|^2) = 0$, i.e., $\alpha(r) = 0$.

D1) (Origin property) The expansion of $\alpha(x)$ is

$$\alpha(x) = \sum_{i=1}^{\infty} a_i x^{p_i} \quad \text{for} \quad x \to 0^+,$$

where $p_i < p_j$ for $i < j$ and a_1 is a positive coefficient.

D2) (Root set) Define a set $\mathbf{R}= \{r_k | \alpha(r_k) = 0, r_k \in (0, +\infty)\} = \bigcup_k [r_k^{(l)}, r_k^{(r)}]$, where $r_k^{(l)}$ and $r_k^{(r)}$ are the left and right boundaries of the interval where $\alpha(x) = 0$. When $r_k^{(l)} = r_k^{(r)}$, that means r_k is a single point root.

D3) (Root approaching property) Approaching the left root boundary from left, the power profile is given as

$$\alpha(x) = \sum_{i=1}^{\infty} a_{ik}^{(l)} (-x + r_k^{(l)})^{p_{ik}^{(l)}} \quad \text{for} \quad x \to (r_k^{(l)})^-,$$

and approaching the right boundary from right,

$$\alpha(x) = \sum_{i=1}^{\infty} a_{ik}^{(r)} (x - r_k^{(r)})^{p_{ik}^{(r)}} \quad \text{for} \quad x \to (r_k^{(r)})^+,$$

where $a_{1k}^{(l)}$, $a_{1k}^{(r)}$ are positive coefficients, and $0 < p_{ik}^{(l)} < p_{jk}^{(l)}$, $0 < p_{ik}^{(r)} < p_{jk}^{(r)}$ for $i < j$.

We will show that the smallest exponents of the expansion at each root, i.e., p_1 in **D1)** and $p_{1k}^{(l)}$, $p_{1k}^{(r)}$ in **D3)**, are important in determining the diversity order achieved at the destination. First, it is shown that the smallest exponent of the expansion at the root characterizes the behavior of a power profile $\alpha(|h_{sr}|^2)$ around its root in the following lemma, and in the next section, we show that the characterized behavior at each root determines the diversity order.

Lemma 2 *Let $\alpha(x) = \sum_{i=1}^{\infty} a_i x^{p_i}$ where $0 < p_i < p_j$ for $i < j$. Suppose that i) $\alpha(x)$ is continuous on $[0, \delta]$ with $\delta > 0$; ii) $0 < \alpha(x) < \infty$ on $(0, \delta]$, and iii) $a_1 > 0$. Then, $\alpha(x)$ is bounded as $c_1 x^{p_1} \leq \alpha(x) \leq c_2 x^{p_1}$ with constants $0 < c_1 < c_2 < \infty$ and $x \in [0, \delta]$.*

Proof: We can rewrite $\alpha(x)$ as

$$\alpha(x) = a_1 x^{p_1} \left(1 + \sum_{i=2}^{\infty} \frac{a_i}{a_1} x^{p_i - p_1} \right) = a_1 x^{p_1} \beta(x),$$

where we have defined $\beta(x)$ as

$$\beta(x) := 1 + \sum_{i=2}^{\infty} \frac{a_i}{a_1} x^{p_i - p_1}.$$

Since $0 < \alpha(x) < \infty$ on $(0, \delta]$ and $a_1 > 0$, $0 < \beta(x) < \infty$ on $(0, \delta]$. Also, we have $\beta(0) = 1$, thus $0 < \beta(x) < \infty$ on $[0, \delta]$. $\beta(x)$ is also continuous on $[0, \delta]$ because $\alpha(x)$

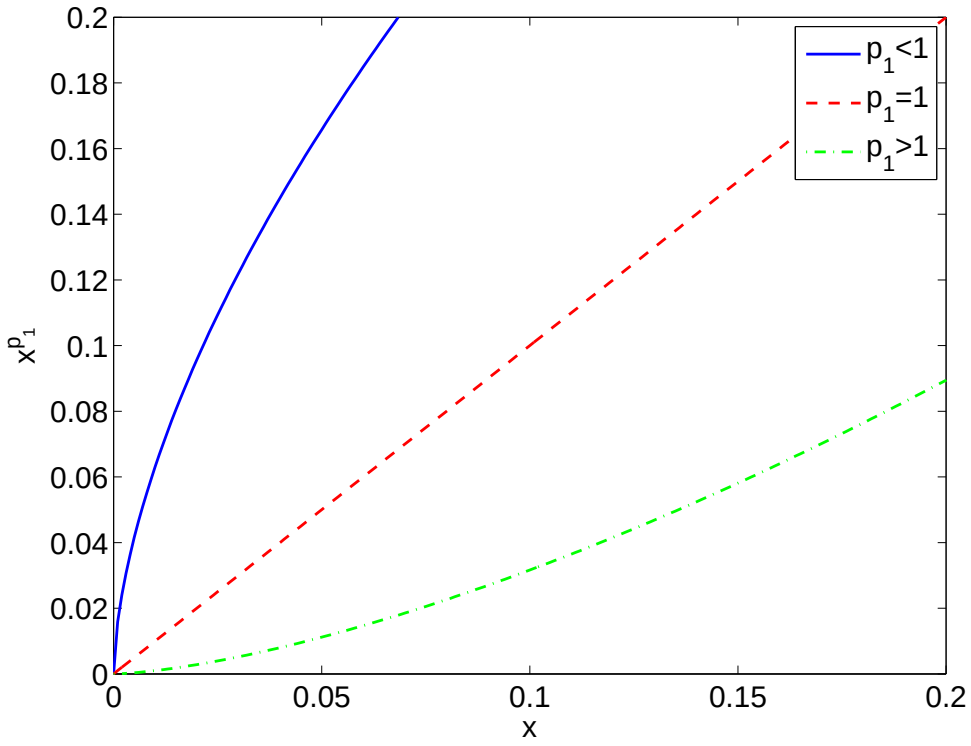

Figure 6: Three cases of the behavior around the origin.

is continuous and finite on $[0, \delta]$. Therefore, by extreme value theorem [58], there exist $m > 0$ and M such that $m \leq \beta(x) \leq M$ for $x \in [0, \delta]$. Since $\alpha(x) = a_1 x^{p_1} \beta(x)$, $\alpha(x)$ can be bounded as $c_1 x^{p_1} \leq \alpha(x) \leq c_2 x^{p_1}$ for $x \in [0, \delta]$ where $c_1 = m a_1 > 0$ and $c_2 = M a_1 > 0$. ■

This lemma states that the behavior of a power series approaching zero is determined by the polynomial term (x^{p_1}) with the lowest exponent. In the literature, this lowest exponent is also called "the order of smoothness" of $\alpha(x)$ at the origin [109]. Depending on the value of p_1, the behavior is divided into three cases: i) $p > 1$; ii) $p = 1$; and $p < 1$ as shown in Figure 6.

In the next section, this characterization will be used to derive the upper and lower bounds of SER and diversity order.

3.3 Performance Analysis

Now, we analyze the diversity performance of the general link-adaptive strategy. Before presenting the diversity claim in Theorem 1, we define three functions that will relate these parameters and the diversity order that $\alpha(|h_{sr}|^2)$ enables.

Definition 2 *Define three special functions $g_1(x)$, $g_2(x)$ and $g_3(x)$ for $x \in [0, \infty)$ as*

$$g_1(x) = \begin{cases} 0, & \text{if } x < 0 \\ x, & \text{if } 0 \le x \le 1 \\ \frac{1}{x}, & \text{if } x > 1 \end{cases},$$

$$g_2(x) = \begin{cases} 1, & \text{if } 0 \le x \le 1 \\ \frac{1}{x}, & \text{if } x > 1 \end{cases},$$

$$\textit{and} \quad g_3(x) = \begin{cases} 0, & \text{if } x \neq 0 \\ 1, & \text{if } x = 0. \end{cases}$$

With these three functions, we find the diversity order of the average SER for the relay system with a power-profile design $\alpha(|h_{sr}|^2)$ as follows:

Theorem 1 *Consider a relay system in* (5) *with a general power-profile design $\alpha(|h_{sr}|^2)$ at the relay node. The diversity order of the average SER at the destination is*

$$G_d = 1 + \min\{g_1(p_1), g_2(p_{1k}^{(l)}), g_2(p_{1k}^{(r)}), g_3(r_k^{(r)} - r_k^{(l)})\}.$$

From Theorem 1, we can see that the diversity order of the general link-adaptive relay system is determined by the behavior of the power profile $\alpha(|h_{sr}|^2)$ at the origin (p_1) and at each positive root approaching from left ($p_{1k}^{(l)}$) and right ($p_{1k}^{(r)}$), and the existence of continuous intervals in $\mathbf{R}$ defined in **D2)**. To enable the cooperative diversity order 2 at the destination, it is required that $g_1(p_1)$, $g_2(p_{1k}^{(l)})$, and $g_2(p_{1k}^{(r)})$ are all ones and also there is no continuous interval in $\mathbf{R}$, e.g., $r_k^{(l)} = r_k^{(r)}$ for all k. Therefore, we obtain the following corollary.

Corollary 2 *Consider a relay system in* (5) *with a general power profile* $\alpha(|h_{sr}|^2)$. *If* $\alpha(|h_{sr}|^2)$ *i) satisfies* $g_1(p_1) = 1$ *at the origin; ii) satisfies* $g_2(p_{1k}^{(l)}) = g_2(p_{1k}^{(r)}) = 1$ *at the roots; and iii) does not have a zero interval, i.e.,* $r_k^{(l)} = r_k^{(r)}$ *for all* k, *i.e.,* $g_3(r_k^{(r)} - r_k^{(l)}) = 1$, *then diversity order of* 2 *is guaranteed at the destination.*

Now, we will prove Theorem 1 by splitting the power-profile design into several cases. We start the proof by considering the power profile α with $\alpha(|h_{sr}|^2) > 0$ when $|h_{sr}|^2 = 0$. Although $|h_{sr}|^2 = 0$ has zero probability, the value of $\alpha(0)$ has a great impact on the diversity at the destination. With Lemma 1, we obtain the following lemma on the diversity enabled by the group of power profiles which satisfy $\alpha(0) > 0$.

Lemma 3 *Suppose that* $\alpha(|h_{sr}|^2)$ *is a nonnegative, continuous function of* $|h_{sr}|^2$ *on the interval* $[0, \infty)$. *If* $\alpha(0) > 0$, *which implies* $p_1 \leq 0$ *and* $g_1(p_1) = 0$ *from* **D1)**, *then the diversity order of the relay systems with the power profile* $\alpha(|h_{sr}|^2)$ *at the relay is always* 1.

Proof: Since $\alpha(|h_{sr}|^2)$ is nonnegative and continuous, $\alpha(0) > 0$ implies that there exist $\delta > 0$ and $C > 0$ such that if $0 \leq |h_{sr}|^2 \leq \delta$, then $\alpha(|h_{sr}|^2) > C$. We bound $E[P_b]$ below by P_{l2} from Lemma 1 and further bound it below by limiting the integration interval to $[0, \delta\bar{\rho}]$ to obtain

$$\begin{aligned}
E[P_b] &\geq P_{l2} \\
&\geq \int_0^{\delta\bar{\rho}} \frac{C\bar{\rho}_{rd}}{\bar{\rho}_{sd} + C\bar{\rho}_{rd}} \frac{\exp(-\rho_{sr} - \frac{\rho_{sr}}{\bar{\rho}_{sr}})}{4\sqrt{\pi}\bar{\rho}_{sr}\sqrt{\rho_{sr}+2}} d\rho_{sr} \\
&\overset{t^2=(\rho_{sr}+2)(1+\frac{1}{\bar{\rho}_{sr}})}{=} \frac{1}{2\sqrt{\pi}\bar{\rho}_{sr}} \left(\frac{C\bar{\rho}_{rd}}{\bar{\rho}_{sd} + C\bar{\rho}_{rd}}\right) \frac{\exp(2 + \frac{2}{\bar{\rho}_{sr}})}{\sqrt{1 + \frac{1}{\bar{\rho}_{sr}}}} \int_{\sqrt{2(1+\frac{1}{\bar{\rho}_{sr}})}}^{\sqrt{(\delta\bar{\rho}+2)(1+\frac{1}{\bar{\rho}_{sr}})}} \exp(-t^2) dt \\
&\overset{\bar{\rho} \text{ is large}}{\geq} \frac{1}{2\sqrt{\pi}\bar{\rho}_{sr}} \left(\frac{C\bar{\rho}_{rd}}{\bar{\rho}_{sd} + C\bar{\rho}_{rd}}\right) \frac{1}{\sqrt{k_1}} \int_{\sqrt{2k_1}}^{\sqrt{k_2+2}} \exp(-t^2) dt \\
&\doteq \bar{\rho}^{-1}.
\end{aligned}$$

The last inequality is obtained if $\bar{\rho}$ is large enough, $1 + \frac{1}{\bar{\rho}_{sr}} < k_1$ and $\delta\bar{\rho} > k_2$ for some constants k_1 and k_2. This derivation shows that the diversity is less than or equal to

1. To prove that the diversity is exactly 1, we need to show that the diversity is also lower bounded by 1. In other words, we need to show that

$$E[P_b] \dot{\leq} \bar{\rho}^{-1}.$$

From Eq. (7), P_b can be bounded above as

$$P_b \leq Q\left(\sqrt{2\rho_{sd}}\right) + Q\left(\sqrt{2\rho_{sr}}\right).$$

Applying the Chernoff bound [21] and taking the expectation on both sides, it is readily seen that

$$E[P_b] \leq \frac{1}{2(1+\bar{\rho}_{sd})} + \frac{1}{2(1+\bar{\rho}_{sr})} \doteq \bar{\rho}^{-1}.$$

Note that this inequality is valid for general power-profile designs $\alpha(|h_{sr}|^2) \geq 0$, which means the diversity of the system is at least 1. Therefore, we have proved that the diversity of the system is 1 for power profiles with $\alpha(0) > 0$. ■

This lemma shows that $\alpha(0) = 0$ is a necessary condition for the power profile $\alpha(|h_{sr}|^2)$ at the relay to enable cooperative diversity at the destination node. The traditional DF strategy can be considered as a special case with the power profile $\alpha = 1$ (or any positive constant). According to [7], the DF relay system only collects diversity 1 at the destination node, which is consistent with the claim in Lemma 3.

Next, we consider $\alpha(|h_{sr}|^2)$ with at least one non-zero measure interval on $|h_{sr}|^2$ such that $\alpha(|h_{sr}|^2) = 0$ for all $|h_{sr}|^2$ in this interval, i.e., there exists k such that $r_k^{(l)} \neq r_k^{(r)}$ as in **D2)**. In short, we call these intervals "zero intervals". One natural example is the binary decision case elaborated in [108], i.e., when $|h_{sr}| < \gamma_{th}$, the relay simply does not forward the packet, and when $|h_{sr}| \geq \gamma_{th}$, the relay forwards the packet with a constant power, where γ_{th} is the threshold value. The following lemma shows that this approach cannot achieve cooperative diversity at the destination node, either.

Lemma 4 *If $\alpha(|h_{sr}|^2)$ is a nonnegative, continuous function of $|h_{sr}|^2$ on $[0,\infty)$, and $\alpha(|h_{sr}|^2)$ has at least one zero interval, i.e., there exists $[r_k^{(l)}, r_k^{(r)}]$ such that $r_k^{(l)} \neq r_k^{(r)}$, then this power-profile design only achieves diversity order of 1 at the destination.*

Proof: Suppose $\alpha(|h_{sr}|^2) = 0$ for $|h_{sr}|^2 \in [a,b]$. We bound $E[P_b]$ below by P_{l1} from Lemma 1 and further bound it below by limiting the integration interval to $[a\bar{\rho}, b\bar{\rho}]$ to obtain

$$\begin{aligned} E[P_b] &\geq P_{l1} \\ &\geq \int_{a\bar{\rho}}^{b\bar{\rho}} \frac{\exp(-\frac{\rho_{sr}}{\bar{\rho}_{sr}})(2-\exp(-\rho_{sr}))}{4\sqrt{\pi}\bar{\rho}_{sr}(2+3\bar{\rho}_{sd})(1+\alpha\bar{\rho}_{rd})} d\rho_{sr} \\ &\geq \int_{a\bar{\rho}}^{b\bar{\rho}} \frac{\exp(-\frac{\rho_{sr}}{\bar{\rho}_{sr}})}{4\sqrt{\pi}\bar{\rho}_{sr}(2+3\bar{\rho}_{sd})} d\rho_{sr} \\ &= \frac{1}{4\sqrt{\pi}(2+3\bar{\rho}_{sd})}\left[\exp\left(-\frac{a\bar{\rho}}{\bar{\rho}_{sr}}\right) - \exp\left(-\frac{b\bar{\rho}}{\bar{\rho}_{sr}}\right)\right] \\ &\doteq \bar{\rho}^{-1}. \end{aligned}$$

Therefore, the diversity order is less than or equal to 1. Combining with the result $E[P_b] \dot{\leq} \bar{\rho}^{-1}$ in Lemma 3, we prove that the diversity order is 1 when $\alpha(|h_{sr}|^2)$ has at least one zero interval. ■

The result is not surprising because if $\alpha(|h_{sr}|^2)$ has zero intervals, the relay node will be shut down with non-zero probability. This means that with a certain probability there is only one path from S to D, and thus, the destination node cannot exploit the cooperative diversity.

Now, suppose that $\alpha(0) = 0$ and $\alpha(|h_{sr}|^2)$ does not have any zero interval. We quantify the diversity G_d enabled by the power-profile design $\alpha(|h_{sr}|^2)$ at the relay node by upper and lower bounding the diversity at the destination node in the following lemmas.

Lemma 5 *For the power-profile design $\alpha(|h_{sr}|^2)$ under* **D1)**, **D2)** *and* **D3)** *with $\alpha(0) = 0$ and no zero interval, we have*

$$E[P_b] \dot{\leq} \bar{\rho}^{-G_d},$$

where $G_d = 1 + \min\{g_1(p_1), g_2(p_{1k}^{(l)}), g_2(p_{1k}^{(r)})\}$.

The proof is provided in the following subsection.

3.3.1 Proof of Lemma 5

When there is no zero interval, i.e., $r_k^{(l)} = r_k^{(r)}$, according to **D1)** and **D3)** in Section 3.2.2 and Lemma 2, $\alpha(|h_{sr}|^2)$ is upper and lower bounded around the origin and its roots, i.e., there exists a constant δ such that

$$\begin{aligned} c_l^o(|h_{sr}|^2)^{p_1} \;\le\; \alpha(|h_{sr}|^2) \le c_u^o(|h_{sr}|^2)^{p_1} \quad \text{for} \quad |h_{sr}|^2 \in [0, \delta], \\ c_l^{kl}(-|h_{sr}|^2 + r_k)^{p_{1k}^{(l)}} \;\le\; \alpha(|h_{sr}|^2) \le c_u^{kl}(-|h_{sr}|^2 + r_k)^{p_{1k}^{(l)}} \quad \text{for} \quad |h_{sr}|^2 \in [(r_k - \delta), r_k], \quad (9) \\ \text{and} \quad c_l^{kr}(|h_{sr}|^2 - r_k)^{p_{1k}^{(r)}} \;\le\; \alpha(|h_{sr}|^2) \le c_u^{kr}(|h_{sr}|^2 - r_k)^{p_{1k}^{(r)}} \quad \text{for} \quad |h_{sr}|^2 \in [r_k, (r_k + \delta)]. \end{aligned}$$

As shown in Lemma 1, the upper bound on the average SER $P_{u1} + P_{u2} + P_{u3}$ is expressed as the integration with respect to ρ_{sr} over the interval $[0, \infty)$. Therefore, we partition the whole integration interval $[0, \infty)$ as

$$L_0 \cup (\cup_{k=1}^N L_{kl}) \cup (\cup_{k=1}^N L_{kr}) \cup L_c,$$

where $L_0 = [0, \delta\bar{\rho}]$, $L_{kl} = [(r_k - \delta)\bar{\rho}, r_k\bar{\rho}]$, $L_{kr} = [r_k\bar{\rho}, (r_k + \delta)\bar{\rho}]$, and L_c denotes the union of the rest intervals. Then, the upper bound on the average SER $E[P_b]$ is expressed as

$$\begin{aligned} E[P_b] \;\le\; & [P_{u1} + P_{u2} + P_{u3}]_{L_0} \\ & + \sum_{k=1}^{N} ([P_{u1} + P_{u2} + P_{u3}]_{L_{kl}} + [P_{u1} + P_{u2} + P_{u3}]_{L_{kr}}) \\ & + [P_{u1} + P_{u2} + P_{u3}]_{L_c}, \end{aligned} \quad (10)$$

where $[P_{u1} + P_{u2} + P_{u3}]_{L_0}$ denotes that the integration interval of $P_{u1} + P_{u2} + P_{u3}$ in Lemma 1 is changed to L_0. Eq. (10) shows that the upper bound on the average SER can be found by integrating over different intervals. In the following subsections, we derive upper bounds for each subinterval, L_0, L_{kl}, L_{kr}, and L_c to obtain an upper bound for $E[P_b]$.

3.3.1.1 The Upper Bound over L_0

From Lemma 1, changing the integration interval of $P_{u1}+P_{u2}+P_{u3}$ to $L_0=[0,\delta\bar{\rho}]$ leads to

$$\begin{aligned}[P_{u1}+P_{u2}+P_{u3}]_{L_0} &\leq \frac{1}{2\bar{\rho}_{sd}\bar{\rho}_{sr}}\int_0^{\delta\bar{\rho}}\frac{\exp(-\frac{\rho_{sr}}{\bar{\rho}_{sr}})}{1+\alpha\bar{\rho}_{rd}}d\rho_{sr}\\ &\quad+\frac{1}{2\bar{\rho}_{sr}}\int_0^{\delta\bar{\rho}}\exp(-\rho_{sr})\left(\frac{1}{2\bar{\rho}_{sd}}+\frac{\pi\sqrt{\alpha\bar{\rho}_{rd}}}{4\bar{\rho}_{sd}}\right)d\rho_{sr}\\ &\quad+\frac{1}{2\bar{\rho}_{sr}}\int_0^{\delta\bar{\rho}}\exp(-\rho_{sr})\frac{\alpha\bar{\rho}_{rd}}{\bar{\rho}_{sd}+\alpha\bar{\rho}_{rd}}d\rho_{sr}. \qquad (11)\end{aligned}$$

Since $c_l^o(\frac{\rho_{sr}}{\bar{\rho}})^{p_1}\leq\alpha(|h_{sr}|^2)\leq c_u^o(\frac{\rho_{sr}}{\bar{\rho}})^{p_1}$ for $\rho_{sr}\in[0,\delta\bar{\rho}]$ from (9), Eq. (11) can be further bounded above as

$$\begin{aligned}[P_{u1}+P_{u2}+P_{u3}]_{L_0} &\leq \frac{1}{2\bar{\rho}_{sd}\bar{\rho}_{sr}}\int_0^{\delta\bar{\rho}}\frac{\exp(-\frac{\rho_{sr}}{\bar{\rho}_{sr}})}{1+c_l^o(\frac{\rho_{sr}}{\bar{\rho}})^{p_1}\bar{\rho}_{rd}}d\rho_{sr}\\ &\quad+\frac{1}{2\bar{\rho}_{sr}}\int_0^{\delta\bar{\rho}}\exp(-\rho_{sr})\left(\frac{1}{2\bar{\rho}_{sd}}+\frac{\pi\sqrt{c_u^o(\frac{\rho_{sr}}{\bar{\rho}})^{p_1}\bar{\rho}_{rd}}}{4\bar{\rho}_{sd}}\right)d\rho_{sr}\\ &\quad+\frac{1}{2\bar{\rho}_{sr}}\int_0^{\delta\bar{\rho}}\exp(-\rho_{sr})\frac{c_u^o(\frac{\rho_{sr}}{\bar{\rho}})^{p_1}\bar{\rho}_{rd}}{\bar{\rho}_{sd}+c_u^o(\frac{\rho_{sr}}{\bar{\rho}})^{p_1}\bar{\rho}_{rd}}d\rho_{sr}\\ &=: P_{u1}^{L_0}+P_{u2}^{L_0}+P_{u3}^{L_0}.\end{aligned}$$

In the following, we derive upper bounds of $P_{u1}^{L_0}$, $P_{u2}^{L_0}$, and $P_{u3}^{L_0}$, respectively.

First, $P_{u1}^{L_0}$ can be simplified and bounded above as

$$\begin{aligned}P_{u1}^{L_0} &= \frac{1}{2\bar{\rho}_{sd}\bar{\rho}_{sr}}\frac{\bar{\rho}^{p_1}}{c_l^o\bar{\rho}_{rd}\bar{\rho}_{sr}^{p_1}}\int_0^{\delta\bar{\rho}}\frac{\exp(-\frac{\rho_{sr}}{\bar{\rho}_{sr}})}{\frac{\bar{\rho}^{p_1}}{c_l^o\bar{\rho}_{rd}\bar{\rho}_{sr}^{p_1}}+(\frac{\rho_{sr}}{\bar{\rho}_{sr}})^{p_1}}d\rho_{sr}\\ &\overset{t=\frac{\rho_{sr}}{\bar{\rho}_{sr}}}{=} \frac{1}{2\bar{\rho}_{sd}}\frac{\bar{\rho}^{p_1}}{c_l^o\bar{\rho}_{rd}\bar{\rho}_{sr}^{p_1}}\int_0^{\delta\frac{\bar{\rho}}{\bar{\rho}_{sr}}}\frac{\exp(-t)}{\frac{\bar{\rho}^{p_1}}{c_l^o\bar{\rho}_{rd}\bar{\rho}_{sr}^{p_1}}+t^{p_1}}dt \qquad (12)\\ &\leq \frac{1}{2\bar{\rho}_{sd}}\frac{\bar{\rho}^{p_1}}{c_l^o\bar{\rho}_{rd}\bar{\rho}_{sr}^{p_1}}\left(\int_0^1\frac{\exp(-t)}{\frac{\bar{\rho}^{p_1}}{c_l^o\bar{\rho}_{rd}\bar{\rho}_{sr}^{p_1}}+t^{p_1}}dt+\int_1^\infty\frac{\exp(-t)}{t^{p_1}}dt\right).\end{aligned}$$

In the last inequality, $P_{u1}^{L_0}$ was bounded above by extending integral interval to $[0,\infty)$.

If $p_1 > 1$, we can derive the upper bound of the first integral as

$$\begin{aligned}
\int_0^1 \frac{\exp(-t)}{\frac{\bar{\rho}^{p_1}}{c_l^o \bar{\rho}_{rd} \bar{\rho}_{sr}^{p_1}} + t^{p_1}} dt &= \frac{c_l^o \bar{\rho}_{rd} \bar{\rho}_{sr}^{p_1}}{\bar{\rho}^{p_1}} \int_0^{\sqrt[p_1]{\frac{c_l^o \bar{\rho}_{rd} \bar{\rho}_{sr}^{p_1}}{\bar{\rho}^{p_1}}}} \frac{\exp\left(-\sqrt[p_1]{\frac{\bar{\rho}^{p_1}}{c_l^o \bar{\rho}_{rd} \bar{\rho}_{sr}^{p_1}}} s\right)}{1+s^{p_1}} \sqrt[p_1]{\frac{\bar{\rho}^{p_1}}{c_l^o \bar{\rho}_{rd} \bar{\rho}_{sr}^{p_1}}} ds \\
&\leq \left(\frac{c_l^o \bar{\rho}_{rd} \bar{\rho}_{sr}^{p_1}}{\bar{\rho}^{p_1}}\right)^{1-\frac{1}{p_1}} \int_0^{\infty} \frac{\exp\left(-\frac{\bar{\rho} s}{(c_l^o \bar{\rho}_{rd})^{1/p_1} \bar{\rho}_{sr}}\right)}{1+s^{p_1}} ds \\
&\leq \left(\frac{c_l^o \bar{\rho}_{rd} \bar{\rho}_{sr}^{p_1}}{\bar{\rho}^{p_1}}\right)^{1-\frac{1}{p_1}} \left(\int_0^1 1 \, ds + \int_1^{\infty} \frac{1}{s^{p_1}} ds\right) \\
&\leq \left(\frac{c_l^o \bar{\rho}_{rd} \bar{\rho}_{sr}^{p_1}}{\bar{\rho}^{p_1}}\right)^{1-\frac{1}{p_1}} \left(1 + \frac{1}{p_1 - 1}\right),
\end{aligned}$$

where we have substituted $s = \left(\frac{\bar{\rho}}{(c_l^o \bar{\rho}_{rd})^{1/p_1} \bar{\rho}_{sr}}\right)^{-1} t$ in the first equality, and used $\exp(-s) \leq 1$ for $s \geq 0$ in the second inequality. Since the second integral $\int_1^{\infty} e^{-t} t^{-p_1} dt$ is finite, we can show that

$$P_{u1}^{L_0} \dot{\leq} \bar{\rho}^{-(1+\frac{1}{p_1})}.$$

Now we find the upper bound of $P_{u1}^{L_0}$ when $0 < p_1 \leq 1$. The integration interval of t from Eq. (12) is $[0, \frac{\delta \bar{\rho}}{\bar{\rho}_{sr}}]$. Since $t^{p_1 - 1}$ is a decreasing function in this interval, we have the inequality $t^{p_1-1} \geq (\frac{\delta \bar{\rho}}{\bar{\rho}_{sr}})^{p_1-1}$, and use this to bound $P_{u1}^{L_0}$ above in Eq. (12) as follows:

$$\begin{aligned}
P_{u1}^{L_0} &\leq \frac{1}{2\bar{\rho}_{sd}} \frac{\bar{\rho}^{p_1}}{c_l^o \bar{\rho}_{rd} \bar{\rho}_{sr}^{p_1}} \int_0^{\delta \frac{\bar{\rho}}{\bar{\rho}_{sr}}} \frac{\exp(-t)}{\frac{\bar{\rho}^{p_1}}{c_l^o \bar{\rho}_{rd} \bar{\rho}_{sr}^{p_1}} + \left(\frac{\delta \bar{\rho}}{\bar{\rho}_{sr}}\right)^{p_1-1} t} dt \\
&\overset{s = \frac{\bar{\rho}}{c_l^o \bar{\rho}_{rd} \bar{\rho}_{sr} \delta^{p_1-1}} + t}{=} \frac{1}{2\bar{\rho}_{sd}} \frac{\bar{\rho}}{c_l^o \bar{\rho}_{rd} \bar{\rho}_{sr} \delta^{p_1-1}} \exp\left(\frac{\bar{\rho}}{c_l^o \bar{\rho}_{rd} \bar{\rho}_{sr} \delta^{p_1-1}}\right) \int_{\frac{\bar{\rho}}{c_l^o \bar{\rho}_{rd} \bar{\rho}_{sr} \delta^{p_1-1}}}^{\frac{\bar{\rho}}{c_l^o \bar{\rho}_{rd} \bar{\rho}_{sr} \delta^{p_1-1}} + \delta \frac{\bar{\rho}}{\bar{\rho}_{sr}}} \frac{\exp(-s)}{s} ds \\
&\leq \frac{1}{2\bar{\rho}_{sd}} \frac{\bar{\rho}}{c_l^o \bar{\rho}_{rd} \bar{\rho}_{sr} \delta^{p_1-1}} \exp\left(\frac{\bar{\rho}}{c_l^o \bar{\rho}_{rd} \bar{\rho}_{sr} \delta^{p_1-1}}\right) E_1\left(\frac{\bar{\rho}}{c_l^o \bar{\rho}_{rd} \bar{\rho}_{sr} \delta^{p_1-1}}\right) \\
&\leq \frac{1}{2\bar{\rho}_{sd}} \frac{\bar{\rho}}{c_l^o \bar{\rho}_{rd} \bar{\rho}_{sr} \delta^{p_1-1}} \ln\left(1 + \frac{c_l^o \bar{\rho}_{rd} \bar{\rho}_{sr} \delta^{p_1-1}}{\bar{\rho}}\right) \\
&\doteq \bar{\rho}^{-2},
\end{aligned}$$

where $E_n(x) = \int_1^{\infty} \exp(-xt)/t^n dt$ and the last inequality comes from $e^x E_1(x) \leq \ln(1 + \frac{1}{x})$ for all $x > 0$ [6, Eq. (5.1.20)]. Thus, considering both cases $p_1 > 1$ and

$0 < p_1 \leq 1$, we can show that

$$P_{u1}^{L_0} \doteq \bar{\rho}^{-\min(2,1+\frac{1}{p_1})}, \quad \forall p_1 > 0. \tag{13}$$

For $P_{u2}^{L_0}$ and $P_{u3}^{L_0}$, we have bounded them above as

$$\begin{aligned} P_{u2}^{L_0} &\leq \frac{1}{4\bar{\rho}_{sr}\bar{\rho}_{sd}} + \frac{\pi}{8\bar{\rho}_{sd}\bar{\rho}_{sr}}\int_0^\infty \exp(-\rho_{sr})\sqrt{c_u^o\left(\frac{\rho_{sr}}{\bar{\rho}}\right)^{p_1}\bar{\rho}_{rd}}d\rho_{sr} \\ &= \frac{1}{4\bar{\rho}_{sr}\bar{\rho}_{sd}} + \frac{\pi}{8\bar{\rho}_{sd}\bar{\rho}_{sr}}\sqrt{c_u^o\frac{\bar{\rho}_{rd}}{\bar{\rho}^{p_1}}}\Gamma\left(\frac{p_1}{2}+1\right) \\ &\doteq \bar{\rho}^{-\min(2,\frac{3}{2}+\frac{p_1}{2})}, \end{aligned} \tag{14}$$

and

$$\begin{aligned} P_{u3}^{L_0} &\leq \frac{1}{2\bar{\rho}_{sr}}\int_0^\infty \exp(-\rho_{sr})\frac{c_u^o(\frac{\rho_{sr}}{\bar{\rho}})^{p_1}\bar{\rho}_{rd}}{\bar{\rho}_{sd}}d\rho_{sr} \\ &= \frac{c_u^o\bar{\rho}_{rd}}{2\bar{\rho}_{sr}\bar{\rho}_{sd}\bar{\rho}^{p_1}}\Gamma(p_1+1) \\ &\doteq \bar{\rho}^{-(1+p_1)}, \end{aligned} \tag{15}$$

where $\Gamma(z) = \int_0^\infty t^{z-1}\exp(-t)dt$. Therefore, summarizing Eqs. (13)-(15) with the function $g_1(\cdot)$ in Definition 2, we conclude that the upper bound over L_0 is

$$[P_{u1} + P_{u2} + P_{u3}]_{L_0} \doteq \bar{\rho}^{-(1+g_1(p_1))}, \tag{16}$$

since the diversity order is dominated by the term with the lowest absolute exponent.

3.3.1.2 The Upper Bound over L_{kl}

When ρ_{sr} belongs to the left margin intervals at nonzero roots, L_{kl}'s, we have

$$c_l^{kl}(-|h_{sr}|^2 + r_k)^{p_{1k}^{(l)}} \leq \alpha(|h_{sr}|^2) \leq c_u^{kl}(-|h_{sr}|^2 + r_k)^{p_{1k}^{(l)}}$$

from (9). Plugging this inequality into Eq. (11) and change the integration interval to L_{kl}, we obtain

$$\begin{aligned}
[P_{u1}+P_{u2}+P_{u3}]_{L_{kl}} \leq & \frac{1}{2\bar{\rho}_{sd}\bar{\rho}_{sr}}\int_{(r_k-\delta)\bar{\rho}}^{r_k\bar{\rho}} \frac{\exp(-\frac{\rho_{sr}}{\bar{\rho}_{sr}})}{1+c_l^{kl}(-\frac{\rho_{sr}}{\bar{\rho}}+r_k)^{p_{1k}^{(l)}}\bar{\rho}_{rd}} d\rho_{sr} \\
& + \frac{1}{2\bar{\rho}_{sr}}\int_{(r_k-\delta)\bar{\rho}}^{r_k\bar{\rho}} \exp(-\rho_{sr}) \left(\frac{1}{2\bar{\rho}_{sd}} + \frac{\pi\sqrt{c_u^{kl}(-\frac{\rho_{sr}}{\bar{\rho}}+r_k)^{p_{1k}^{(l)}}\bar{\rho}_{rd}}}{4\bar{\rho}_{sd}} \right) d\rho_{sr} \\
& + \frac{1}{2\bar{\rho}_{sr}}\int_{(r_k-\delta)\bar{\rho}}^{r_k\bar{\rho}} \exp(-\rho_{sr}) \frac{c_u^{kl}(-\frac{\rho_{sr}}{\bar{\rho}}+r_k)^{p_{1k}^{(l)}}\bar{\rho}_{rd}}{\bar{\rho}_{sd}+c_u^{kl}(-\frac{\rho_{sr}}{\bar{\rho}}+r_k)^{p_{1k}^{(l)}}\bar{\rho}_{rd}} d\rho_{sr} \\
=: & \ P_{u1}^{L_{kl}}+P_{u2}^{L_{kl}}+P_{u3}^{L_{kl}}. \qquad (17)
\end{aligned}$$

Similar to the derivation of the upper bound over L_0, we will derive the upper bounds of $P_{u1}^{L_{kl}}$, $P_{u2}^{L_{kl}}$, and $P_{u3}^{L_{kl}}$, respectively.

$P_{u1}^{L_{kl}}$ in Eq. (17) can be expressed as

$$P_{u1}^{L_{kl}} \overset{t=\frac{(r_k\bar{\rho}-\rho_{sr})}{\bar{\rho}_{sr}}}{=} \frac{\exp(-\frac{r_k\bar{\rho}}{\bar{\rho}_{sr}})}{2\bar{\rho}_{sd}} \frac{\bar{\rho}^{p_{1k}^{(l)}}}{c_l^{kl}\bar{\rho}_{rd}\bar{\rho}_{sr}^{p_{1k}^{(l)}}} \int_0^{\delta\frac{\bar{\rho}}{\bar{\rho}_{sr}}} \frac{\exp(t)}{\frac{\bar{\rho}^{p_{1k}^{(l)}}}{c_l^{kl}\bar{\rho}_{rd}\bar{\rho}_{sr}^{p_{1k}^{(l)}}}+t^{p_{1k}^{(l)}}} dt.$$

Using $\exp(-x)\leq 1$ for $x\geq 0$ and $\exp(t)\leq\exp(\frac{2\delta\bar{\rho}}{\bar{\rho}_{sr}}-t)$ for $0\leq t\leq\frac{\delta\bar{\rho}}{\bar{\rho}_{sr}}$, we bound it above as

$$P_{u1}^{L_{kl}} \leq \frac{1}{2\bar{\rho}_{sd}} \frac{\bar{\rho}^{p_{1k}^{(l)}}}{c_l^{kl}\bar{\rho}_{rd}\bar{\rho}_{sr}^{p_{1k}^{(l)}}} \exp\left(\frac{2\delta\bar{\rho}}{\bar{\rho}_{sr}}\right) \int_0^{\delta\frac{\bar{\rho}}{\bar{\rho}_{sr}}} \frac{\exp(-t)}{\frac{\bar{\rho}^{p_{1k}^{(l)}}}{c_l^{kl}\bar{\rho}_{rd}\bar{\rho}_{sr}^{p_{1k}^{(l)}}}+t^{p_{1k}^{(l)}}} dt. \qquad (18)$$

It can be seen that the upper bound of Eq. (18) can be derived similarly as that of Eq. (12), and we have the following result analogous to Eq. (13).

$$P_{u1}^{L_{kl}} \dot{\leq} \bar{\rho}^{-\min(2,1+\frac{1}{p_{1k}^{(l)}})}. \qquad (19)$$

We can also bound $P_{u2}^{L_{kl}}$ and $P_{u3}^{L_{kl}}$ as

$$\begin{aligned}
P_{u2}^{L_{kl}} & \leq \frac{1}{4\bar{\rho}_{sr}\bar{\rho}_{sd}} + \frac{\pi}{8\bar{\rho}_{sr}\bar{\rho}_{sd}}\sqrt{c_u^{kl}\frac{\bar{\rho}_{rd}}{\bar{\rho}^{p_{1k}^{(l)}}}} \int_{(r_k-\delta)\bar{\rho}}^{r_k\bar{\rho}} (\delta\bar{\rho})^{\frac{p_{1k}^{(l)}}{2}} \exp(-\rho_{sr}) d\rho_{sr} \\
& \leq \frac{1}{4\bar{\rho}_{sr}\bar{\rho}_{sd}} + \frac{\pi}{8\bar{\rho}_{sr}\bar{\rho}_{sd}}\sqrt{c_u^{kl}\bar{\rho}_{rd}}\delta^{\frac{p_{1k}^{(l)}}{2}} \exp\left[-(r_k-\delta)\bar{\rho}\right] \\
& \doteq \bar{\rho}^{-2}, \qquad (20)
\end{aligned}$$

and

$$\begin{aligned} P_{u3}^{L_{kl}} &\leq \frac{1}{2\bar{\rho}_{sr}} \int_{(r_k-\delta)\bar{\rho}}^{r_k\bar{\rho}} \exp(-\rho_{sr}) d\rho_{sr} \\ &\leq \frac{1}{2\bar{\rho}_{sr}} \exp\left[-(r_k-\delta)\bar{\rho}\right] \\ &\dot{\leq} \bar{\rho}^{-2}, \end{aligned} \tag{21}$$

where the inequality $(r_k - \delta)\bar{\rho} \leq \rho_{sr}$ was used to derive the upper bound for $P_{u2}^{L_{kl}}$. Combining Eqs. (19)-(21), with the function $g_2(\cdot)$ in Definition 2, we conclude that the upper bound over L_{kl} is

$$[P_{u1} + P_{u2} + P_{u3}]_{L_{kl}} \dot{\leq} \bar{\rho}^{-(1+g_2(p_{1k}^{(l)}))}. \tag{22}$$

3.3.1.3 The Upper Bound over L_{kr}

When ρ_{sr} belongs to L_{kl}, we have upper and lower bounds of $\alpha(|h_{sr}|^2)$ from (9) as

$$c_l^{kr}(|h_{sr}|^2 - r_k)^{p_{1k}^{(r)}} \leq \alpha(|h_{sr}|^2) \leq c_u^{kr}(|h_{sr}|^2 - r_k)^{p_{1k}^{(r)}}.$$

We change the integration interval of the upper bound in Lemma 1 to L_{kr} and use above bounds to obtain

$$\begin{aligned} [P_{u1} + P_{u2} + P_{u3}]_{L_{kr}} \leq\ & \frac{1}{2\bar{\rho}_{sd}\bar{\rho}_{sr}} \int_{r_k\bar{\rho}}^{(r_k+\delta)\bar{\rho}} \frac{\exp(-\frac{\rho_{sr}}{\bar{\rho}_{sr}})}{1 + c_l^{kr}(\frac{\rho_{sr}}{\bar{\rho}} - r_k)^{p_{1k}^r}\bar{\rho}_{rd}} d\rho_{sr} \\ & + \frac{1}{2\bar{\rho}_{sr}} \int_{r_k\bar{\rho}}^{(r_k+\delta)\bar{\rho}} \exp(-\rho_{sr}) \left(\frac{1}{2\bar{\rho}_{sd}} + \frac{\pi\sqrt{c_u^{kr}(\frac{\rho_{sr}}{\bar{\rho}} - r_k)^{p_{1k}^{(r)}}\bar{\rho}_{rd}}}{4\bar{\rho}_{sd}} \right) d\rho_{sr} \\ & + \frac{1}{2\bar{\rho}_{sr}} \int_{r_k\bar{\rho}}^{(r_k+\delta)\bar{\rho}} \exp(-\rho_{sr}) \frac{c_u^{kr}(\frac{\rho_{sr}}{\bar{\rho}} - r_k)^{p_{1k}^{(r)}}\bar{\rho}_{rd}}{\bar{\rho}_{sd} + c_u^{kr}(\frac{\rho_{sr}}{\bar{\rho}} - r_k)^{p_{1k}^{(r)}}\bar{\rho}_{rd}} d\rho_{sr} \\ =:\ & P_{u1}^{L_{kr}} + P_{u2}^{L_{kr}} + P_{u3}^{L_{kr}}. \end{aligned} \tag{23}$$

In the following, we will derive the upper bounds of $P_{u1}^{L_{kl}}$, $P_{u2}^{L_{kl}}$, and $P_{u3}^{L_{kl}}$, respectively. First, $P_{u1}^{L_{kr}}$ can be expressed and bounded above as

$$\begin{aligned} P_{u1}^{L_{kr}} &\overset{\rho'=\rho_{sr}-r_k\bar{\rho}}{=} \frac{\exp(-\frac{r_k\bar{\rho}}{\bar{\rho}_{sr}})}{2\bar{\rho}_{sd}\bar{\rho}_{sr}} \frac{\bar{\rho}^{p_{1k}^{(r)}}}{c_l^{kr}\bar{\rho}_{rd}\bar{\rho}_{sr}^{p_{1k}^{(r)}}} \int_0^{\delta\bar{\rho}} \frac{\exp(-\frac{\rho'}{\bar{\rho}_{sr}})}{\frac{\bar{\rho}^{p_{1k}^{(r)}}}{c_l^{kr}\bar{\rho}_{rd}\bar{\rho}_{sr}^{p_{1k}^{(r)}}} + (\frac{\rho'}{\bar{\rho}_{sr}})^{p_{1k}^{(r)}}} d\rho' \\ &\overset{t=\frac{\rho'}{\bar{\rho}_{sr}}}{=} \frac{\exp(-\frac{r_k\bar{\rho}}{\bar{\rho}_{sr}})}{2\bar{\rho}_{sd}} \frac{\bar{\rho}^{p_{1k}^{(r)}}}{c_l^{kr}\bar{\rho}_{rd}\bar{\rho}_{sr}^{p_{1k}^{(r)}}} \int_0^{\delta\frac{\bar{\rho}}{\bar{\rho}_{sr}}} \frac{\exp(-t)}{\frac{\bar{\rho}^{p_{1k}^{(r)}}}{c_l^{kr}\bar{\rho}_{rd}\bar{\rho}_{sr}^{p_{1k}^{(r)}}} + t^{p_{1k}^{(r)}}} d\rho' \\ &\dot{\leq} \quad \bar{\rho}^{-\min(2,1+\frac{1}{p_{1k}^{(r)}})}, \end{aligned} \tag{24}$$

where the upper bound Eq. (24) can be obtained by following the similar procedure of bounding Eq. (12) above to get Eq. (13). For $P_{u2}^{L_{kr}}$ and $P_{u3}^{L_{kr}}$, we have

$$\begin{aligned} P_{u2}^{L_{kr}} &\leq \frac{1}{4\bar{\rho}_{sr}\bar{\rho}_{sd}} + \frac{\pi}{8\bar{\rho}_{sr}\bar{\rho}_{sd}} \sqrt{c_u^{kr}\frac{\bar{\rho}_{rd}}{\bar{\rho}^{p_{1k}^{(r)}}}} \int_{r_k\bar{\rho}}^{(r_k+\delta)\bar{\rho}} (\delta\bar{\rho})^{\frac{p_{1k}^{(r)}}{2}} \exp(-\rho_{sr}) d\rho_{sr} \\ &\leq \frac{1}{4\bar{\rho}_{sr}\bar{\rho}_{sd}} + \frac{\pi}{8\bar{\rho}_{sr}\bar{\rho}_{sd}} \sqrt{c_u^{kr}\bar{\rho}_{rd}}\delta^{\frac{p_{1k}^{(r)}}{2}} \exp(-r_k\bar{\rho}) \\ &\doteq \bar{\rho}^{-2}, \end{aligned} \tag{25}$$

and

$$\begin{aligned} P_{u3}^{L_{kr}} &\leq \frac{1}{2\bar{\rho}_{sr}} \int_{r_k\bar{\rho}}^{(r_k+\delta)\bar{\rho}} \exp(-\rho_{sr}) d\rho_{sr} \\ &\leq \frac{1}{2\bar{\rho}_{sr}} \exp(-r_k\bar{\rho}) \\ &\dot{\leq} \bar{\rho}^{-2}, \end{aligned} \tag{26}$$

where the inequality $r_k\bar{\rho} \leq \rho_{sr}$ was used to derive the upper bound for $P_{u2}^{L_{kr}}$. Combining Eqs. (23)-(26), we conclude that

$$[P_{u1} + P_{u2} + P_{u3}]_{L_{kr}} \dot{\leq} \bar{\rho}^{-(1+g_2(p_{1k}^{(r)}))}. \tag{27}$$

3.3.1.4 The Upper Bound over L_c

Since there are $N+1$ roots including the origin, L_c consists of N bounded intervals and one unbounded interval. For k^{th} bounded interval $L_{ck} = [(r_{k-1}+\delta)\bar{\rho}, (r_k-\delta)\bar{\rho}]$,

$\alpha(|h_{sr}|^2)$ has a lower bound C' and we have

$$\begin{aligned}
[P_{u1}+P_{u2}+P_{u3}]_{L_{ck}} &\leq \frac{1}{2\bar{\rho}_{sd}\bar{\rho}_{sr}}\int_0^{\infty}\frac{\exp(-\frac{\rho_{sr}}{\bar{\rho}_{sr}})}{1+C'\bar{\rho}_{rd}}d\rho_{sr} \\
&\quad +\frac{1}{2\bar{\rho}_{sr}}\int_{(r_{k-1}+\delta)\bar{\rho}}^{\infty}\exp(-\rho_{sr})\left\{\frac{1}{2\bar{\rho}_{sd}}+\frac{\pi\sqrt{\bar{\rho}_{sd}}}{4C'\bar{\rho}_{rd}}\right\}d\rho_{sr} \\
&\quad +\frac{1}{2\bar{\rho}_{sr}}\int_{(r_{k-1}+\delta)\bar{\rho}}^{\infty}\exp(-\rho_{sr})d\rho_{sr} \\
&= \frac{1}{2\bar{\rho}_{sd}}\frac{1}{1+C'\bar{\rho}_{rd}} \\
&\quad +\left(\frac{1}{4\bar{\rho}_{sr}\bar{\rho}_{sd}}+\frac{\pi\sqrt{\bar{\rho}_{sd}}}{8C'\bar{\rho}_{rd}\bar{\rho}_{sr}}+\frac{1}{2\bar{\rho}_{sr}}\right)\exp\left[-(r_{k-1}+\delta)\bar{\rho}\right] \\
&\doteq \bar{\rho}^{-2}.
\end{aligned}$$

For the unbounded interval $L_{c(N+1)}=[(r_N+\delta)\bar{\rho},\infty)$, if $\alpha(|h_{sr}|^2)$ has a lower bound, similar procedures can be applied to obtain the same result as above. If $\alpha(|h_{sr}|^2)$ does not have a lower bound and strictly decreasing, i.e., $\alpha(|h_{sr}|^2)=(1/|h_{sr}|^2)^d$ for $d>0$,

$$\begin{aligned}
[P_{u1}+P_{u2}+P_{u3}]_{L_{c(N+1)}} &\leq \frac{1}{2\bar{\rho}_{sd}\bar{\rho}_{sr}}\int_0^{\infty}\frac{\rho_{sr}^d\exp(-\frac{\rho_{sr}}{\bar{\rho}_{sr}})}{\bar{\rho}_{sr}^d\bar{\rho}_{rd}}d\rho_{sr} \\
&\quad +\frac{1}{2\bar{\rho}_{sr}}\int_{(r_N+\delta)\bar{\rho}}^{\infty}\exp(-\rho_{sr})\left\{\frac{1}{2\bar{\rho}_{sd}}+\frac{\pi\sqrt{(\frac{\bar{\rho}_{rd}}{\rho_{sr}})^d\bar{\rho}_{rd}}}{4\bar{\rho}_{sd}}\right\}d\rho_{sr} \\
&\quad +\frac{1}{2\bar{\rho}_{sr}}\int_{(r_N+\delta)\bar{\rho}}^{\infty}\exp(-\rho_{sr})d\rho_{sr} \\
&\doteq \bar{\rho}^{-2}.
\end{aligned}$$

Thus, we obtain that

$$[P_{u1}+P_{u2}+P_{u3}]_{L_c}=\sum_{k=1}^{N+1}[P_{u1}+P_{u2}+P_{u3}]_{L_{ck}} \;\dot{\leq}\; \bar{\rho}^{-2}. \tag{28}$$

Combining Eqs. (10), (16), (22), (27), and (28), we have shown that

$$E[P_b] \;\dot{\leq}\; \bar{\rho}^{-G_d},$$

where

$$G_d=1+\min\{g_1(p_1),g_2(p_{1k}^{(l)}),g_2(p_{1k}^{(r)})\}. \;\blacksquare$$

Next, we provide upper bound of the diversity and its proof in the following when $\alpha(0) = 0$ and it has no zero interval.

Lemma 6 *For the power-profile design* $\alpha(|h_{sr}|^2)$ *under* **D1)**, **D2)** *and* **D3)** *with* $\alpha(0) = 0$ *and no zero interval, we have*

$$E[P_b] \dot{\geq} \bar{\rho}^{-G_d},$$

where $G_d = 1 + \min\{g_1(p_1), g_2(p_{1k}^{(l)}), g_2(p_{1k}^{(r)})\}$.

3.3.2 Proof of Lemma 6

As shown in Lemma 1, the lower bound $P_{l1} + P_{l2}$ is expressed as the integration with respect to ρ_{sr} over $[0, \infty)$. Similarly, we partition the integration interval $[0, \infty)$ as

$$L_0 \cup (\cup_{k=1}^{N} L_{kl}) \cup (\cup_{k=1}^{N} L_{kr}) \cup L_c$$

as in Lemma 5. Therefore, the lower bound of $E[P_b]$ is expressed as

$$E[P_b] \;\geq\; [P_{l1} + P_{l2}]_{L_0} + \sum_{k=1}^{N} \left([P_{l1} + P_{l2}]_{L_{kl}} + [P_{l1} + P_{l2}]_{L_{kr}} \right), \tag{29}$$

where we have ignored the interval L_c. In the following subsections, we find the lower bound of $E[P_b]$ for each subinterval, L_0, L_{kl}, and L_{kr}.

3.3.2.1 The Lower Bound over L_0

If $\rho_{sr} \in [0, \delta\bar{\rho}]$, we have

$$c_l^o(|h_{sr}|^2)^{p_1} \leq \alpha(|h_{sr}|^2) \leq c_u^o(|h_{sr}|^2)^{p_1}$$

from (9). Therefore, by plugging this inequality into Lemma 1, the lower bound over L_0 can be further relaxed as

$$\begin{aligned}
[P_{l1} + P_{l2}]_{L_0} \;\geq\; & \frac{1}{4\sqrt{\pi}\bar{\rho}_{sr}(2 + 3\bar{\rho}_{sd})} \int_0^{\delta\bar{\rho}} \frac{\exp(-\frac{\rho_{sr}}{\bar{\rho}_{sr}})}{1 + c_u^o(\frac{\rho_{sr}}{\bar{\rho}})^{p_1}\bar{\rho}_{rd}} d\rho_{sr} \\
& + \frac{1}{4\sqrt{\pi}\bar{\rho}_{sr}} \int_0^{\delta\bar{\rho}} \frac{c_l^o(\frac{\rho_{sr}}{\bar{\rho}})^{p_1}\bar{\rho}_{rd}}{\bar{\rho}_{sd} + c_l^o(\frac{\rho_{sr}}{\bar{\rho}})^{p_1}\bar{\rho}_{rd}} \frac{\exp(-\rho_{sr} - \frac{\rho_{sr}}{\bar{\rho}_{sr}})}{\sqrt{\rho_{sr} + 2}} d\rho_{sr} \\
=:\; & P_{l1}^{L_0} + P_{l2}^{L_0}.
\end{aligned}$$

To further simplify the lower bound $[P_{l1}+P_{l2}]_{L_0}$, we will analyze based on the value of p_1 as we did for $P_{u1}^{L_0}$ in Lemma 5. If $0<p_1\leq 1$, the lower bound over L_0 is relaxed as

$$\begin{aligned}
[P_{l1}+P_{l2}]_{L_0} &\geq P_{l2}^{L_0} \\
&\overset{\bar{\rho}\text{ is large}}{\geq} \frac{1}{4\sqrt{\pi}\bar{\rho}_{sr}}\int_0^1 \frac{c_l^o(\frac{\rho_{sr}}{\bar{\rho}})^{p_1}\bar{\rho}_{rd}}{\bar{\rho}_{sd}+c_l^o(\frac{\rho_{sr}}{\bar{\rho}})^{p_1}\bar{\rho}_{rd}}\frac{\exp(-\rho_{sr}-\frac{\rho_{sr}}{\bar{\rho}_{sr}})}{\sqrt{\rho_{sr}+2}}d\rho_{sr} \\
&\geq \frac{c_l^o\bar{\rho}_{rd}}{4\sqrt{3\pi}\bar{\rho}_{sr}}\int_0^1 \frac{\rho_{sr}}{\bar{\rho}_{sd}\bar{\rho}^{p_1}+c_l^o\bar{\rho}_{rd}}\exp\left(-\rho_{sr}-\frac{\rho_{sr}}{\bar{\rho}_{sr}}\right)d\rho_{sr} \\
&\overset{t=\rho_{sr}(1+\frac{1}{\bar{\rho}_{sr}})}{=} \frac{c_l^o\bar{\rho}_{rd}}{4\sqrt{3\pi}\bar{\rho}_{sr}(\bar{\rho}_{sd}\bar{\rho}^{p_1}+c_l^o\bar{\rho}_{rd})}\left(\frac{\bar{\rho}_{sr}}{1+\bar{\rho}_{sr}}\right)^2\int_0^1 t\exp(-t)dt \\
&\doteq \bar{\rho}^{-(1+p_1)}, \qquad (30)
\end{aligned}$$

where we have assumed $\delta\bar{\rho}>1$ when $\bar{\rho}$ is large enough to obtain the second inequality. For the last inequality, $\rho_{sr}\leq\rho_{sr}^{p_1}\leq 1$ for $0\leq\rho_{sr}\leq 1$ and $0<p_1\leq 1$ was used. On the other hand, if $p_1>1$, the lower bound is relaxed as

$$\begin{aligned}
[P_{l1}+P_{l2}]_{L_0} &\geq P_{l1}^{L_0} \\
&\overset{s=(c_u^o\bar{\rho}_{rd})^{\frac{1}{p_1}}\frac{\rho_{sr}}{\bar{\rho}}}{=} \frac{1}{4\sqrt{\pi}(2+3\bar{\rho}_{sd})}\sqrt[p_1]{\frac{\bar{\rho}^{p_1}}{c_u^o\bar{\rho}_{rd}\bar{\rho}_{sr}^{p_1}}}\int_0^{\delta\sqrt[p_1]{c_u^o\bar{\rho}_{rd}}}\frac{\exp\left(-\sqrt[p_1]{\frac{\bar{\rho}^{p_1}}{c_u^o\bar{\rho}_{rd}\bar{\rho}_{sr}^{p_1}}}s\right)}{1+s^{p_1}}ds \\
&\overset{\bar{\rho}\text{ is large}}{\geq} \frac{1}{4\sqrt{\pi}(2+3\bar{\rho}_{sd})}\sqrt[p_1]{\frac{\bar{\rho}^{p_1}}{c_u^o\bar{\rho}_{rd}\bar{\rho}_{sr}^{p_1}}}\int_0^1\frac{\exp\left(-\sqrt[p_1]{\frac{\bar{\rho}^{p_1}}{c_u^o\bar{\rho}_{rd}\bar{\rho}_{sr}^{p_1}}}s\right)}{1+s^{p_1}}ds \\
&\geq \frac{1}{8\sqrt{\pi}(2+3\bar{\rho}_{sd})}\sqrt[p_1]{\frac{\bar{\rho}^{p_1}}{c_u^o\bar{\rho}_{rd}\bar{\rho}_{sr}^{p_1}}}\int_0^1\exp\left(-\sqrt[p_1]{\frac{\bar{\rho}^{p_1}}{c_u^o\bar{\rho}_{rd}\bar{\rho}_{sr}^{p_1}}}s\right)ds \\
&= \frac{1}{8\sqrt{\pi}(2+3\bar{\rho}_{sd})}\left[1-\exp\left(-\sqrt[p_1]{\frac{\bar{\rho}^{p_1}}{c_u^o\bar{\rho}_{rd}\bar{\rho}_{sr}^{p_1}}}\right)\right] \\
&\doteq \bar{\rho}^{-(1+\frac{1}{p_1})}, \qquad (31)
\end{aligned}$$

where the second inequality is obtained by assuming $\delta(c_u^o\bar{\rho}_{rd})^{\frac{1}{p_1}}>1$ when $\bar{\rho}$ is large enough. Therefore, based on Eqs. (30) and (31), the lower bound over L_0 is relaxed as

$$[P_{l1}+P_{l2}]_{L_0} \;\dot{\geq}\; \bar{\rho}^{-(1+g_1(p_1))}. \qquad (32)$$

3.3.2.2 The Lower Bound over L_{kl}'s

When ρ_{sr} belongs to L_{kl}, we have upper and lower bounds of $\alpha(|h_{sr}|^2)$ as

$$c_l^{kl}(-|h_{sr}|^2+r_k)^{p_{1k}^{(l)}} \le \alpha(|h_{sr}|^2) \le c_u^{kl}(-|h_{sr}|^2+r_k)^{p_{1k}^{(l)}}$$

from (9). Plugging it into the expression of P_{l1} in Lemma 1 and changing the integration interval to L_{kl} yield the lower bound as

$$\begin{aligned}
[P_{l1}+P_{l2}]_{L_{kl}} &\ge [P_{l1}]_{L_{kl}} \\
&\ge \frac{1}{4\sqrt{\pi}\bar{\rho}_{sr}(2+3\bar{\rho}_{sd})}\int_{(r_k-\delta)\bar{\rho}}^{r_k\bar{\rho}} \frac{\exp(-\frac{\rho_{sr}}{\bar{\rho}_{sr}})}{1+c_u^{kl}(-\frac{\rho_{sr}}{\bar{\rho}}+r_k)^{p_{1k}^{(l)}}\bar{\rho}_{rd}}d\rho_{sr} \\
&=: P_{l1}^{L_{kl}}. \qquad (33)
\end{aligned}$$

Since $\exp(-t) \le \exp(t)$ for $0 \le t \le \frac{\delta\bar{\rho}}{\bar{\rho}_{sr}}$, the lower bound of $P_{l1}^{L_{kl}}$ is relaxed as

$$\begin{aligned}
P_{l1}^{L_{kl}} &\overset{t=\frac{r_k\bar{\rho}-\rho_{sr}}{\bar{\rho}_{sr}}}{=} \frac{\exp(-\frac{r_k\bar{\rho}}{\bar{\rho}_{sr}})}{4\sqrt{\pi}(2+3\bar{\rho}_{sd})}\int_0^{\delta\frac{\bar{\rho}}{\bar{\rho}_{sr}}} \frac{\exp(t)}{1+c_u^{kl}(\frac{\bar{\rho}_{sr}}{\bar{\rho}}t)^{p_{1k}^{(l)}}\bar{\rho}_{rd}}dt \\
&\ge \frac{\exp(-\frac{r_k\bar{\rho}}{\bar{\rho}_{sr}})}{4\sqrt{\pi}(2+3\bar{\rho}_{sd})}\int_0^{\delta\frac{\bar{\rho}}{\bar{\rho}_{sr}}} \frac{\exp(-t)}{1+c_u^{kl}(\frac{\bar{\rho}_{sr}}{\bar{\rho}}t)^{p_{1k}^{(l)}}\bar{\rho}_{rd}}dt. \qquad (34)
\end{aligned}$$

We substitute t in Eq. (34) with $s = \sqrt[p_{1k}^{(l)}]{c_u^{kl}\bar{\rho}_{rd}}\frac{\bar{\rho}_{sr}}{\bar{\rho}}t$ and follow the same procedures as in (31) to obtain the lower bound as

$$\begin{aligned}
P_{l1}^{L_{kl}} &\ge \frac{\exp(-\frac{r_k\bar{\rho}}{\bar{\rho}_{sr}})}{4\sqrt{\pi}(2+3\bar{\rho}_{sd})}\sqrt[p_{1k}^{(l)}]{\frac{\bar{\rho}^{p_{1k}^{(l)}}}{c_u^{kl}\bar{\rho}_{rd}\bar{\rho}_{sr}^{p_{1k}^{(l)}}}}\int_0^{\delta\sqrt[p_{1k}^{(l)}]{c_u^{kl}\bar{\rho}_{rd}}} \frac{\exp\left(-\sqrt[p_{1k}^{(l)}]{\frac{\bar{\rho}^{p_{1k}^{(l)}}}{c_u^{kl}\bar{\rho}_{rd}\bar{\rho}_{sr}^{p_{1k}^{(l)}}}}s\right)}{1+s^{p_{1k}^{(l)}}}ds \\
&\dot{\ge} \bar{\rho}^{-\left(1+\frac{1}{p_{1k}^{(l)}}\right)}, \qquad (35)
\end{aligned}$$

since the lower bound in the first line of (35) and $P_{l1}^{L_0}$ in (31) have the same form except for a constant term. Thus, combining Eqs. (33) and (35), the lower bound over L_{kl} is relaxed as

$$[P_{l1}+P_{l2}]_{L_{kl}} \dot{\ge} \bar{\rho}^{-\left(1+\frac{1}{p_{1k}^{(l)}}\right)}. \qquad (36)$$

3.3.2.3 The Lower Bound over L_{kr}'s

From (9), $\alpha(|h_{sr}|^2)$ is upper and lower bounded as

$$c_l^{kr}(|h_{sr}|^2 - r_k)^{p_{1k}^{(r)}} \leq \alpha(|h_{sr}|^2) \leq c_u^{kr}(|h_{sr}|^2 - r_k)^{p_{1k}^{(r)}},$$

when ρ_{sr} belongs to L_{kr}. Plugging it into the expression of P_{l1} in Lemma 1 and changing the integration interval to L_{kr} yield the lower bound as follows:

$$\begin{aligned} E[P_{l1} + P_{l2}]_{L_{kr}} &\geq [P_{l1}]_{L_{kr}} \\ &\geq \frac{1}{4\sqrt{\pi}\bar{\rho}_{sr}(2 + 3\bar{\rho}_{sd})} \int_{r_k\bar{\rho}}^{(r_k+\delta)\bar{\rho}} \frac{\exp(-\frac{\rho_{sr}}{\bar{\rho}_{sr}})}{1 + c_u^{kr}(\frac{\rho_{sr}}{\bar{\rho}} - r_k)^{p_{1k}^{(r)}}\bar{\rho}_{rd}} d\rho_{sr} \\ &=: P_{l1}^{L_{kr}}. \end{aligned} \tag{37}$$

After simple calculations, $P_{l1}^{L_{kr}}$ can be expressed as

$$\begin{aligned} P_{l1}^{L_{kr}} &\overset{\rho' = \rho_{sr} - r_k\bar{\rho}}{=} \frac{1}{4\sqrt{\pi}\bar{\rho}_{sr}(2 + 3\bar{\rho}_{sd})} \int_0^{\delta\bar{\rho}} \frac{\exp(-\frac{\rho' + r_k\bar{\rho}}{\bar{\rho}_{sr}})}{1 + c_u^{kr}(\frac{\rho'}{\bar{\rho}})^{p_{1k}^{(r)}}\bar{\rho}_{rd}} d\rho' \\ &\overset{t = \frac{\rho'}{\bar{\rho}_{sr}}}{=} \frac{\exp(-\frac{r_k\bar{\rho}}{\bar{\rho}_{sr}})}{4\sqrt{\pi}(2 + 3\bar{\rho}_{sd})} \int_0^{\delta\frac{\bar{\rho}}{\bar{\rho}_{sr}}} \frac{\exp(-t)}{1 + c_u^{kr}(\frac{\bar{\rho}_{sr}}{\bar{\rho}}t)^{p_{1k}^{(r)}}\bar{\rho}_{rd}} dt. \end{aligned} \tag{38}$$

Since Eq. (38) and Eq. (34) have the same form, we follow the similar procedure as in Eq. (35) to get

$$P_{l1}^{L_{kr}} \doteq \bar{\rho}^{-\left(1 + \frac{1}{p_{1k}^{(r)}}\right)}. \tag{39}$$

Combining Eq. (37) and Eq. (39), we conclude

$$[P_{l1} + P_{l2}]_{L_{kr}} \doteq \bar{\rho}^{-\left(1 + \frac{1}{p_{1k}^{(r)}}\right)}. \tag{40}$$

Finally, from Eqs. (29), (32), (36) and (40), we further bound $E[P_b]$ below by a term with the lowest absolute exponent and conclude that

$$E[P_b] \doteq \bar{\rho}^{-G_d},$$

where $G_d = 1 + \min\{g_1(p_1), \frac{1}{p_{1k}^{(l)}}, \frac{1}{p_{1k}^{(r)}}\}$. Since the maximum of $g_1(p_1)$ is 1, this is equivalent to

$$G_d = 1 + \min\{g_1(p_1), g_2(p_{1k}^{(l)}), g_2(p_{1k}^{(r)})\}. \ \blacksquare$$

With the upper and lower bounds on the average SER as given in Lemmas 5 and 6, we have shown that the behavior of $\alpha(|h_{sr}|^2)$ approaching each root determines the diversity at the destination node. Summarizing the above lemmas, it is easy to prove Theorem 1.

It is interesting to note that the result in Theorem 1 bears some similarities with that in [109] which shows that the diversity gain provided by fading channels depends on the PDF of the channel around the origin. Our result confirms that the behavior of power profile at the origin also plays an important role in determining the diversity gains in DF relay systems. The difference between our result and the one in [109] is two-fold: (i) [109] finds the relationship in point-to-point communications with inherent channel statistics, but the diversity for our design depends on two-hop channel information which is more general than the one in [109]; and (ii) the relay power-profile design depends on the channel state information of the first hop, but it will affect the diversity at the next hop. In summary, applying [109] directly cannot solve the technical problem we are facing here.

3.3.3 Necessary and Sufficient Conditions for Cooperative Diversity

Previously, we have analyzed the average SER performance of the general link-adaptive strategy and the diversity order at the destination is presented in Theorem 1. Based on our analysis, we summarize the necessary and sufficient conditions on $\alpha(|h_{sr}|^2)$ under **D1)**, **D2)** and **D3)** to enable cooperative diversity 2 for the single relay system in the following:

NSC1) $\alpha(|h_{sr}|^2 = 0) = 0$.

NSC2) The set $\{x : \alpha(x) = 0\}$ is measure zero, i.e., no zero interval, so that $g_3(r_k^{(r)} - r_k^{(l)}) = 1$.

NSC3) The behavior of $\alpha(|h_{sr}|^2)$ approaching the origin point is linear ($p_1 = 1$) so that $g_1(p_1) = 1$.

NSC4) If $\alpha(|h_{sr}|^2) = 0$ has roots other than the origin, the behavior of $\alpha(|h_{sr}|^2)$ near those roots must satisfy $p_{1k}^{(l)} \leq 1$ and $p_{1k}^{(r)} \leq 1$ so that $g_2(p_{1k}^{(l)}) = 1$ and $g_2(p_{1k}^{(r)}) = 1$.

As shown in Lemmas 3 and 4, if $\alpha(|h_{sr}|^2)$ fails to satisfy **NSC1)** or **NSC2)**, we can only achieve the diversity order of 1. According to Theorem 1, if either **NSC3)** or **NSC4)** is violated, the diversity order is real number between 1 and 2, depending on the behavior of $\alpha(|h_{sr}|^2)$ near the roots of $\alpha(|h_{sr}|^2) = 0$.

3.4 Simulation Results

Power profiles can be designed to satisfy the conditions **NSC1)**$\sim$**NSC4**), such as the ideal soft-limiter design in [108], to enable full cooperative diversity. However, they may not be implemented perfectly in practice because of the non-idealness of real systems (e.g. nonlinear power amplifier). In this section, we present some numerical examples to verify the diversity order for a general shape of the power profile. According to Theorem 1, the factors that determine the diversity order are $\alpha(0)$, the existence of zero interval, and the behavior of α near each root. From each test case, we will see how they affect the diversity order.

We plot the average SER curves versus $\bar{\rho}$ by assigning $(\bar{\rho}_{sr}, \bar{\rho}_{rd}, \bar{\rho}_{sd}) = (\bar{\rho}, \bar{\rho}, \bar{\rho})$. BPSK modulation is adopted through this section unless otherwise mentioned. For the fair comparisons among different power-profile designs, we normalize the average scaling power to $E[\alpha] = 1$.

Test case 3.1 (The effects of $\alpha(0)$, tail and zero intervals): Four different power-profile designs are considered in this test case (see in Figure 7). The corresponding SER performance at the destination is plotted in Figure 8. The well-known AF and DF strategies are also plotted as benchmarks. Diversity order of 2 is obtained for α_{Aa} and α_{Ac} in [108], as expected. The tail of α_{Ac} has a function $(1/|h_{sr}|^2)^5$ which is strictly decreasing. For the power profile α_{Ab} and the DF strategy (or equivalently $\alpha = 1$), the diversity collected at the destination is only 1, which verifies Lemma 3

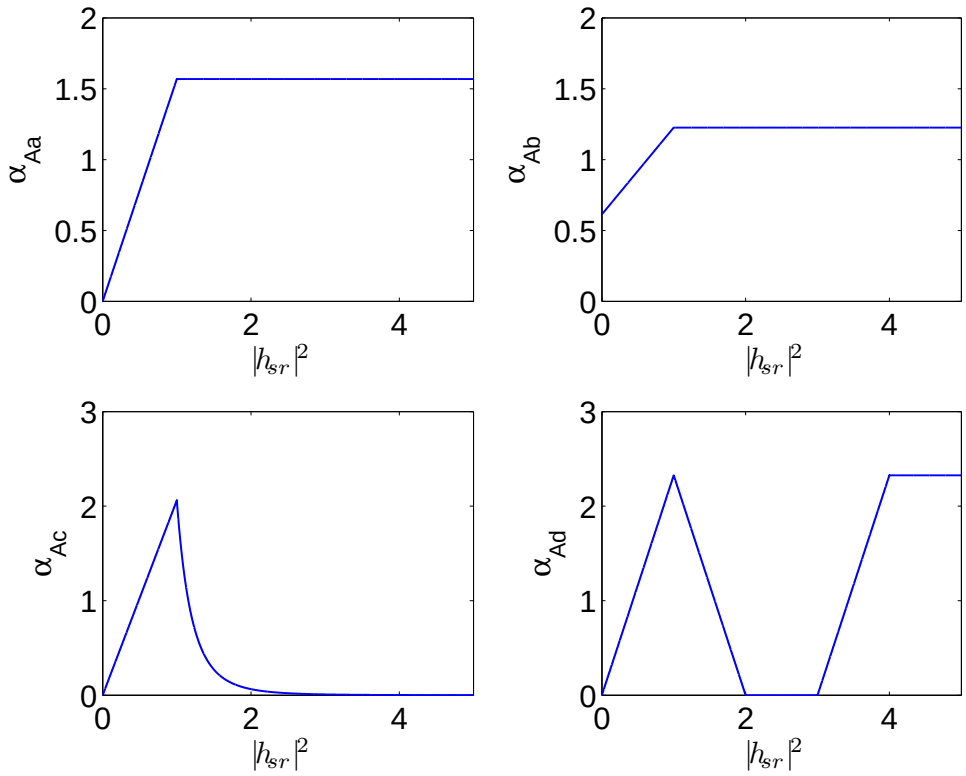

Figure 7: Power profiles α_{Aa}, α_{Ab}, α_{Ac}, and α_{Ad}.

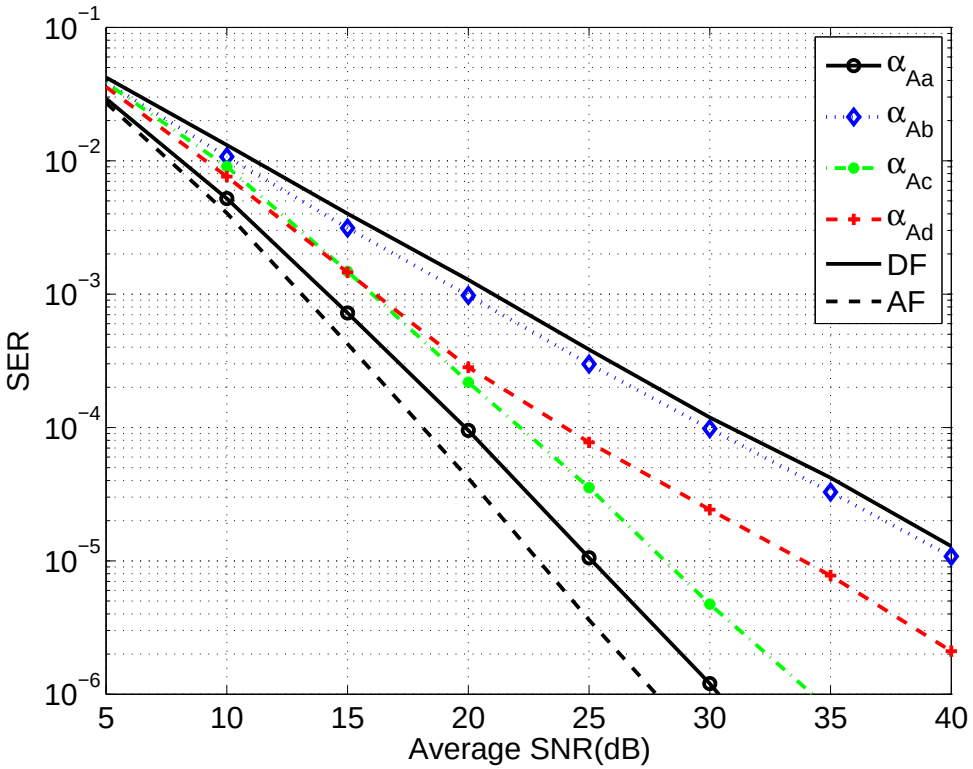

Figure 8: SER performance of α_{Aa}, α_{Ab}, α_{Ac}, and α_{Ad}.

Table 1: Diversity order of α_{Ba}, α_{Bb}, α_{Bc}, and α_{Bd}.

	p_1	$g_1(p_1)$	Diversity order G_d $= 1 + g_1(p_1)$
α_{Ba}	4	0.25	1.25
α_{Bb}	2	0.5	1.5
α_{Bc}	0.5	0.5	1.5
α_{Bd}	0.25	0.25	1.25

because both of them satisfy $\alpha(0) > 0$, i.e., $p_1 \leq 0$. For α_{Ad} which has one zero interval, the relay system only achieves diversity order of 1 according to Lemma 4.

Test case 3.2 (The effect of the behavior of α at the origin - p_1): To verify the effect of the behavior of α at the origin, we design four power profiles in Figure 9 with the origin point as the only root of $\alpha(|h_{sr}|^2) = 0$ but different behaviors at the origin. Before being clipped to a constant, the power profile is selected as $\alpha(|h_{sr}|^2) = (|h_{sr}|^2)^{p_1}$. The parameter p_1 of α_{Ba}, α_{Bb}, α_{Bc}, and α_{Bd} is 4, 2, 0.5, and 0.25, respectively. The average SER performance of these designs is depicted in Figure 10. Both α_{Bb} and α_{Bc} have the same diversity order of $1 + g_1(2) = 1 + g_1(0.5) = 1.5$, while α_{Ba} and α_{Bd} enable diversity order of $1 + g_1(4) = 1 + g_1(0.25) = 1.25$, which verifies Theorem 1. The parameter p_1 and the diversity order for each power profile are summarized in Table 1. It is shown that only when the expansion of α at the origin has lowest exponent $p_1 = 1$, is the full cooperative diversity possible. If p keeps increasing and approaches infinity, the power profile will become a step function which causes diversity loss as shown in [108]. On the other hand, if p keeps decreasing and approaches zero, the power profile becomes 1 as in the DF strategy which also loses diversity. This is well explained by Theorem 1 since $G_d = 1 + g_1(p)$ approaches 1 as $p \to 0$ or $p \to \infty$.

Test case 3.3 (The effect of the behavior of α at positive roots - $p_{1k}^{(l)}$, $p_{1k}^{(r)}$): In this example, we illustrate the performance of power profiles with positive roots and

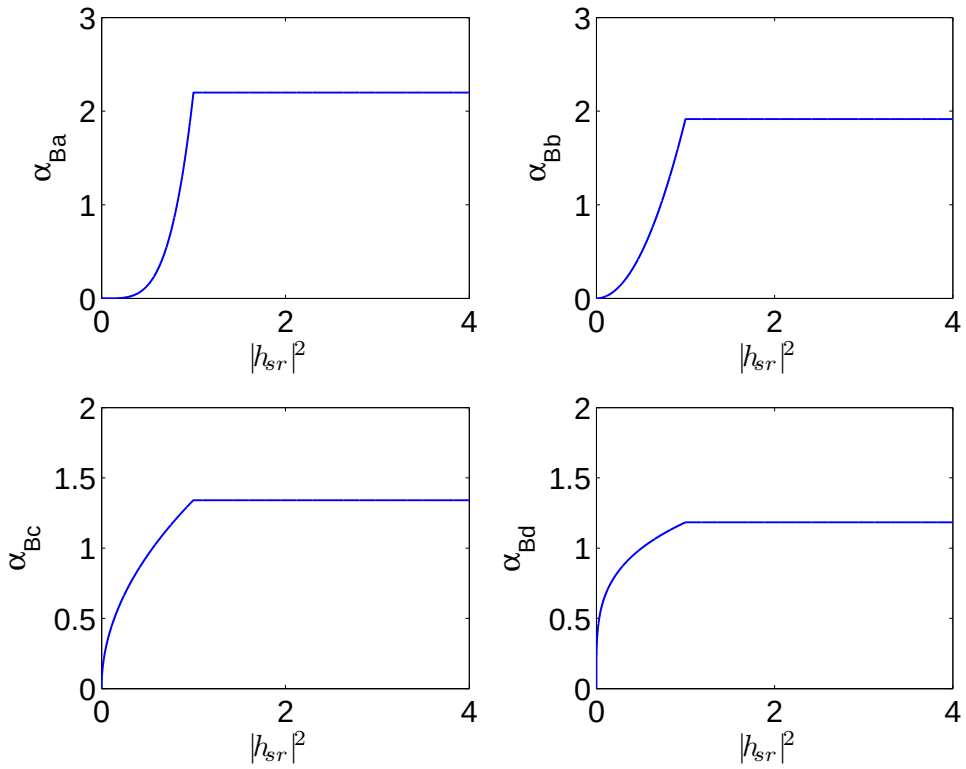

Figure 9: Power profiles α_{Ba}, α_{Bb}, α_{Bc}, and α_{Bd}.

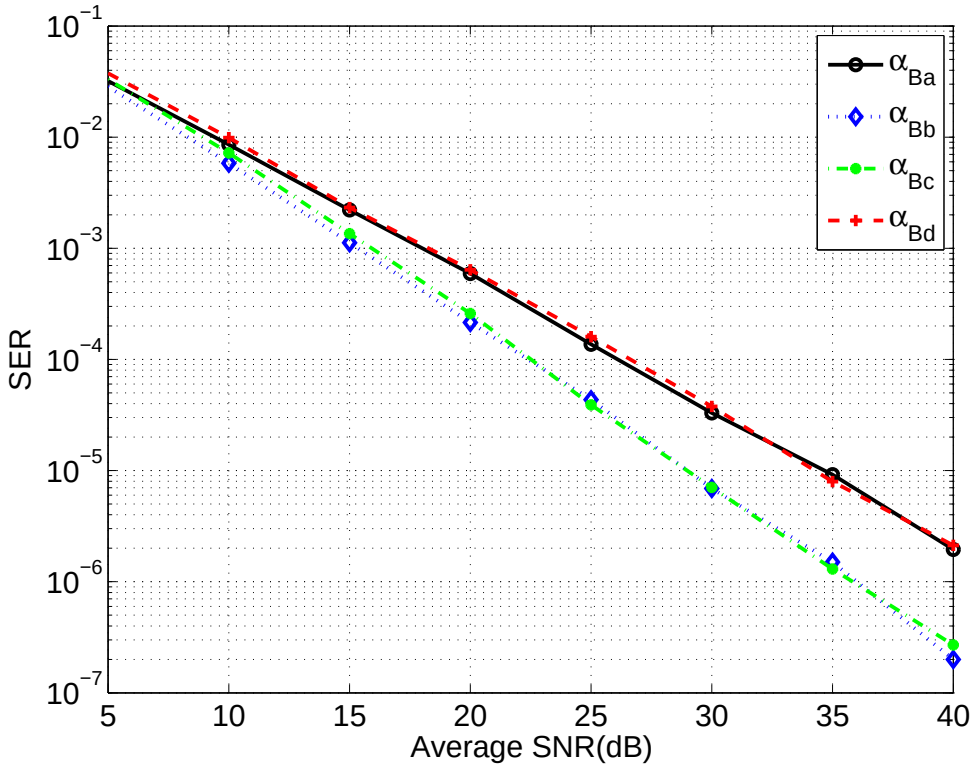

Figure 10: SER performance of α_{Ba}, α_{Bb}, α_{Bc}, and α_{Bd}.

Table 2: Diversity order of α_{Ca}, α_{Cb}, α_{Cc}, α_{Cd}, α_{Ce}, and α_{Cf}.

	p_1	$p_{11}^{(l)}$	$p_{11}^{(r)}$	$g_1(p_1)$	$g_2(p_{11}^{(l)})$	$g_2(p_{11}^{(r)})$	Diversity order G_d $= 1+\min\{g_1(p_1), g_2(p_{11}^{(l)}), g_2(p_{11}^{(r)})\}$
α_{Ca}	1	8	8	1	1/8	1/8	9/8
α_{Cb}	1	8	0.5	1	1/8	1	9/8
α_{Cc}	1	0.5	0.5	1	1	1	2
α_{Cd}	2	0.5	0.5	0.5	1	1	1.5
α_{Ce}	0.5	0.5	0.5	0.5	1	1	1.5
α_{Cf}	2	8	8	0.5	1/8	1/8	9/8

verify our Theorem 1. Six different power profiles are depicted in Figure 11, which can be described as $(|h_{sr}|^2)^{p_1}$ for $|h_{sr}|^2 \in [0,1]$, $(-|h_{sr}|^2+2)^{p_{11}^{(l)}}$ for $|h_{sr}|^2 \in [1,2]$, and $(|h_{sr}|^2-2)^{p_{11}^{(r)}}$ for $|h_{sr}|^2 \in [2,3]$. The SER curves corresponding to triplets $(p_1, p_{11}^{(l)}, p_{11}^{(r)})$ are presented in Figure 12. To see the effect of the behavior at the positive root on the diversity order, we compare the SER of α_{Ca}, α_{Cb}, and α_{Cc} in Figure 12, all of which have linearity at the origin. When either $p_{11}^{(l)}$ or $p_{11}^{(r)}$ is greater than 1 as in α_{Ca} and α_{Cb}, the power profile cannot achieve the diversity order of 2 since $g_2(p_{11}^{(l)})$ or $g_2(p_{11}^{(r)}) < 1$, which leads to $G_d < 2$ according to Theorem 1. Both α_{Ca} and α_{Cb} achieve diversity order of 9/8 since $g_2(8) = 1/8$. However, if both $p_{11}^{(l)}$ and $p_{11}^{(r)}$ are less than 1 as in α_{Cc}, we have $g_2(p_{11}^{(l)}) = g_2(p_{11}^{(r)}) = 1$, and thus, $G_d = 2$. For α_{Cc}, α_{Cd}, and α_{Ce}, their behaviors are same at the positive root ($p_{11}^{(l)} = p_{11}^{(r)} = 0.5$) but different at the origin. Depending on the behavior at the origin, α_{Cc}, α_{Cd}, and α_{Ce} enable diversity order of 2, 1.5, and 1.5, respectively, since $g_1(1) = 1$ and $g_1(2) = g_1(0.5) = 0.5$. α_{Cf} is an example where the power profile behaviors at both the origin and the positive root prevent the destination from achieving full cooperative diversity. The behavior at the positive root dominates the diversity performance of α_{Cf} since $g_2(p_{11}^{(l)})(= 1/8)$ is less than $g_1(p_1)(= 0.5)$. Thus, the diversity order enabled by α_{Cf} is 9/8. The parameters p_1, $p_{11}^{(l)}$ and $p_{11}^{(r)}$ and the diversity order for each power profile are summarized in Table 2.

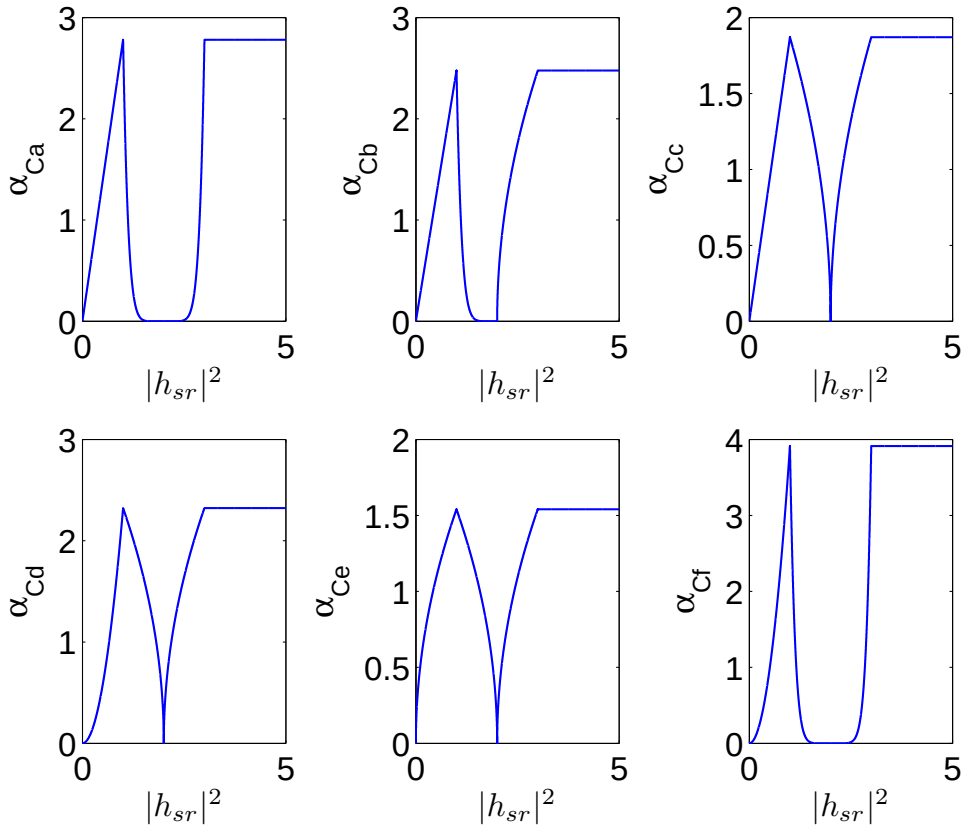

Figure 11: Power profiles α_{Ca}, α_{Cb}, α_{Cc}, α_{Cd}, α_{Ce}, and α_{Cf}.

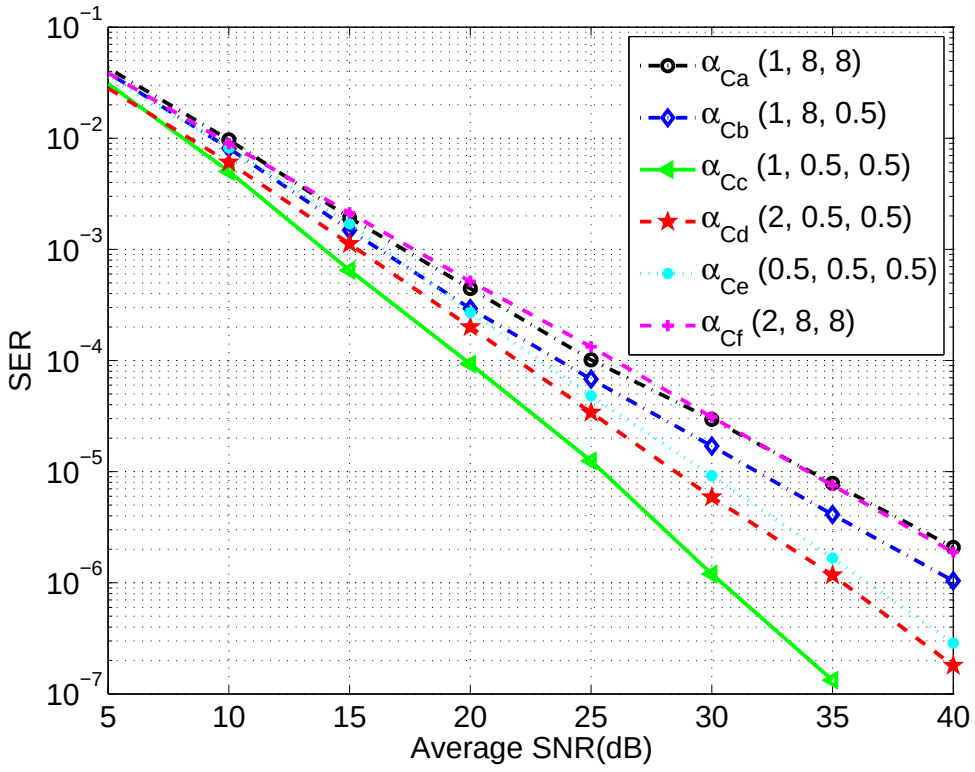

Figure 12: SER performance of α_{Ca}, α_{Cb}, α_{Cc}, α_{Cd}, α_{Ce}, and α_{Cf}.

Table 3: Diversity order of α_{Da} and α_{Db}.

	p_1	$p_{11}^{(l)}$	$p_{11}^{(r)}$	$g_1(p_1)$	$g_2(p_{11}^{(l)})$	$g_2(p_{11}^{(r)})$	Diversity order G_d $= 1+\min\{g_1(p_1), g_2(p_{11}^{(l)}), g_2(p_{11}^{(r)})\}$
α_{Da}	2/3	·	·	2/3	·	·	5/3
α_{Db}	2/3	8	8	2/3	1/8	1/8	9/8

If $p_{11}^{(l)}$ and $p_{11}^{(r)}$ in α_{Ca} are increased to infinity, the power profile near the positive root becomes a zero interval in $[1, 3]$ which causes diversity loss. According to Theorem 1, diversity order G_d decreases to 1 as $p_{11}^{(l)}$ and $p_{11}^{(r)}$ approach infinity. However, when $p_{11}^{(l)}$ and $p_{11}^{(r)}$ are decreasing to 0, the power profile approaches that of α_{Aa} in Figure 7 which achieves diversity order of 2. This is also verified by Theorem 1, from which we find $G_d = 2$ if $p_1 = 1$, $0 \leq p_{11}^{(l)} \leq 1$, and $0 \leq p_{11}^{(r)} \leq 1$.

Test case 3.4 (The effect of general power profiles): Now we turn to the case when the behavior of α approaching its roots can be represented as the summation of multiple polynomial terms. We design α_{Da} and α_{Db} in Figure 13 to be $(|h_{sr}|^2)^{2/3}\exp(|h_{sr}|^2)$ for $|h_{sr}|^2 \in [0, 1]$, but α_{Db} has an additional root at $|h_{sr}|^2 = 2$ and α_{Db} is designed as $(|h_{sr}|^2 - 2)^8\exp(||h_{sr}|^2 - 2|)$ for $|h_{sr}|^2 \in [1, 3]$. According to Theorem 1, the diversity order of α_{Da} will be determined by p_1 only, but for α_{Db}, $p_{11}^{(l)}$ and $p_{11}^{(r)}$ will also affect the diversity performance. Since the Taylor expansion of $\exp(|x - a|)$ near $x = a$ is expressed as

$$\exp(|x - a|) = \sum_{k=0}^{\infty} \frac{|x - a|^k}{k!},$$

the order of smoothness p_1 for α_{Da} is 2/3, and $(p_1, p_{11}^{(l)}, p_{11}^{(r)})$ for α_{Db} is $(2/3, 8, 8)$. Thus, according to Theorem 1, diversity orders enabled by α_{Da} and α_{Db} are $1+g_1(2/3) = 5/3$ and $1 + \min\{g_1(2/3), g_2(8), g_2(8)\} = 9/8$, respectively. The parameters p_1, $p_{11}^{(l)}$ and $p_{11}^{(r)}$ and the diversity order for α_{Da} and α_{Db} are summarized in Table 3. The result is corroborated by the simulation in Figure 14.

Test case 3.5 (Higher-order constellations): It was explained in (8) that our

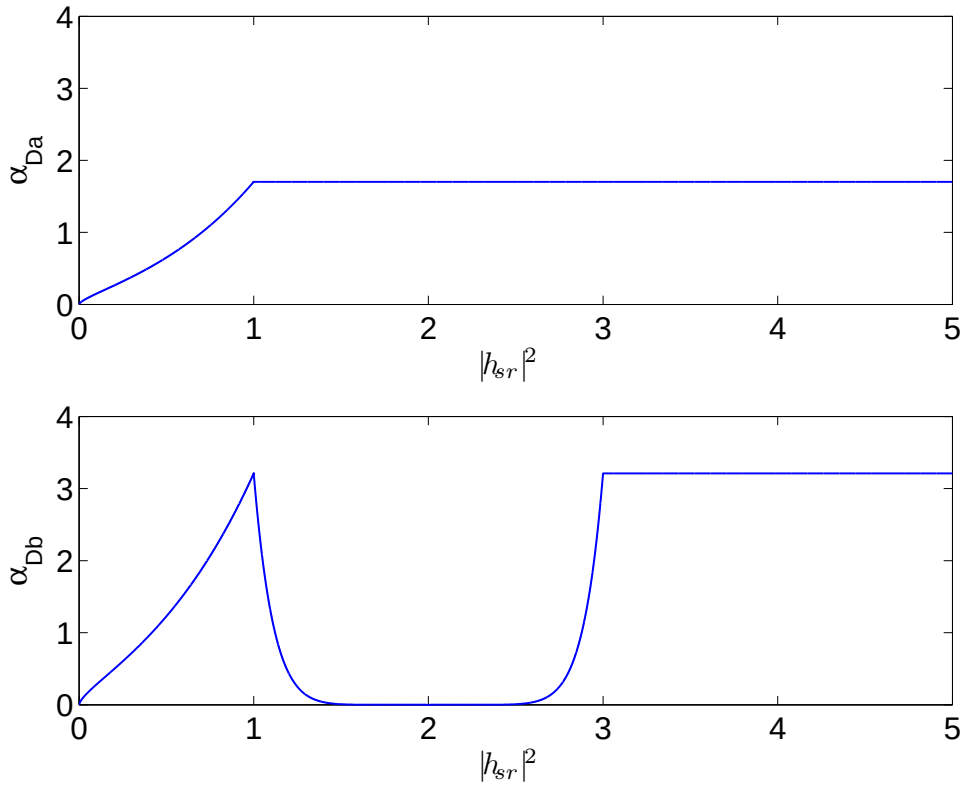

Figure 13: Power profiles α_{Da} and α_{Db}.

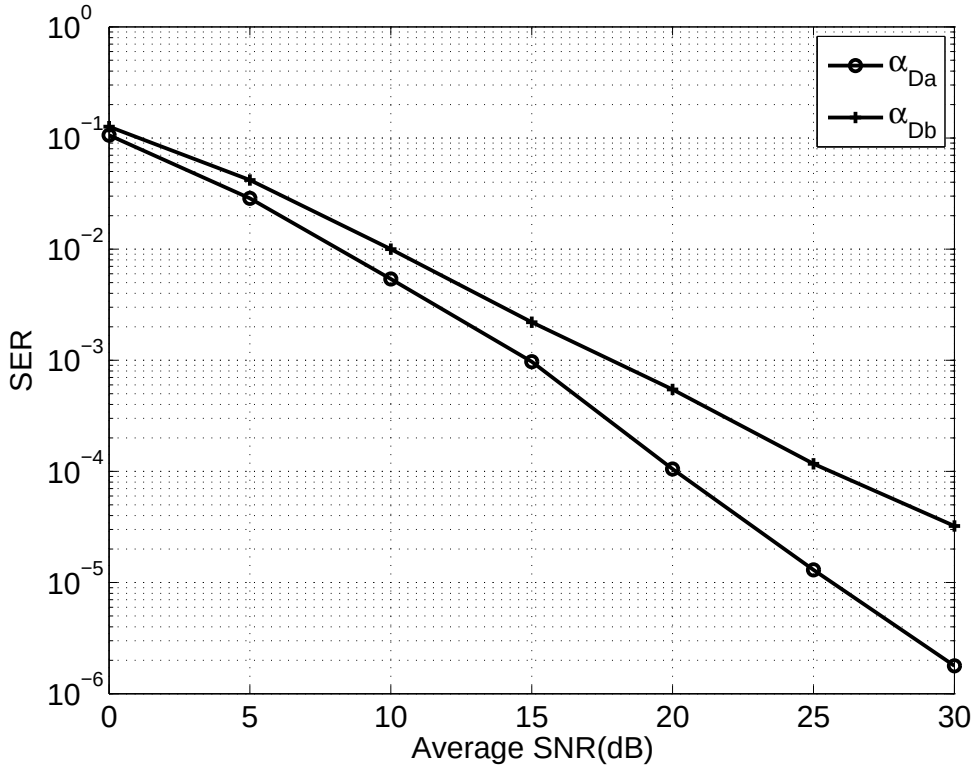

Figure 14: SER performance of α_{Da} and α_{Db} with BPSK modulation.

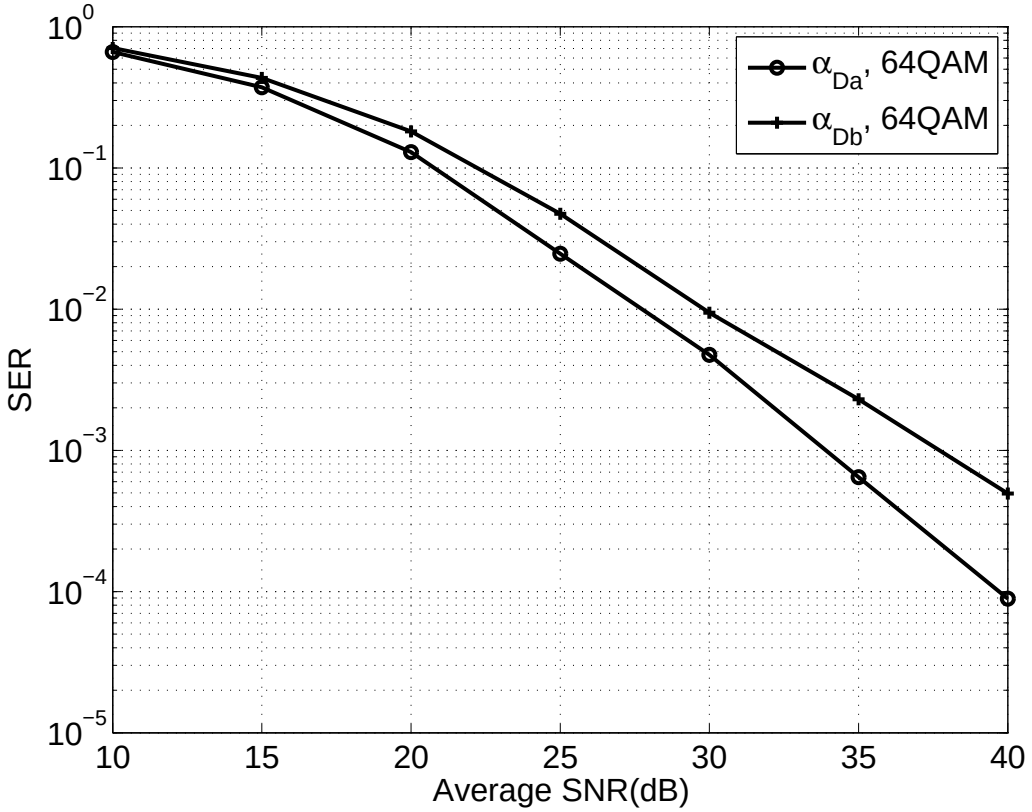

Figure 15: SER performance of α_{Da} and α_{Db} with 64-QAM.

diversity order analysis applies to any constellation size. To verify the diversity claim for higher-order constellations, the SER performance of α_{Da} and α_{Db} in Figure 13 is plotted in Figure 15 for 64-QAM modulation. Comparing Figure 14 and Figure 15, we find that BPSK and 64-QAM have the same diversity order, validating Theorem 1 for general constellations.

Test case 3.6 (Power profile coefficients from an actual class AB power amplifier): To validate our theoretical results, we shall also consider a power profile of third-order nonlinearity $\alpha_{classAB} = a_1(|h_{sr}|^2)+a_3(|h_{sr}|^2)^3$ with nonlinear coefficients $a_1 = 1.0144$ and $a_3 = 0.181$ extracted from an actual class AB power amplifier [32]. The power profile $\alpha_{classAB}$ and the SER performance with $\alpha_{classAB}$ are shown in Figure 16 and 17, respectively. Since the order of smoothness of $\alpha_{classAB}$ at the origin is 1, cooperative diversity 2 is achieved according to Theorem 1. Figure 17 verifies this.

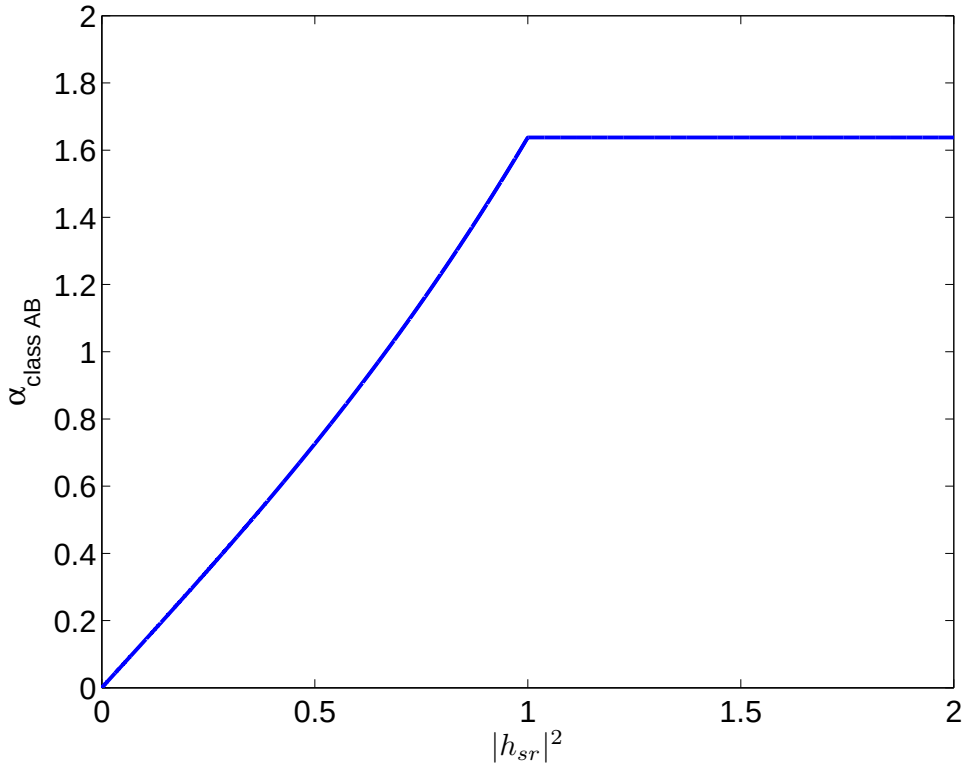

Figure 16: A power profile with coefficients from an actual class AB PA.

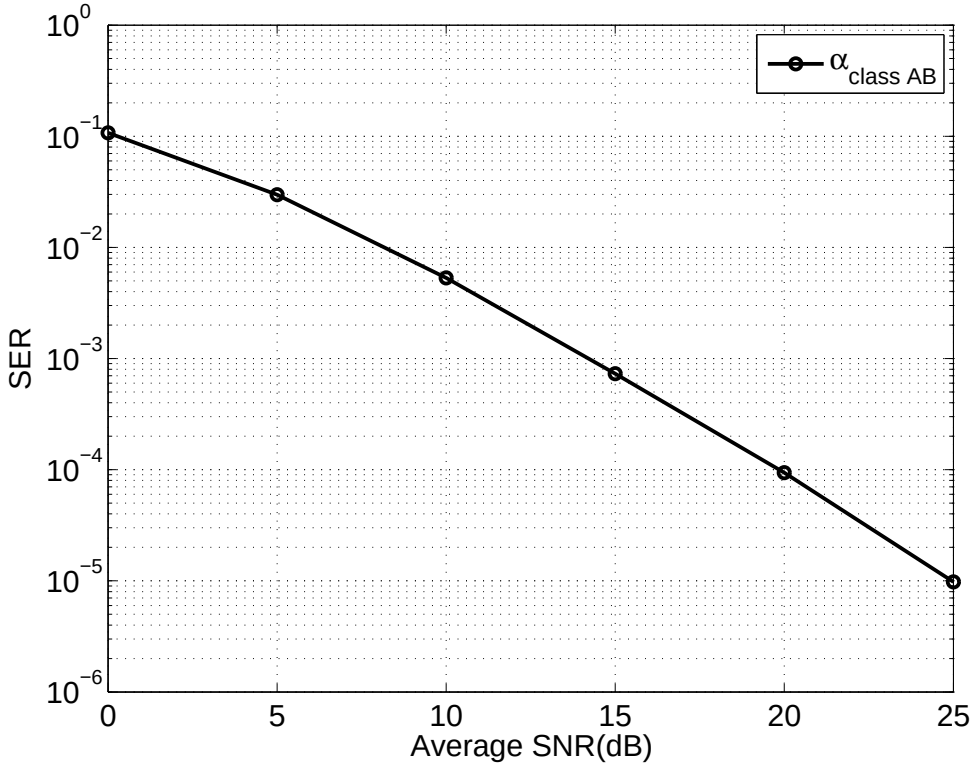

Figure 17: SER with power profile coefficients from an actual class AB PA.

Table 4: Diversity order for multi-relay transmissions.

	p_1	$g_1(p_1)$	N_R	Diversity order G_{d,N_R} $= 1 + N_R g_1(p_1)$
α_{Bb}	0.5	0.5	1	1.5
			2	2
			3	2.5
α_{Aa}	1	1	1	2
			2	3
			3	4

Test case 3.7 (Multi-relay transmissions): In this example, we show that the general link-adaptive relay strategy is applicable to multi-relay transmissions, where N_R relay nodes operate in parallel over orthogonal channels. The number of arriving paths to D is $1 + N_R$ including one direct link. In Theorem 1, the diversity order G_d for single-relay transmissions is $1 + \min\{g_1(p_1), g_2(p_{1k}^{(l)}), g_2(p_{1k}^{(r)}), g_3(r_k^{(r)} - r_k^{(l)})\}$, where "1" is from the direct link and the second term "$\min\{g_1(p_1), g_2(p_{1k}^{(l)}), g_2(p_{1k}^{(r)}), g_3(r_k^{(r)} - r_k^{(l)})\}$" comes from $S - R - D$ path. Thus, the diversity order can be generalized to $G_{d,N_R} = 1 + N_R \min\{g_1(p_1), g_2(p_{1k}^{(l)}), g_2(p_{1k}^{(r)}), g_3(r_k^{(r)} - r_k^{(l)})\}$ for multi-relay transmissions. Figure 18 tests generalizations and validates the diversity claims for multiple relay nodes. We assume every relay node adopts the same power profile. Two schemes, α_{Bb} from Figure 9 and α_{Aa} from Figure 7, are tested. By inspecting the slope of the average SER curves, we can verify that in each scheme, diversity order of G_{d,N_R} is achieved. The results are summarized in Table 4.

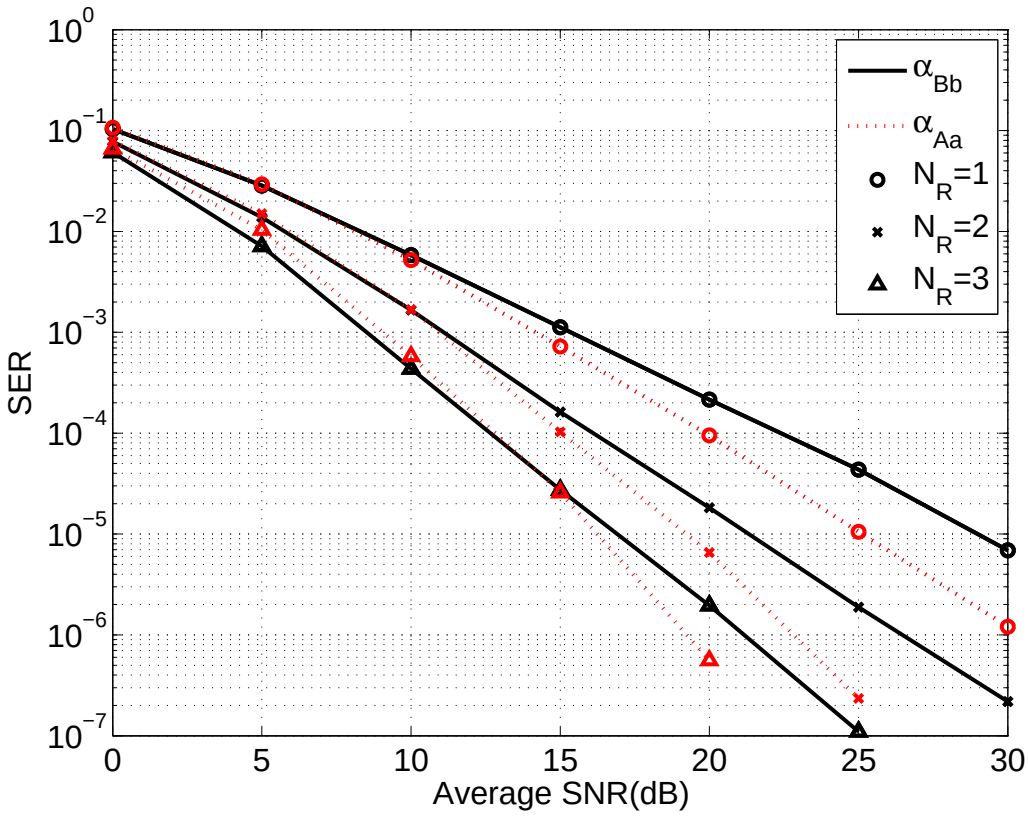

Figure 18: SER performance comparison for multiple relay nodes.

3.5 Conclusions

In this chapter, we have investigated the diversity order enabled by general power profiles at the relay for DF cooperative systems without any feedback information. We have shown that the behavior of the power profile near its roots plays an important role in determining the diversity order at the destination. In general, the diversity order for a single-relay system is a real number between 1 and 2. The necessary and sufficient conditions for the power-profile design to enable full cooperative diversity 2 have been summarized. Theoretical claims have been verified by simulations.

CHAPTER IV

JOINT DIVERSITY IN DECODE-AND-FORWARD MIMO RELAY NETWORKS WITH LOW-COMPLEXITY EQUALIZERS

Recently, MIMO techniques have been applied to relay networks to provide higher rate and reliability and are receiving significant interest [5, 14, 16, 23, 17, 20, 37, 55, 90, 95, 105, 113, 117, 118]. However, most of MIMO relay techniques require high-complexity equalizers, such as maximum-likelihood equalizers (MLEs) or near-MLEs, and also error free forwarding at the relay to collect spatial diversity, which is impractical and thus may not be suitable for low-complexity communication environments. In this chapter, we propose high-rate and low-complexity DF MIMO relay designs that achieve cooperative diversity, receive diversity or joint diversity. The main contributions of this chapter are: (i) Design of a power scaling matrix at the relay so that cooperative diversity can be achieved at the destination; (ii) Combining zero-forcing equalizers (ZFEs) with a novel channel-controlled ARQ (CC-ARQ) technique so that the receive-antenna diversity can be collected at the destination even with ZFEs; (iii) Development of a low-complexity relay strategy to achieve joint diversity without any feedback or CRC. We prove these claims mathematically and verify them numerically with simulations.

4.1 System Model of DF MIMO Relay Networks

As shown in Figure 19, we consider a simple single-relay network which consists of three nodes: source (S), relay (R), and destination (D). Without loss of generality, we assume that each node is equipped with N antennas. All channels are considered

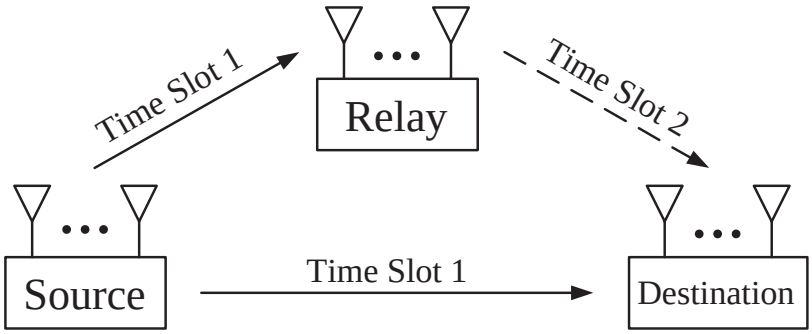

Figure 19: Block diagram of a MIMO relay network.

to be flat, quasi-static and mutually independent. We assume half duplex relaying and divide one transmission period into two time slots. In the first time slot, the source node S transmits the $N \times 1$ information symbol vector $\boldsymbol{s}$ to the relay node R and the destination node D. In the second time slot, the relay node R helps transmit the information of the source node S by decoding the received signal and forwarding re-encoded symbols to the destination node D. Note that here we fully take multiple antennas for spatial multiplexity.

With subscripts signifying the corresponding link, e.g., $_{sr}$ denotes the link from S to R, the mathematical formulation of the baseband equivalent model can be written as

$$\begin{aligned} \boldsymbol{y}_{\mathrm{sr}} &= \boldsymbol{H}_{\mathrm{sr}}\boldsymbol{s} + \boldsymbol{w}_{\mathrm{sr}}, \\ \boldsymbol{y}_{\mathrm{sd}} &= \boldsymbol{H}_{\mathrm{sd}}\boldsymbol{s} + \boldsymbol{w}_{\mathrm{sd}}, \\ \boldsymbol{y}_{\mathrm{rd}} &= \boldsymbol{H}_{\mathrm{rd}}\boldsymbol{A}^{\frac{1}{2}}\hat{\boldsymbol{s}}_{\mathrm{r}} + \boldsymbol{w}_{\mathrm{rd}}, \end{aligned} \tag{41}$$

where $\boldsymbol{y}$ is the $N \times 1$ received signal, $\hat{\boldsymbol{s}}_{\mathrm{r}}$ is the $N \times 1$ information vector transmitted by the relay node. Diagonal matrix $\boldsymbol{A} = \mathrm{diag}[\alpha_1, \alpha_2, \cdots, \alpha_N]$ is the power scaling factor (PSF) matrix at the relay node. Matrix $\boldsymbol{H}_{\mathrm{ij}}$ is the $N \times N$ random channel with all entries being i.i.d. complex Gaussian variables with zero mean and variance σ_{ij}^2 for i-j link. We assume all channel matrices are estimated and known at the corresponding receiver side. The $N \times 1$ noise vector $\boldsymbol{w}$ is i.i.d. complex Gaussian

distributed with zero mean and variance N_0, i.e., $E[\boldsymbol{w}\boldsymbol{w}^{\mathcal{H}}] = N_0\boldsymbol{I}_N$. The average power of each transmitted symbol s_i and $\hat{s}_{\mathrm{r},i}$ is 1. Therefore, the average SNR at each hop is defined as $\bar{\rho} = 1/N_0$.

In this chapter, we use diversity order, defined in Eq. (3), as a performance indicator. It is well known that the diversity order depends on the degrees of freedom provided by the underlying fading channels. Note that for the three-node MIMO relay network setup in (41), there are two types of diversity: the cooperative diversity 2 due to the multi-access to destination and the receive diversity N introduced by the multi-antenna at each node. For simplicity, here we do not consider transmit diversity. Accordingly, the appropriate design will collect a diversity order of $2N$.

In this chapter, we focus on DF MIMO relay networks, where $\hat{\boldsymbol{s}}_{\mathrm{r}}$ in (41) is taken as the estimate of $\boldsymbol{s}$ at the relay. The MLE is often used as the optimal estimation method, which considers multiple spatial streams as a whole. However, the complexity of MLE is very high, which increases exponentially with the number of antennas [103]. To reduce the decoding complexity, some near-MLEs have been proposed, e.g., sphere decoding (SD) method [49]. However, it has been shown that MLE and near-MLEs suffer from high complexity and thus not efficient for hardware implementation [119]. In practice, ZFEs are favored for their low decoding complexity. Here, we adopt ZFE at the relay to estimate the transmitted symbol vector $\boldsymbol{s}$ as

$$\begin{aligned} \boldsymbol{x}_{\mathrm{sr}} &= \boldsymbol{H}_{\mathrm{sr}}^{\dagger}\boldsymbol{y}_{\mathrm{sr}} = \boldsymbol{s} + \boldsymbol{H}_{\mathrm{sr}}^{\dagger}\boldsymbol{w}_{\mathrm{sr}} = \boldsymbol{s} + \boldsymbol{n}_{\mathrm{sr}}, \\ \hat{s}_{\mathrm{r},i} &= \mathcal{Q}\left(x_{\mathrm{sr},i}\right) = \mathcal{Q}\left(s_i + n_{\mathrm{sr},i}\right), \end{aligned} \tag{42}$$

where $\boldsymbol{H}^{\dagger} = (\boldsymbol{H}^{\mathcal{H}}\boldsymbol{H})^{-1}\boldsymbol{H}^{\mathcal{H}}$ denotes the Moore-Penrose pseudo-inverse of the channel matrix $\boldsymbol{H}$ and $E[|n_{\mathrm{sr},i}|^2] = N_0\left(\boldsymbol{H}_{\mathrm{sr}}^{\mathcal{H}}\boldsymbol{H}_{\mathrm{sr}}\right)_{i,i}^{-1}$. The quantization step $\mathcal{Q}$ maps each entry to the nearest symbol in the alphabet $\mathcal{S}$. Then, in the second time slot, the relay forwards the scaled version of $\hat{\boldsymbol{s}}_{\mathrm{r}}$, $\boldsymbol{A}^{\frac{1}{2}}\hat{\boldsymbol{s}}_{\mathrm{r}}$, to the destination. Upon receiving two signals $\boldsymbol{y}_{\mathrm{sd}}$ and $\boldsymbol{y}_{\mathrm{rd}}$ from the source and the relay, the destination applies ZFE to each

received signal vector as

$$\begin{aligned} \boldsymbol{x}_{\mathrm{sd}} &= \boldsymbol{H}_{\mathrm{sd}}^{\dagger}\boldsymbol{y}_{\mathrm{sd}} = \boldsymbol{s} + \boldsymbol{H}_{\mathrm{sd}}^{\dagger}\boldsymbol{w}_{\mathrm{sd}} = \boldsymbol{s} + \boldsymbol{n}_{\mathrm{sd}}, \\ \boldsymbol{x}_{\mathrm{rd}} &= \left(\boldsymbol{H}_{\mathrm{rd}}\boldsymbol{A}^{\frac{1}{2}}\right)^{\dagger}\boldsymbol{y}_{\mathrm{rd}} = \hat{\boldsymbol{s}}_{\mathrm{r}} + \left(\boldsymbol{H}_{\mathrm{rd}}\boldsymbol{A}^{\frac{1}{2}}\right)^{\dagger}\boldsymbol{w}_{\mathrm{rd}} = \hat{\boldsymbol{s}}_{\mathrm{r}} + \boldsymbol{A}^{-\frac{1}{2}}\boldsymbol{n}_{\mathrm{rd}}. \end{aligned} \tag{43}$$

Now, each MIMO channel is converted into multiple parallel single-input single-output (SISO) channels. Each SISO channel associated with the i^{th} symbol can be written as

$$\begin{aligned} x_{\mathrm{sd},i} &= s_i + n_{\mathrm{sd},i}, \\ x_{\mathrm{rd},i} &= \hat{s}_{\mathrm{r},i} + \frac{n_{\mathrm{rd},i}}{\sqrt{\alpha_i}}, \end{aligned} \tag{44}$$

where $E[|n_{\mathrm{sd},i}|^2] = N_0\left(\boldsymbol{H}_{\mathrm{sd}}^{\mathcal{H}}\boldsymbol{H}_{\mathrm{sd}}\right)_{i,i}^{-1}$ and $E[|n_{\mathrm{rd},i}|^2] = N_0\left(\boldsymbol{H}_{\mathrm{rd}}^{\mathcal{H}}\boldsymbol{H}_{\mathrm{rd}}\right)_{i,i}^{-1}$. Since the destination has two estimates for the i^{th} symbol, it combines these equalized signals and estimates the signal as

$$\hat{s}_{\mathrm{d},i} = \arg\min_{s\in\mathcal{S}} \left|\rho_{\mathrm{sd},i}x_{\mathrm{sd},i} + \alpha_i\rho_{\mathrm{rd},i}x_{\mathrm{rd},i} - \left(\rho_{\mathrm{sd},i} + \alpha_i\rho_{\mathrm{rd},i}\right)s\right|^2, \tag{45}$$

where

$$\rho_i := \frac{1}{E[|n_i|^2]} = \frac{\bar{\rho}}{\left(\boldsymbol{H}^{\mathcal{H}}\boldsymbol{H}\right)_{i,i}^{-1}} \tag{46}$$

is defined as the instantaneous SNR of the i^{th} symbol for the corresponding link.

In DF MIMO relay networks, where the relay forwards the estimate of the information symbols, the PSF α_i is set to a constant (say 1), i.e., decoded symbols at the relay are not scaled in power. Furthermore, with this constant PSF α_i, ZFE in Eq. (43), and combining detector in Eq. (45), the destination cannot collect either cooperative diversity or receive diversity. The cooperative diversity is lost because of the inherent decoding error propagations from the relay in DF strategy [108]. The loss of receive diversity comes from the use of simple ZFE at both relay and destination, which provides inferior performance compared to MLE.

In this chapter, we propose diversity-enabling DF strategies for MIMO relay networks to collect cooperative diversity, receive diversity, or joint cooperative and receive diversity while keeping the decoding complexity low by employing ZFEs at the relay and the destination.

4.2 Power-Scaling MIMO Relay

In this section, we develop an MIMO relay design that achieves cooperative diversity. It is well known in the literature [22, 108] that cooperative diversity can be collected for single-antenna DF relay networks if the PSF at the relay is designed appropriately and MRC is adopted at the destination. Since MIMO channel is converted into multiple parallel SISO channels with the use of ZFE as we have seen in Eq. (44), we apply the idea of PSF to DF MIMO relay networks and propose to design a diagonal PSF matrix $\boldsymbol{A} = \mathrm{diag}[\alpha_1, \alpha_2, \cdots, \alpha_N]$ with

$$\alpha_i = \lambda \min\left(\frac{1}{\left(\boldsymbol{H}_{\mathrm{sr}}^{\mathcal{H}}\boldsymbol{H}_{\mathrm{sr}}\right)_{i,i}^{-1}}, \xi\right), \tag{47}$$

where ξ is a positive constant. PSF is limited to ξ because practical power amplifiers are always peak-power constrained. Then, λ normalizes the average power to make $E[\alpha_i] = 1$. We adopt $\frac{1}{\left(\boldsymbol{H}_{\mathrm{sr}}^{\mathcal{H}}\boldsymbol{H}_{\mathrm{sr}}\right)_{i,i}^{-1}}$ to represent the "quality" of the $S - R$ link for the i^{th} symbol and thus the reliability of the estimate $\boldsymbol{s}$ at the relay. Note that for single-antenna case, i.e., when $N = 1$, the PSF design in Eq. (47) becomes $\alpha_i = \lambda \min\left(|h_{\mathrm{sr}}|^2, \xi\right)$ which satisfies necessary and sufficient conditions in Section 3.3.3 for single-antenna relay networks. Intuitively, when the channel between the source and the relay is weak, the relay scales down the transmission power by a factor proportional to the channel quality in Eq. (47), and thus mitigates the effect of possible decoding errors at the relay. On the other hand, when the channel between the source and the relay is strong, most likely the estimated symbol $\hat{\boldsymbol{s}}_{\mathrm{r}}$ is correct, and the relay just forwards the symbol with a constant power.

With the PSF design in Eq. (47), the destination combines two estimates and detects the original signal $\boldsymbol{s}$ as described in Eq. (45). Note here, the destination applies ZFE by assuming the forwarded signal $\hat{\boldsymbol{s}}_{\mathrm{r}}$ from the relay is the same as the original signal $\boldsymbol{s}$ from the source. We summarize the power-scaling MIMO relay design as follows.

Design 1 (Power-Scaling MIMO Relay) *Given the DF MIMO relay network system model in* (41)*, the relay decodes* $\boldsymbol{s}$ *from the source using ZFE in Eq.* (42) *and forwards the estimate* $\hat{\boldsymbol{s}}_{\mathrm{r}}$ *after scaling it with PSF in Eq.* (47)*. The destination applies ZFE onto received signals* $\boldsymbol{y}_{\mathrm{sd}}$ *and* $\boldsymbol{y}_{\mathrm{rd}}$ *as in Eq.* (43) *and then applies the detector on each element as in Eq.* (45)*.*

In the next subsection, we will analyze the diversity performance of Design 1 presented above to show that power-scaling MIMO relay achieves cooperative diversity of 2 for each i^{th} transmitted symbol of $\boldsymbol{s}$.

4.2.1 Performance Analysis

First, we assess the performance of the design when BPSK is employed, and then the result will be extended to higher-order constellations later.

We give the expression for the instantaneous pairwise error probability of the i^{th} transmitted symbol s_i in the following lemma.

Lemma 7 *Given BPSK modulation and the set of three channel matrices* $\mathcal{H} = \{\boldsymbol{H}_{\mathrm{sr}}, \boldsymbol{H}_{\mathrm{sd}}, \boldsymbol{H}_{\mathrm{rd}}\}$ *for DF MIMO relay networks* (41) *with ZFEs in Eq.* (43) *and combination in Eq.* (45) *at the destination, the instantaneous pairwise error probability of the* i^{th} *symbol* s_i *at the destination is expressed as*

$$\begin{aligned} P_{\mathrm{e},i|\mathcal{H}} &= \left\{1 - Q\left(\sqrt{2\rho_{\mathrm{sr},i}}\right)\right\} Q\left(\sqrt{2\left(\rho_{\mathrm{sd},i} + \alpha_i \rho_{\mathrm{rd},i}\right)}\right) \\ &+ Q\left(\sqrt{2\rho_{\mathrm{sr},i}}\right) Q\left(\frac{\sqrt{2}\left(\rho_{\mathrm{sd},i} - \alpha_i \rho_{\mathrm{rd},i}\right)}{\sqrt{\rho_{\mathrm{sd},i} + \alpha_i \rho_{\mathrm{rd},i}}}\right), \end{aligned} \tag{48}$$

where $\rho_{\mathrm{sr},i}$*,* $\rho_{\mathrm{rd},i}$*, and* $\rho_{\mathrm{sd},i}$ *are defined in Eq.* (46)*.*

Proof: Suppose that s_i is transmitted for the i^{th} symbol from the source, and at the destination, it is erroneously detected as $\tilde{s} = -s_i$. Given the set of three channel matrices $\mathcal{H} = \{\boldsymbol{H}_{\rm sr}, \boldsymbol{H}_{\rm sd}, \boldsymbol{H}_{\rm rd}\}$, the instantaneous pairwise error probability can be expressed as

$$\begin{aligned} P_{{\rm e},i|\mathcal{H}} &= P(\hat{s}_{{\rm r},i} = s_i|\mathcal{H}) P(s_i \to \tilde{s}_i|\hat{s}_{{\rm r},i} = s_i, \mathcal{H}) \\ &\quad + P(\hat{s}_{{\rm r},i} = -s_i|\mathcal{H}) P(s_i \to \tilde{s}_i|\hat{s}_{{\rm r},i} = -s_i, \mathcal{H}). \end{aligned} \tag{49}$$

A MIMO channel for the $S-R$ link is decomposed into N SISO channels after applying ZFE as in Eq. (42) and we get

$$\begin{aligned} P(\hat{s}_{{\rm r},i} = -s_i|\mathcal{H}) &= Q\left(\sqrt{2\rho_{{\rm sr},i}}\right) \\ P(\hat{s}_{{\rm r},i} = s_i|\mathcal{H}) &= 1 - Q\left(\sqrt{2\rho_{{\rm sr},i}}\right). \end{aligned} \tag{50}$$

First, we find the conditional error probability at the destination when the relay estimates s_i correctly. From Eqs. (44) and (45), we have

$$\begin{aligned} P(s_i \to \tilde{s}_i|\hat{s}_{{\rm r},i} = s_i, \mathcal{H}) &= P(|\rho_{{\rm sd},i} x_{{\rm sd},i} + \alpha_i \rho_{{\rm rd},i} x_{{\rm rd},i} - (\rho_{{\rm sd},i} + \alpha_i \rho_{{\rm rd},i})(-s_i)|^2 < \\ &\qquad |\rho_{{\rm sd},i} x_{{\rm sd},i} + \alpha_i \rho_{{\rm rd},i} x_{{\rm rd},i} - (\rho_{{\rm sd},i} + \alpha_i \rho_{{\rm rd},i}) s_i|^2 \,|\hat{s}_{{\rm r},i} = s_i, \mathcal{H}) \\ &= P(|\rho_{{\rm sd,i}}(s_{\rm i} + n_{\rm sd,i}) + \alpha_{\rm i}\rho_{\rm rd,i}\left(s_{\rm i} + \frac{n_{\rm rd,i}}{\sqrt{\alpha_{\rm i}}}\right) - (\rho_{\rm sd,i} + \alpha_{\rm i}\rho_{\rm rd,i})(-s_{\rm i})|^2 \\ &\qquad < |\rho_{{\rm sd,i}}(s_{\rm i} + n_{\rm sd,i}) + \alpha_{\rm i}\rho_{\rm rd,i}\left(s_{\rm i} + \frac{n_{\rm rd,i}}{\sqrt{\alpha_{\rm i}}}\right) - (\rho_{\rm sd,i} + \alpha_{\rm i}\rho_{\rm rd,i}) s_{\rm i}|^2 | \boldsymbol{H}) \\ &= P(|\rho_{{\rm sd},i} n_{{\rm sd},i} + \sqrt{\alpha_i}\rho_{{\rm rd},i} n_{{\rm rd},i} + 2(\rho_{{\rm sd},i} + \alpha_i \rho_{{\rm rd},i}) s_i|^2 \\ &\qquad < |\rho_{{\rm sd},i} n_{{\rm sd},i} + \sqrt{\alpha_i}\rho_{{\rm rd},i} n_{{\rm rd},i}|^2 \mid \mathcal{H}) \\ &= P\left(\rho_{{\rm sd},i} + \alpha_i \rho_{{\rm rd},i} < -\Re[s_i(\rho_{{\rm sd},i} n_{{\rm sd},i} + \sqrt{\alpha_i}\rho_{{\rm rd},i} n_{{\rm rd},i})] | \mathcal{H}\right). \end{aligned} \tag{51}$$

Since $\Re[s_i(\rho_{{\rm sd},i} n_{{\rm sd},i} + \sqrt{\alpha_i}\rho_{{\rm rd},i} n_{{\rm rd},i})]$ is a real Gaussian random variable with zero mean and variance $\sigma_{\rm v}^2 = (\rho_{{\rm sd},i} + \alpha_i \rho_{{\rm rd},i})/2$,

$$\begin{aligned} P(s_i \to \tilde{s}_i|\hat{s}_{{\rm r},i} = s_i, \mathcal{H}) &= \frac{1}{\sqrt{2\pi\sigma_{\rm v}^2}} \int_{2\sigma_{\rm v}^2}^{\infty} \exp\left(-\frac{x^2}{2\sigma_{\rm v}^2}\right) dx \\ &= Q(2\sigma_{\rm v}) \\ &= Q\left(\sqrt{2(\rho_{{\rm sd},i} + \alpha_i \rho_{{\rm rd},i})}\right). \end{aligned} \tag{52}$$

Now, we consider $P(s_i \to \tilde{s}_i | \hat{s}_{\mathrm{r},i} = -s_i, \mathcal{H})$ in Eq. (49), which is the conditional error probability at the destination when the estimate at the relay is $\hat{s}_{\mathrm{r},i} = -s_i$. We derive this term similarly as in Eq. (51) and Eq. (52),

$$\begin{aligned} P(s_i \to \tilde{s}_i | \hat{s}_{\mathrm{r},i} = -s_i, \mathcal{H}) &= P(|\rho_{\mathrm{sd},i} n_{\mathrm{sd},i} + \sqrt{\alpha_i}\rho_{\mathrm{rd},i} n_{\mathrm{rd},i} + 2\rho_{\mathrm{sd},i} s_i|^2 < \\ &\qquad |\rho_{\mathrm{sd},i} n_{\mathrm{sd},i} + \sqrt{\alpha_i}\rho_{\mathrm{rd},i} n_{\mathrm{rd},i} - 2\alpha_i \rho_{\mathrm{rd},i} s_i|^2 \mid \mathcal{H}) \\ &= P\left(\frac{\rho_{\mathrm{sd,i}}^2 - \alpha_{\mathrm{i}}^2 \rho_{\mathrm{rd,i}}^2}{\rho_{\mathrm{sd,i}} + \alpha_{\mathrm{i}}\rho_{\mathrm{rd,i}}} < -\Re[s_{\mathrm{i}}(\rho_{\mathrm{sd,i}} n_{\mathrm{sd,i}} + \sqrt{\alpha_{\mathrm{i}}}\rho_{\mathrm{rd,i}} n_{\mathrm{rd,i}})] \mid \mathcal{H} \right) \\ &= P\left(\rho_{\mathrm{sd},i} - \alpha_i \rho_{\mathrm{rd},i} < -\Re[s_i(\rho_{\mathrm{sd},i} n_{\mathrm{sd},i} + \sqrt{\alpha_i}\rho_{\mathrm{rd},i} n_{\mathrm{rd},i})] | \mathcal{H} \right) \\ &= \frac{1}{\sqrt{2\pi\sigma_{\mathrm{v}}^2}} \int_{\rho_{\mathrm{sd},i} - \alpha_i \rho_{\mathrm{rd},i}}^{\infty} \exp\left(-\frac{x^2}{2\sigma_{\mathrm{v}}^2} \right) dx \\ &= Q\left(\frac{\sqrt{2}\left(\rho_{\mathrm{sd},i} - \alpha_i \rho_{\mathrm{rd},i}\right)}{\sqrt{\rho_{\mathrm{sd},i} + \alpha_i \rho_{\mathrm{rd},i}}} \right). \end{aligned} \tag{53}$$

Plugging Eqs. (50), (52), (53) into Eq. (49), we arrive at

$$\begin{aligned} P_{\mathrm{e},i|\mathcal{H}} &= \left\{1 - Q\left(\sqrt{2\rho_{\mathrm{sr},i}}\right)\right\} Q\left(\sqrt{2\left(\rho_{\mathrm{sd},i} + \alpha_i \rho_{\mathrm{rd},i}\right)} \right) \\ &\quad + Q\left(\sqrt{2\rho_{\mathrm{sr},i}}\right) Q\left(\frac{\sqrt{2}\left(\rho_{\mathrm{sd},i} - \alpha_i \rho_{\mathrm{rd},i}\right)}{\sqrt{\rho_{\mathrm{sd},i} + \alpha_i \rho_{\mathrm{rd},i}}} \right). \ \blacksquare \end{aligned}$$

The average SER of the i^{th} symbol $P_{\mathrm{e},i}$ can be obtained by averaging $P_{\mathrm{e},i|\mathcal{H}}$ with respect to random channel matrices. Then, diversity order can be obtained from $P_{\mathrm{e},i}$ using Definition 1.

Based on the instantaneous pairwise error probability provided in Lemma 7, the diversity order achieved by the power-scaling MIMO relay design is proved in Proposition 1.

Proposition 1 *Given the DF MIMO relay network system model in* (41)*, the power-scaling MIMO relay scheme proposed in Design 1 achieves cooperative diversity* 2 *at the destination, i.e.,* $G_d = 2$.

Proof: From Eq. (48) in Lemma 7, the instantaneous pairwise error probability of

the i^{th} symbol at the destination (with ZFE in Eq. (45)) is given as

$$\begin{aligned} P_{\mathrm{e},i|\mathcal{H}} &= \left\{1 - Q\left(\sqrt{2\rho_{\mathrm{sr},i}}\right)\right\} Q\left(\sqrt{2\left(\rho_{\mathrm{sd},i} + \alpha_i \rho_{\mathrm{rd},i}\right)}\right) \\ &\quad + Q\left(\sqrt{2\rho_{\mathrm{sr},i}}\right) Q\left(\frac{\sqrt{2}\left(\rho_{\mathrm{sd},i} - \alpha_i \rho_{\mathrm{rd},i}\right)}{\sqrt{\rho_{\mathrm{sd},i} + \alpha_i \rho_{\mathrm{rd},i}}}\right). \end{aligned}$$

Thanks to ZFE at the destination, for each symbol, the instantaneous pairwise error probability has exactly the same form as P_{b} in Eq. (7), which we repeat here,

$$\begin{aligned} P_{\mathrm{b}} &= \left\{1 - Q\left(\sqrt{2\rho_{\mathrm{sr}}}\right)\right\} Q\left(\sqrt{2(\rho_{\mathrm{sd}} + \alpha\rho_{\mathrm{rd}})}\right) \\ &\quad + Q\left(\sqrt{2\rho_{\mathrm{sr}}}\right) Q\left(\frac{\sqrt{2}(\rho_{\mathrm{sd}} - \alpha\rho_{\mathrm{rd}})}{\sqrt{\rho_{\mathrm{sd}} + \alpha\rho_{\mathrm{rd}}}}\right), \end{aligned}$$

where P_{b} is the instantaneous pairwise error probability at the destination for single-antenna relay networks.

To make the diversity claim for the power-scaling MIMO relay design, we will first show that $\rho_{\mathrm{sr},i}$ and ρ_{sr} have the same distribution, where $\rho_{\mathrm{sr}} = |h_{\mathrm{sr}}|^2\bar{\rho}$ from Eq. (6). When h_{sr} is complex Gaussian distributed with zero mean and unit variance, ρ_{sr} is a chi-squared random variable with degree 2.

On the other hand, in [67, Appendix A], it is proved that $\frac{1}{\left(\boldsymbol{H}^{\mathcal{H}}\boldsymbol{H}\right)^{-1}_{i,i}}$ is a chi-squared random variable with $2(N_{\mathrm{r}} - N_{\mathrm{t}} + 1)$ degrees of freedom when $\boldsymbol{H}$ is the $N_{\mathrm{r}} \times N_{\mathrm{t}}$ random channel with all the entries i.i.d. complex Gaussian distributed with zero mean and unit variance. Since we have $\rho_{\mathrm{sr},i} = \frac{\bar{\rho}}{\left(\boldsymbol{H}_{\mathrm{sr}}^{\mathcal{H}}\boldsymbol{H}_{\mathrm{sr}}\right)^{-1}_{i,i}}$ from Eq. (46), and $\boldsymbol{H}_{\mathrm{sr}}$ is $N \times N$ complex Gaussian channel matrices, we know that $\rho_{\mathrm{sr},i}$ is also a chi-squared random variable with degree 2. Thus, $\rho_{\mathrm{sr},i}$ and ρ_{sr} have the same distribution. Same results can be obtained for $\rho_{\mathrm{rd},i}$ and $\rho_{\mathrm{sd},i}$.

Now, given $\rho_{\mathrm{sr},i}$ and ρ_{sr} have the same distribution, α_i can be designed so that $E[P_{\mathrm{e},i|\mathcal{H}}]$ and $E[P_{\mathrm{b}}]$ have the same diversity order. For single-antenna relay networks, it is shown in Section 3.3.3 that $E[P_{\mathrm{b}}]$ achieves cooperative diversity 2 if PSF α satisfies the necessary and sufficient conditions **NSC1)-NSC4)** such as

$$\alpha = \lambda \min\left(|h_{sr}|^2, \xi\right) = \lambda \min\left(\frac{\rho_{\mathrm{sr}}}{\bar{\rho}}, \xi\right).$$

Since $\rho_{\mathrm{sr},i}$ and ρ_{sr} are analogous, if PSF α_i for DF MIMO relay networks is designed as

$$\alpha_i = \lambda \min\left(\frac{\rho_{\mathrm{sr},i}}{\bar{\rho}}, \xi\right) = \lambda \min\left(\frac{1}{\left(\boldsymbol{H}_{\mathrm{sr}}^{\mathcal{H}}\boldsymbol{H}_{\mathrm{sr}}\right)_{i,i}^{-1}}, \xi\right),$$

then $P_{\mathrm{e},i} = E[P_{\mathrm{e},i|\mathcal{H}}]$ also has a diversity order of 2. ■

We have proved that cooperative diversity 2 is achieved by power-scaling MIMO relay design. Note that, as discussed in [22, 108], the diversity order of the average SER is not affected by the underlying modulation constellations. General constellations are considered in [22] by using the upper and lower bounds of the average SER, and thus, the diversity claims extend to higher order constellation schemes. Through the rest of this chapter, the diversity order is proved for the average SER with BPSK.

4.2.2 General Link-Adaptive Relay Strategy for Power-Scaling MIMO Relay

In Chapter 3, general link-adaptive relay strategy was studied for single-antenna cooperative relay networks. Since the instantaneous pairwise error probability for MIMO relay networks derived in Lemma 7 has the same form as that for single-antenna relay networks which is shown in Eq. (7), and distributions of $\rho_{\mathrm{sr},i}$ and ρ_{sr} are identical as shown in Proposition 1, general link-adaptive relay strategy introduced in Chapter 3 can be applied to power-scaling MIMO relay design. As a result, diversity claim in Theorem 1 can be easily extended to power-scaling MIMO relay case.

Using the same descriptions **D1)-D3)** in Section 3.2.2 for $\alpha_i\left(\frac{1}{(\boldsymbol{H}_{\mathrm{sr}}^{\mathcal{H}}\boldsymbol{H}_{\mathrm{sr}})_{i,i}^{-1}}\right)$, the diversity order achieved by general power-profile design $\boldsymbol{A}$ with $\alpha_i\left(\frac{1}{(\boldsymbol{H}_{\mathrm{sr}}^{\mathcal{H}}\boldsymbol{H}_{\mathrm{sr}})_{i,i}^{-1}}\right)$ for power-scaling MIMO relay design is presented in the following.

Corollary 3 *Consider a relay system in* (41) *with a general power-profile design* $\alpha_i\left(\frac{1}{(\boldsymbol{H}_{\mathrm{sr}}^{\mathcal{H}}\boldsymbol{H}_{\mathrm{sr}})_{i,i}^{-1}}\right)$ *for* i^{th} *antenna at the relay node. The diversity order of the average SER at the destination is*

$$G_d = 1 + \min\{g_1(p_1), g_2(p_{1k}^{(l)}), g_2(p_{1k}^{(r)}), g_3(r_k^{(r)} - r_k^{(l)})\},$$

where p_1, $p_{1k}^{(l)}$, $p_{1k}^{(r)}$, $r_k^{(l)}$, *and* $r_k^{(r)}$ *are defined in* **D1)-D3)**, *and* $g_1(\cdot)$, $g_2(\cdot)$, *and* $g_3(\cdot)$ *are from Definition 2.*

Note that, α_i is now a function of $\frac{1}{(\boldsymbol{H}_{\text{sr}}^{\mathcal{H}}\boldsymbol{H}_{\text{sr}})_{i,i}^{-1}}$ instead of $|h_{sr}|^2$ as in Section 3.2.2.

Accordingly, the necessary and sufficient conditions to enable cooperative diversity 2 for power-scaling MIMO relay can be summarized as follows.

NSC1) $\alpha_i\left(\frac{1}{(\boldsymbol{H}_{\text{sr}}^{\mathcal{H}}\boldsymbol{H}_{\text{sr}})_{i,i}^{-1}}=0\right)=0$.

NSC2) The set $\{x:\alpha(x)=0\}$ is measure zero, i.e., no zero interval, so that $g_3(r_k^{(r)}-r_k^{(l)})=1$.

NSC3) The behavior of $\alpha_i\left(\frac{1}{(\boldsymbol{H}_{\text{sr}}^{\mathcal{H}}\boldsymbol{H}_{\text{sr}})_{i,i}^{-1}}\right)$ approaching the origin point is linear ($p_1=1$) so that $g_1(p_1)=1$.

NSC4) If $\alpha_i\left(\frac{1}{(\boldsymbol{H}_{\text{sr}}^{\mathcal{H}}\boldsymbol{H}_{\text{sr}})_{i,i}^{-1}}\right)=0$ has roots other than the origin, the behavior of $\alpha_i\left(\frac{1}{(\boldsymbol{H}_{\text{sr}}^{\mathcal{H}}\boldsymbol{H}_{\text{sr}})_{i,i}^{-1}}\right)$ near those roots must satisfy $p_{1k}^{(l)}\leq 1$ and $p_{1k}^{(r)}\leq 1$ so that $g_2(p_{1k}^{(l)})=1$ and $g_2(p_{1k}^{(r)})=1$.

Now, we validate Corollary 3 with some examples. Power profile designs α_{Aa} and α_{Ad} from Figure 7 and α_{Ba} and α_{Bc} from Figure 9 are shown in Figure 20 and the bit-error rate (BER) for each power profile for power-scaling MIMO relay with $N=2$ is plotted in Figure 21. For each design, the same power profile function is used for all antennas, but the instantaneous PSF may be different for each symbol since the $\frac{1}{(\boldsymbol{H}_{\text{sr}}^{\mathcal{H}}\boldsymbol{H}_{\text{sr}})_{i,i}^{-1}}$ may be different for different i. α_{Aa} is a power profile designed in Eq. (47) and it was proved in Proposition 1 that cooperative diversity 2 is achieved with this PSF. α_{Ad} has a zero interval, i.e., there exists a k such that $g_3(r_k^{(r)}-r_k^{(l)})=0$. Thus, diversity order achieved is 1 according to Corollary 3. For α_{Ba} and α_{Bc}, the behavior is described as $\left(\frac{1}{(\boldsymbol{H}_{\text{sr}}^{\mathcal{H}}\boldsymbol{H}_{\text{sr}})_{i,i}^{-1}}\right)^4$ and $\left(\frac{1}{(\boldsymbol{H}_{\text{sr}}^{\mathcal{H}}\boldsymbol{H}_{\text{sr}})_{i,i}^{-1}}\right)^{\frac{1}{2}}$ around the origin, and according to Corollary 3, they enable diversity order of $1+g_1(4)=1.25$ and $1+g_1(1/2)=1.5$, respectively. The results are verified in Figure 21.

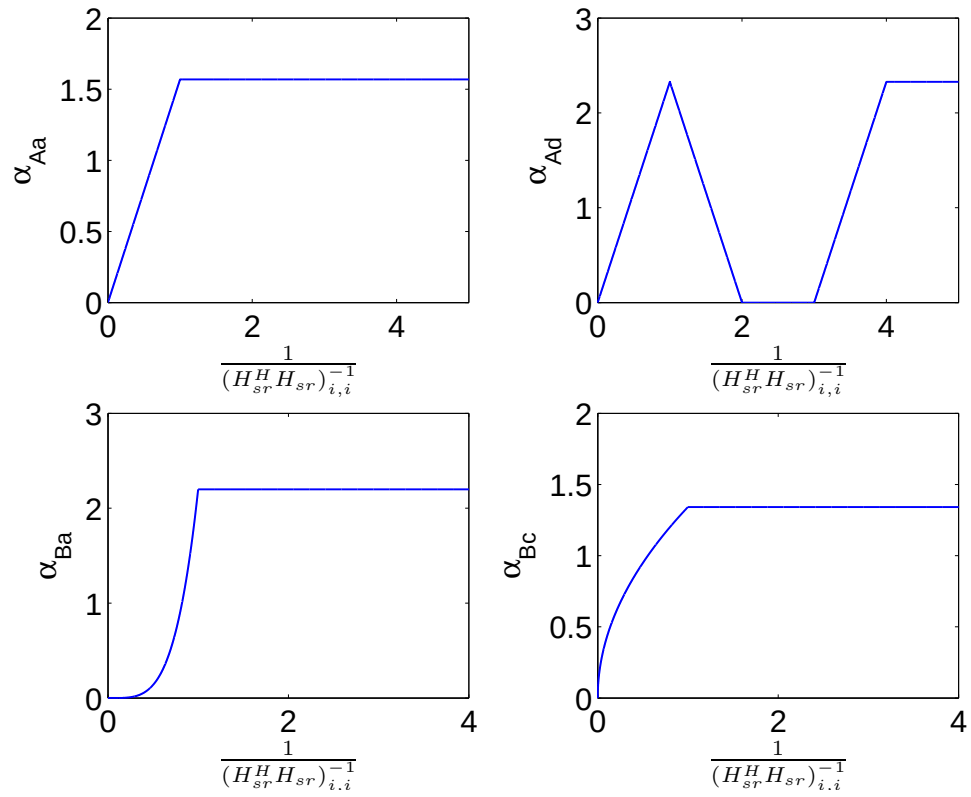

Figure 20: Power profiles α_{Aa}, α_{Ad}, α_{Ba}, and α_{Bc} for power-scaling MIMO relay.

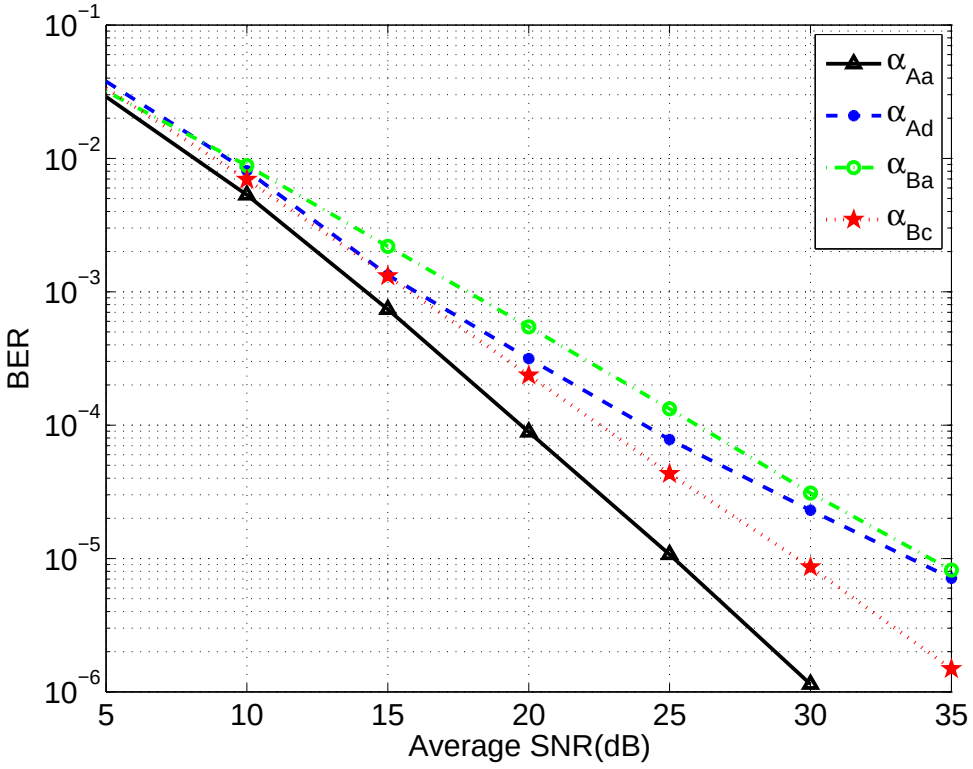

Figure 21: BER of α_{Aa}, α_{Ad}, α_{Ba}, and α_{Bc} for power-scaling MIMO relay with $N = 2$.

4.3 MIMO Relay with CC-ARQ

In the previous design, multiple antennas are used at receiver sides, however, receiver diversity is not collected at the destination. ZFE comes with low complexity, but provides inferior error performance. As shown in [66], the performance of ZFE is directly linked to the orthogonality deficiency (*od*) of channel matrices, which we introduce below.

Definition 3 *For an $M \times N$ matrix $\boldsymbol{B} = [\boldsymbol{b}_1, \boldsymbol{b}_2, \ldots, \boldsymbol{b}_N]$, with $\boldsymbol{b}_n$ being the n^{th} column of $\boldsymbol{B}$, its orthogonality deficiency (od) is defined as*

$$od(\boldsymbol{B}) = 1 - \frac{\det(\boldsymbol{B}^{\mathcal{H}}\boldsymbol{B})}{\prod_{n=1}^{N} \|\boldsymbol{b}_n\|^2},$$

where $\|\boldsymbol{b}_n\|, 1 \leq n \leq N$ is the norm of the n^{th} column of $\boldsymbol{B}$.

As revealed in [66], the fundamental condition for ZFE to collect receive diversity as MLE does is that the *od* of channel matrices is bounded above by a constant strictly less than 1. However, the *od* of channel matrices with i.i.d. complex Gaussian distributed does not meet the fundamental condition [66].

In this section, we propose a channel-controlled (CC-) ARQ design which depends on the *od* of channel matrices. Alternative to diversity techniques in physical layer, this ARQ scheme helps to achieve reliable transmission over MIMO fading channels in data link layer. Different from traditional ARQ techniques for which the retransmission request is sent if error is detected using CRC, CC-ARQ requires retransmission when *od* of the channel matrix is higher than a fixed threshold ϵ_{th}, which is strictly less than 1, and thus satisfying the fundamental condition when ZFE is applied.

We will prove that discarding packets transmitted through poor channels before decoding restores receive diversity for ZFEs and is more power efficient than the use of CRC because: (i) no need to insert extra bits for error detecting; (ii) no need to decode CRC for retransmissions; and (iii) no need to assume perfect CRC to guarantee diversity. We summarize the design of MIMO relay with CC-ARQ as follows.

Design 2 (MIMO Relay with CC-ARQ) *Given the DF MIMO relay network system model in* (41) *and a threshold* $\epsilon_{\text{th}} \in (0,1)$*, the protocol of MIMO relay with CC-ARQ is designed as in Figure 22. Here, the relay adopts an identity PSF matrix* $\boldsymbol{A}^{\frac{1}{2}} = \boldsymbol{I}_N$ *in* (41).

The CC-ARQ transmission protocol in Figure 22 can be divided into two phases. In the first phase, the source transmits and the relay and/or the destination request retransmissions to the source until both $od(\boldsymbol{H}_{\text{sr}}) \leq \epsilon_{\text{th}}$ and $od(\boldsymbol{H}_{\text{sd}}) \leq \epsilon_{\text{th}}$ are satisfied. If $\boldsymbol{H}_{\text{sr}}$ ($\boldsymbol{H}_{\text{sd}}$) satisfies the *od* condition, but $\boldsymbol{H}_{\text{sd}}$ ($\boldsymbol{H}_{\text{sr}}$) does not, the destination (relay) sends the retransmission requests until $od(\boldsymbol{H}_{\text{sd}}) \leq \epsilon_{\text{th}}$ ($od(\boldsymbol{H}_{\text{sr}}) \leq \epsilon_{\text{th}}$). In the meantime, the relay (destination) hears another copy of $\boldsymbol{y}_{\text{sr}}$ ($\boldsymbol{y}_{\text{sd}}$), and chooses the one with the smaller corresponding $od(\boldsymbol{H}_{\text{sr}})$ ($od(\boldsymbol{H}_{\text{sd}})$). The relay decodes and forwards in the second phase and the destination requests retransmission to the relay if $od(\boldsymbol{H}_{\text{rd}}) \leq \epsilon_{\text{th}}$ is not satisfied during the phase. In this way, all channels meet the *od* condition. At the final step, the destination has one $\boldsymbol{y}_{\text{sd}}$ and one $\boldsymbol{y}_{\text{rd}}$ to combine for each packet.

Now, performance analysis of the diversity order of the proposed MIMO relay with CC-ARQ scheme is provided in the following.

4.3.1 Performance Analysis

Before the diversity order of the average SER of the proposed MIMO relay with CC-ARQ is established, we find upper and lower bounds of the channel gain in the following lemma.

Lemma 8 *Let* $\boldsymbol{h}_i$ *be the* i^{th} *column of* $\boldsymbol{H}$*. Provided* $od(\boldsymbol{H}) \leq \epsilon_{\text{th}}$*,* $\frac{1}{\left(\boldsymbol{H}^{\mathcal{H}}\boldsymbol{H}\right)^{-1}_{i,i}}$ *is bounded above and below by*

$$(1-\epsilon_{\text{th}})\left\|\boldsymbol{h}_i\right\|^2 \leq \frac{1}{\left(\boldsymbol{H}^{\mathcal{H}}\boldsymbol{H}\right)^{-1}_{i,i}} \leq \left\|\boldsymbol{h}_i\right\|^2.$$

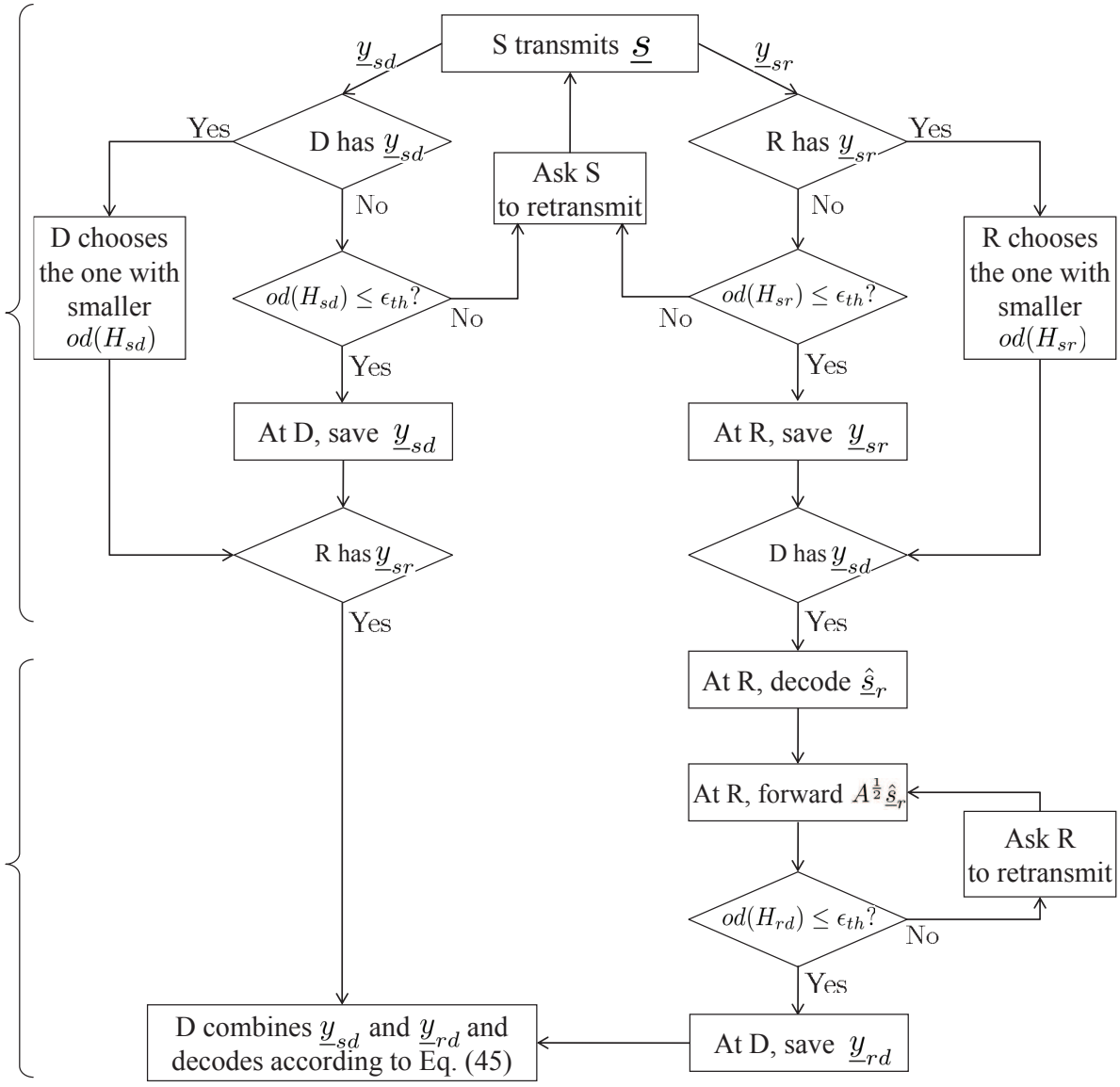

Figure 22: CC-ARQ protocol for DF MIMO relay networks.

Proof: Let $\boldsymbol{a}_i^T$ be the i^{th} row of $\boldsymbol{H}^\dagger = (\boldsymbol{H}^{\mathcal{H}}\boldsymbol{H})^{-1}\boldsymbol{H}^{\mathcal{H}}$. Then, $\boldsymbol{a}_i$ is the i^{th} column of $(\boldsymbol{H}^\dagger)^{\mathcal{H}}$. Since $\boldsymbol{H}^\dagger(\boldsymbol{H}^\dagger)^{\mathcal{H}} = \left(\boldsymbol{H}^{\mathcal{H}}\boldsymbol{H}\right)^{-1}$, we arrive at

$$\left(\boldsymbol{H}^{\mathcal{H}}\boldsymbol{H}\right)^{-1}_{i,i} = \boldsymbol{a}_i^T\boldsymbol{a}_i = \|\boldsymbol{a}_i^T\|^2. \tag{54}$$

Also, from $\boldsymbol{H}^\dagger\boldsymbol{H} = \boldsymbol{I}_N$, it is shown that $1 = \boldsymbol{a}_i^T\boldsymbol{h}_i$. By Cauchy-Schwarz inequality, we obtain

$$1 \leq \|\boldsymbol{a}_i^T\|^2\|\boldsymbol{h}_i\|^2. \tag{55}$$

The upper bound can be derived from Eqs. (54) and (55).

The proof for the lower bound can be derived from [94, Lemma 1] where orthogonality defect δ is defined as $\delta = \frac{1}{1-od(\boldsymbol{H})}$. From Eq. (3) in [94], if δ is bounded, or $od(\boldsymbol{H}) \leq \epsilon_{\text{th}}$, we have

$$\|\boldsymbol{h}_i\|^2 \leq \frac{\delta}{\|\boldsymbol{a}_i^T\|^2},$$

and, from the definition of δ and Eq. (54), this is equivalent to

$$(1-\epsilon_{\text{th}})\|\boldsymbol{h}_i\|^2 \leq \frac{1}{\left(\boldsymbol{H}^{\mathcal{H}}\boldsymbol{H}\right)^{-1}_{i,i}}. \quad \blacksquare$$

Using the above upper and lower bounds of $\frac{1}{\left(\boldsymbol{H}^{\mathcal{H}}\boldsymbol{H}\right)^{-1}_{i,i}}$, the diversity order of the average SER of the proposed MIMO relay with the CC-ARQ scheme is established as follows.

Proposition 2 *Given the DF MIMO relay network system model in* (41)*, MIMO relay with the CC-ARQ scheme proposed in Design 2 achieves full receive diversity at the destination, i.e.,* $G_d = N$.

Proof: Since $\alpha_i = 1$ (no power scaling) in this scheme, the instantaneous pairwise error probability of s_i in Eq. (48) can be written as

$$\begin{aligned} P_{\text{e},i|\mathcal{H}} &= \left\{1 - Q\left(\sqrt{2\rho_{\text{sr},i}}\right)\right\} Q\left(\sqrt{2\left(\rho_{\text{sd},i}+\rho_{\text{rd},i}\right)}\right) \\ &\quad + Q\left(\sqrt{2\rho_{\text{sr},i}}\right) Q\left(\frac{\sqrt{2}\left(\rho_{\text{sd},i}-\rho_{\text{rd},i}\right)}{\sqrt{\rho_{\text{sd},i}+\rho_{\text{rd},i}}}\right). \end{aligned}$$

The average of $P_{\mathrm{e},i|\mathcal{H}}$ is bounded below by the average of the second term, which is derived as

$$\begin{aligned}
P_{\mathrm{e},i} &\geq E\left[Q\left(\sqrt{2\rho_{\mathrm{sr},i}}\right)\right] E\left[Q\left(\frac{\sqrt{2}\left(\rho_{\mathrm{sd},i}-\rho_{\mathrm{rd},i}\right)}{\sqrt{\rho_{\mathrm{sd},i}+\rho_{\mathrm{rd},i}}}\right)\right] \\
&\geq E\left[Q\left(\sqrt{\frac{2\bar{\rho}}{\left(\boldsymbol{H}_{\mathrm{sr}}^{\mathcal{H}}\boldsymbol{H}_{\mathrm{sr}}\right)_{i,i}^{-1}}}\right)\right] P(\rho_{\mathrm{sd},i}<\rho_{\mathrm{rd},i})\; E\left[Q\left(\frac{\sqrt{2}\left(\rho_{\mathrm{sd},i}-\rho_{\mathrm{rd},i}\right)}{\sqrt{\rho_{\mathrm{sd},i}+\rho_{\mathrm{rd},i}}}\right)\Bigg|\rho_{\mathrm{sd},i}<\rho_{\mathrm{rd},i}\right] \\
&\geq \frac{1}{2}\; P(\rho_{\mathrm{sd},i}<\rho_{\mathrm{rd},i})\; E\left[Q\left(\sqrt{2\bar{\rho}\|\boldsymbol{h}_{\mathrm{sr},i}\|^2}\right)\right] \\
&= \frac{1}{2}\; P(\rho_{\mathrm{sd},i}<\rho_{\mathrm{rd},i})\; E\left[Q\left(\sqrt{\sigma_{\mathrm{sr}}^2\bar{\rho}\frac{2\|\boldsymbol{h}_{\mathrm{sr},i}\|^2}{\sigma_{\mathrm{sr}}^2}}\right)\right], \qquad (56)
\end{aligned}$$

where the last inequality is based on Lemma 8 and the inequality $Q(x)\geq 1/2$ for $x\leq 0$. Since $\boldsymbol{H}_{\mathrm{sr}}$ is the $N\times N$ random channel with all entries being i.i.d. complex Gaussian variables with zero mean and variance σ_{sr}^2, it can be seen that $\frac{2\|\boldsymbol{h}_{\mathrm{sr},i}\|^2}{\sigma_{\mathrm{sr}}^2}$ is a chi-squared random variable with $2N$ degrees of freedom. According to [109, Proposition 1], if we integrate the last term in Eq. (56) with respect to $\frac{2\|\boldsymbol{h}_{\mathrm{sr},i}\|^2}{\sigma_{\mathrm{sr}}^2}$, the diversity order of Eq. (56) is at most N. Therefore, we obtain

$$P_{\mathrm{e},i}\;\dot{\geq}\;\bar{\rho}^{-N}. \qquad (57)$$

Now, we consider the upper bound of $P_{\mathrm{e},i|\mathcal{H}}$. From $Q(x)\leq 1$ and Lemma 8, we bound $P_{\mathrm{e},i|\mathcal{H}}$ above as

$$\begin{aligned}
P_{\mathrm{e},i|\mathcal{H}} &\leq Q\left(\sqrt{2\left(\rho_{\mathrm{sd},i}+\rho_{\mathrm{rd},i}\right)}\right)+Q\left(\sqrt{2\rho_{\mathrm{sr},i}}\right) \\
&= Q\left(\sqrt{\frac{2\bar{\rho}}{\left(\boldsymbol{H}_{\mathrm{sd}}^{\mathcal{H}}\boldsymbol{H}_{\mathrm{sd}}\right)_{i,i}^{-1}}+\frac{2\bar{\rho}}{\left(\boldsymbol{H}_{\mathrm{rd}}^{\mathcal{H}}\boldsymbol{H}_{\mathrm{rd}}\right)_{i,i}^{-1}}}\right)+Q\left(\sqrt{\frac{2\bar{\rho}}{\left(\boldsymbol{H}_{\mathrm{sr}}^{\mathcal{H}}\boldsymbol{H}_{\mathrm{sr}}\right)_{i,i}^{-1}}}\right) \\
&\leq Q\left(\sqrt{\frac{2\bar{\rho}}{\left(\boldsymbol{H}_{\mathrm{sd}}^{\mathcal{H}}\boldsymbol{H}_{\mathrm{sd}}\right)_{i,i}^{-1}}}\right)+Q\left(\sqrt{\frac{2\bar{\rho}}{\left(\boldsymbol{H}_{\mathrm{sr}}^{\mathcal{H}}\boldsymbol{H}_{\mathrm{sr}}\right)_{i,i}^{-1}}}\right) \\
&\leq Q\left(\sqrt{2\bar{\rho}(1-\epsilon_{\mathrm{th}})\|\boldsymbol{h}_{\mathrm{sd},i}\|^2}\right)+Q\left(\sqrt{2\bar{\rho}(1-\epsilon_{\mathrm{th}})\|\boldsymbol{h}_{\mathrm{sr},i}\|^2}\right). \qquad (58)
\end{aligned}$$

Since both $\frac{2\|\boldsymbol{h}_{\mathrm{sd},i}\|^2}{\sigma_{\mathrm{sd}}^2}$ and $\frac{2\|\boldsymbol{h}_{\mathrm{sr},i}\|^2}{\sigma_{\mathrm{sr}}^2}$ are chi-squared random variables with $2N$ degrees of freedom, we integrate Eq. (58) with respect to $\frac{2\|\boldsymbol{h}_{\mathrm{sd},i}\|^2}{\sigma_{\mathrm{sd}}^2}$ and $\frac{2\|\boldsymbol{h}_{\mathrm{sr},i}\|^2}{\sigma_{\mathrm{sr}}^2}$ to get

$$P_{\mathrm{e},i} \dot{\leq} \bar{\rho}^{-N}. \tag{59}$$

From Eqs. (57) and (59), we conclude that $P_{\mathrm{e},i} \doteq \bar{\rho}^{-N}$. Thus, MIMO relay with the CC-ARQ scheme achieves full receive diversity, which is N. ■

As we have seen, discarding packets transmitted through high *od* channels before decoding is a good choice to improve the reliability of the transmission and power efficiency, though the discarded packets do not necessarily contain errors. Receive diversity is collected at the destination without the use of CRC. However, the disadvantage of CC-ARQ is that similar to all other ARQ methods, it causes long delay and low throughput when experiencing a deep fading in a slow-fading environment. That means retransmissions may be required for many times until the link recovers from deep fading. For practical systems, truncated CC-ARQ can be applied by limiting the maximum number of retransmissions to reduce the packet delay.

4.4 Power-Scaling MIMO Relay with CC-ARQ

In previous sections, we have developed two schemes that enabled cooperative diversity or receive diversity. However, neither of them can achieve joint cooperative and receive diversity $2N$. Here, we combine those two schemes to enable joint diversity for DF MIMO relay networks. The design of the power-scaling MIMO relay with CC-ARQ is given in the following.

Design 3 (Power-Scaling MIMO Relay with CC-ARQ) *Given the DF MIMO relay network system model in* (41) *and a threshold* $\epsilon_{\mathrm{th}} \in (0, 1)$*, the protocol of power-scaling MIMO relay with CC-ARQ is designed as in Figure 22. Here, the relay employs the PSF matrix and transmits* $\boldsymbol{A}^{\frac{1}{2}}\hat{\boldsymbol{s}}_{\mathrm{r}}$ *with* α_i *in Eq.* (47)*.*

The design of power-scaling MIMO relay with CC-ARQ is the same as that of MIMO relay with CC-ARQ in Design 2 except for the PSF matrix $\boldsymbol{A}$.

4.4.1 Performance Analysis

Now, we quantify the performance of the power-scaling MIMO relay with the CC-ARQ scheme in the following proposition.

Proposition 3 *Given the DF MIMO relay network system model in* (41)*, the power-scaling MIMO relay with the CC-ARQ scheme proposed in Design 3 achieves joint cooperative and receive diversity at the destination, i.e.,* $G_d = 2N$.

Proof: Here, we repeat the $P_{\mathrm{e},i|\mathcal{H}}$ expression in Eq. (48),

$$\begin{aligned} P_{\mathrm{e},i|\mathcal{H}} &= \left\{1 - Q\left(\sqrt{2\rho_{\mathrm{sr},i}}\right)\right\} Q\left(\sqrt{2\left(\rho_{\mathrm{sd},i} + \alpha_i \rho_{\mathrm{rd},i}\right)}\right) \\ &\quad + Q\left(\sqrt{2\rho_{\mathrm{sr},i}}\right) Q\left(\frac{\sqrt{2}\left(\rho_{\mathrm{sd},i} - \alpha_i \rho_{\mathrm{rd},i}\right)}{\sqrt{\rho_{\mathrm{sd},i} + \alpha_i \rho_{\mathrm{rd},i}}}\right) \\ &=: P_{\mathrm{e1},i|\mathcal{H}} + P_{\mathrm{e2},i|\mathcal{H}}. \end{aligned} \tag{60}$$

First, we find upper and lower bounds of $P_{\mathrm{e1},i|\mathcal{H}}$ in the following,

$$\begin{aligned} & \frac{1}{2} Q\left(\sqrt{\bar{\rho}\sigma_{\mathrm{sd}}^2 \left(\frac{2\|\boldsymbol{h}_{\mathrm{sd},i}\|^2}{\sigma_{\mathrm{sd}}^2} + \lambda\xi \frac{\sigma_{\mathrm{rd}}^2}{\sigma_{\mathrm{sd}}^2} \frac{2\|\boldsymbol{h}_{\mathrm{rd},i}\|^2}{\sigma_{\mathrm{rd}}^2}\right)}\right) \\ \leq\ & P_{\mathrm{e1},i|\mathcal{H}} \\ \leq\ & Q\left(\sqrt{2\bar{\rho}\left(1 - \epsilon_{\mathrm{th}}\right)\left(\|\boldsymbol{h}_{\mathrm{sd},i}\|^2 + \alpha_i \|\boldsymbol{h}_{\mathrm{rd},i}\|^2\right)}\right), \end{aligned} \tag{61}$$

where Lemma 8 is used. Since both $\frac{2\|\boldsymbol{h}_{\mathrm{sd},i}\|^2}{\sigma_{\mathrm{sd}}^2}$ and $\frac{2\|\boldsymbol{h}_{\mathrm{rd},i}\|^2}{\sigma_{\mathrm{rd}}^2}$ are independent chi-squared random variables with $2N$ degrees of freedom, the upper bound of the diversity order based on the left-hand-side (LHS) of (61) is $2N$. Thus, we have

$$P_{\mathrm{e1},i} \dot{\geq} \bar{\rho}^{-2N}. \tag{62}$$

For the upper bound of $P_{\mathrm{e1},i|\mathcal{H}}$, we use Lemma 8 and Chernoff bound [21] on Q-function to derive,

$$\begin{aligned} P_{\mathrm{e1},i|\mathcal{H}} &\leq \exp\left(-\bar{\rho}\left(1-\epsilon_{\mathrm{th}}\right)\left(\|\boldsymbol{h}_{\mathrm{sd},i}\|^2+\alpha_i\|\boldsymbol{h}_{\mathrm{rd},i}\|^2\right)\right) \\ &\leq \exp\left(-\left(1-\epsilon_{\mathrm{th}}\right)\left(\rho'_{\mathrm{sd},i}\sigma^2_{\mathrm{sd}}+\alpha'_i\rho'_{\mathrm{rd},i}\sigma^2_{\mathrm{rd}}\right)\right), \end{aligned} \tag{63}$$

where we defined

$$\begin{aligned} \rho'_{\mathrm{sr},i} &:= \frac{\|\boldsymbol{h}_{\mathrm{sr},i}\|^2}{\sigma^2_{\mathrm{sr}}N_0}, \\ \rho'_{\mathrm{sd},i} &:= \frac{\|\boldsymbol{h}_{\mathrm{sd},i}\|^2}{\sigma^2_{\mathrm{sd}}N_0}, \\ \rho'_{\mathrm{rd},i} &:= \frac{\|\boldsymbol{h}_{\mathrm{rd},i}\|^2}{\sigma^2_{\mathrm{rd}}N_0}, \\ \text{and}\ \ \alpha'_i &:= \lambda\min\left(\frac{\left(1-\epsilon_{\mathrm{th}}\right)\rho'_{\mathrm{sr},i}\sigma^2_{\mathrm{sr}}}{\bar{\rho}},\xi\right). \end{aligned} \tag{64}$$

Now, we integrate Eq. (63) with respect to $\rho'_{\mathrm{sd},i}$, $\rho'_{\mathrm{sr},i}$ and $\rho'_{\mathrm{rd},i}$ to obtain the upper bound of $P_{\mathrm{e1},i}$ as

$$\begin{aligned} P_{\mathrm{e1},i} &\leq \int_0^\infty\int_0^\infty\int_0^\infty \exp\left(-\left(1-\epsilon_{\mathrm{th}}\right)\left(\rho'_{\mathrm{sd},i}\sigma^2_{\mathrm{sd}}+\alpha'_i\rho'_{\mathrm{rd},i}\sigma^2_{\mathrm{rd}}\right)\right) \\ &\quad\times f(\rho'_{\mathrm{sd},i})f(\rho'_{\mathrm{rd},i})f(\rho'_{\mathrm{sr},i})d\rho'_{\mathrm{sd},i}d\rho'_{\mathrm{rd},i}d\rho'_{\mathrm{sr},i} \\ &= \int_0^\infty \exp\left(-\left(1-\epsilon_{\mathrm{th}}\right)\rho'_{\mathrm{sd},i}\sigma^2_{\mathrm{sd}}\right)f(\rho'_{\mathrm{sd},i})d\rho'_{\mathrm{sd},i} \\ &\quad\times\int_0^\infty\int_0^\infty \exp\left(-\left(1-\epsilon_{\mathrm{th}}\right)\alpha'_i\rho'_{\mathrm{rd},i}\sigma^2_{\mathrm{rd}}\right)f(\rho'_{\mathrm{rd},i})f(\rho'_{\mathrm{sr},i})d\rho'_{\mathrm{rd},i}d\rho'_{\mathrm{sr},i} \\ &= \left(\frac{\bar{\rho}}{1+(1-\epsilon_{\mathrm{th}})\bar{\rho}\sigma^2_{\mathrm{sd}}}\right)^N\left(\frac{1}{\bar{\rho}}\right)^N \\ &\quad\times\int_0^\infty f(\rho'_{\mathrm{sr},i})\left(\int_0^\infty \exp\left(-\left(1-\epsilon_{\mathrm{th}}\right)\alpha'_i\rho'_{\mathrm{rd},i}\sigma^2_{\mathrm{rd}}\right)f(\rho'_{\mathrm{rd},i})d\rho'_{\mathrm{rd},i}\right)d\rho'_{\mathrm{sr},i} \\ &= \left(\frac{\bar{\rho}}{1+(1-\epsilon_{\mathrm{th}})\bar{\rho}\sigma^2_{\mathrm{sd}}}\right)^N\left(\frac{1}{\bar{\rho}}\right)^{2N}\int_0^\infty f(\rho'_{\mathrm{sr},i})\left(\frac{\bar{\rho}}{1+(1-\epsilon_{\mathrm{th}})\alpha'_i\bar{\rho}\sigma^2_{\mathrm{rd}}}\right)^N d\rho'_{\mathrm{sr},i}, \end{aligned} \tag{65}$$

where the PDF of ρ' is

$$f(\rho') = \frac{1}{\Gamma(N)}\left(\frac{1}{\bar{\rho}}\right)^N(\rho')^{N-1}\exp\left(-\frac{\rho'}{\bar{\rho}}\right),$$

since $2\rho'_{\mathrm{sd},i}/\bar{\rho}$, $2\rho'_{\mathrm{rd},i}/\bar{\rho}$, and $2\rho'_{\mathrm{sr},i}/\bar{\rho}$ are all chi-squared random variables with $2N$ degrees of freedom with $\Gamma(N) = (N-1)!$. Substituting α'_i from Eq. (64) to the integral in Eq. (65), we have

$$\begin{aligned}
&\int_0^{\infty} f(\rho'_{\mathrm{sr},i}) \left(\frac{\bar{\rho}}{1+(1-\epsilon_{\mathrm{th}})\alpha'_i\bar{\rho}\sigma^2_{\mathrm{rd}}}\right)^N d\rho'_{\mathrm{sr},i} \\
\leq\ & \frac{1}{\Gamma(N)} \int_0^{\frac{\xi\bar{\rho}}{(1-\epsilon_{\mathrm{th}})\sigma^2_{\mathrm{sr}}}} \left(\rho'_{\mathrm{sr},i}\right)^{N-1} \left(\frac{1}{1+\lambda(1-\epsilon_{\mathrm{th}})^2\rho'_{\mathrm{sr},i}\sigma^2_{\mathrm{sr}}\sigma^2_{\mathrm{rd}}}\right)^N d\rho'_{\mathrm{sr},i} + \left(\frac{1}{\lambda(1-\epsilon_{\mathrm{th}})\xi\sigma^2_{\mathrm{rd}}}\right)^N \\
=\ & \frac{1}{\Gamma(N)} \int_0^{\lambda(1-\epsilon_{\mathrm{th}})\xi\bar{\rho}\sigma^2_{\mathrm{rd}}} \left(\frac{t}{\lambda(1-\epsilon_{\mathrm{th}})^2\sigma^2_{\mathrm{sr}}\sigma^2_{\mathrm{rd}}}\right)^{N-1} \left(\frac{1}{1+t}\right)^N \frac{1}{\lambda(1-\epsilon_{\mathrm{th}})^2\sigma^2_{\mathrm{sr}}\sigma^2_{\mathrm{rd}}} dt \\
&+ \left(\frac{1}{\lambda(1-\epsilon_{\mathrm{th}})\xi\sigma^2_{\mathrm{rd}}}\right)^N \\
\leq\ & \frac{1}{\Gamma(N)} \left(\frac{1}{\lambda(1-\epsilon_{\mathrm{th}})^2\sigma^2_{\mathrm{sr}}\sigma^2_{\mathrm{rd}}}\right)^N \int_0^{\lambda(1-\epsilon_{\mathrm{th}})\xi\bar{\rho}\sigma^2_{\mathrm{rd}}} \frac{1}{1+t} dt + \left(\frac{1}{\lambda(1-\epsilon_{\mathrm{th}})\xi\sigma^2_{\mathrm{rd}}}\right)^N \\
=\ & \frac{1}{\Gamma(N)} \left(\frac{1}{\lambda(1-\epsilon_{\mathrm{th}})^2\sigma^2_{\mathrm{sr}}\sigma^2_{\mathrm{rd}}}\right)^N \ln\left(1+\lambda(1-\epsilon_{\mathrm{th}})\xi\bar{\rho}\sigma^2_{\mathrm{rd}}\right) + \left(\frac{1}{\lambda(1-\epsilon_{\mathrm{th}})\xi\sigma^2_{\mathrm{rd}}}\right)^N. \qquad (66)
\end{aligned}$$

Combining Eq. (65) and Eq. (66), we obtain

$$P_{\mathrm{e1},i} \dot{\leq} \bar{\rho}^{-2N}. \qquad (67)$$

For the second item in Eq. (60), we bound $P_{\mathrm{e2},i|\mathcal{H}}$ above using Lemma 8 and Chernoff bound [21] on Q-function to obtain

$$\begin{aligned}
P_{\mathrm{e2},i|\mathcal{H}} &\leq \exp\left(-\rho_{\mathrm{sr},i}\right) Q\left(\frac{\sqrt{2}\left(\rho_{\mathrm{sd},i} - \alpha_i\rho_{\mathrm{rd},i}\right)}{\sqrt{\rho_{\mathrm{sd},i} + \alpha_i\rho_{\mathrm{rd},i}}}\right) \\
&\leq \exp\left(-(1-\epsilon_{\mathrm{th}})\rho'_{\mathrm{sr},i}\right)\ Q\left(\frac{\sqrt{2}\left((1-\epsilon_{\mathrm{th}})\rho'_{\mathrm{sd},i} - \rho'_{\mathrm{sr},i}\|\boldsymbol{h}_{\mathrm{rd},i}\|^2\right)}{\sqrt{(1-\epsilon_{\mathrm{th}})\rho'_{\mathrm{sd},i} + \rho'_{\mathrm{sr},i}\|\boldsymbol{h}_{\mathrm{rd},i}\|^2}}\right). \qquad (68)
\end{aligned}$$

Because $\rho'_{\mathrm{sr},i} \sim \mathrm{Gamma}(N, \bar{\rho}\sigma^2_{\mathrm{sr}})$ and $\rho'_{\mathrm{sd},i} \sim \mathrm{Gamma}(N, \bar{\rho}\sigma^2_{\mathrm{sd}})$, we can apply [107, Lemma 2] to claim that the last term in Eq. (68) leads to diversity $2N$ when averaging over random channel matrices, which means

$$P_{\mathrm{e2},i} \dot{\leq} \bar{\rho}^{-2N}. \qquad (69)$$

Since $P_{\mathrm{e},i} = E[P_{\mathrm{e1},i|\mathcal{H}} + P_{\mathrm{e2},i|\mathcal{H}}] = P_{\mathrm{e1},i} + P_{\mathrm{e2},i}$, with Eqs. (62), (67), and (69), we arrive at

$$P_{\mathrm{e},i} \doteq \bar{\rho}^{-2N}.$$

Thus, we have proved that power-scaling MIMO relay with CC-ARQ achieves the joint cooperative and receive diversity order of $2N$. ■

So far, we have proposed three MIMO relay designs: power-scaling MIMO relay, MIMO relay with CC-ARQ, and power-scaling MIMO relay with CC-ARQ. Proposed MIMO relay designs keep the low-complexity property in three-fold: (i) ZFEs are applied at receivers to decode the transmitted signal; (ii) CRC is not required for cooperative diversity; and (iii) no space-time cooperation between source and relay is required. In the following, we show numerical examples to verify Propositions 1, 2 and 3, where the diversity orders claimed by our proposed DF MIMO relay designs are verified.

4.5 Simulation Results

In this section, we present some numerical examples for a DF MIMO relay network depicted in Figure 19 with various designs proposed. We plot the average BER curves versus the average SNR $\bar{\rho} = 1/N_0$. The number of antennas at each node is N. We normalize the average PSF for the i^{th} antenna ($E[\alpha_i]$) at the relay node to 1.

Test case 4.1 (BER comparison of different designs): We first verify the performance of MIMO relay designs in Designs 1, 2 and 3. In Figure 23, we plot the BER performance for $N = 2$ and quadrature phase-shift keying (QPSK) modulation. The relay is located equidistant from the source and the destination, i.e., $\sigma^2_{\rm sr} = \sigma^2_{\rm rd} = \sigma^2_{\rm sd} = 1$. Seven designs are plotted: ZFE for the source-destination link only networks, ZFEs at the relay and destination, ZFEs with CC-ARQ with $\epsilon_{\rm th} = 0.93$, ZFEs with PSF, ZFEs with PSF and CC-ARQ with $\epsilon_{\rm th} = 0.93$, MLEs with PSF, and ZF-MLE with PSF and CC-ARQ, which means ZFE is adopted at the relay while MLE is applied at the destination and the CC-ARQ is applied on the source-relay link. Observed from the figure, ZFE for the source-destination link only and ZFEs at the relay and destination achieve diversity 1, while receive diversity $N = 2$ is achieved

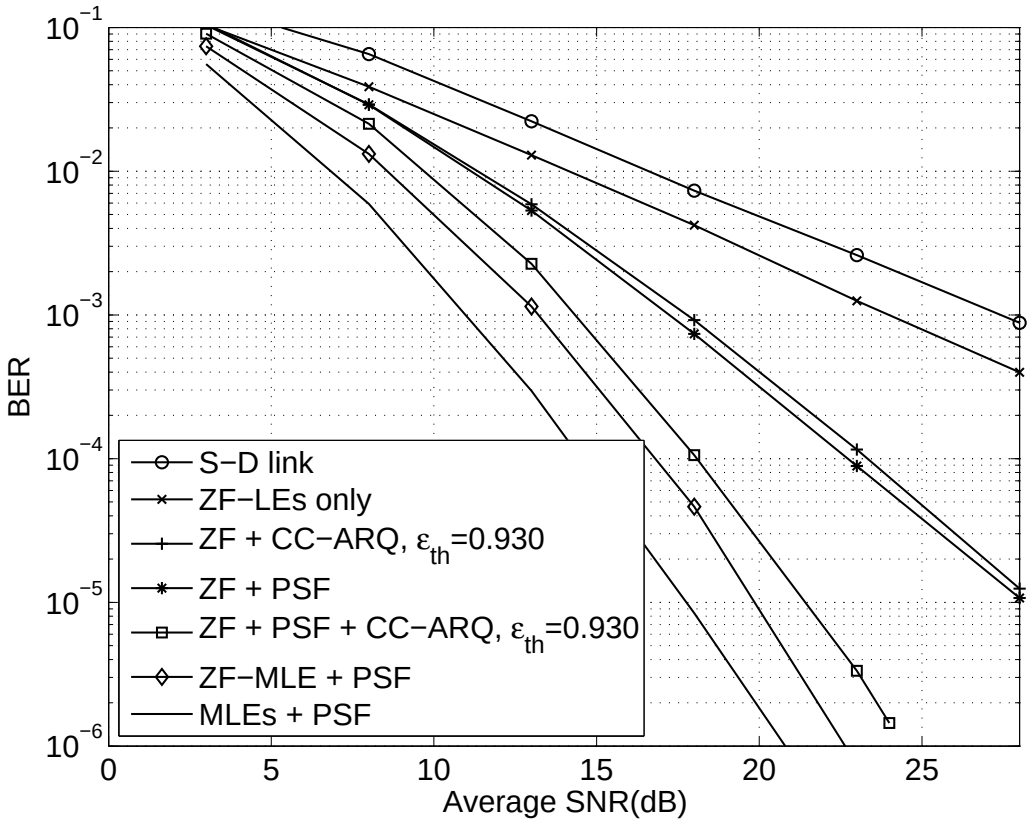

Figure 23: BER comparison of different schemes with $N = 2$ and QPSK.

for ZFEs with CC-ARQ and cooperative diversity 2 is achieved for ZFEs with PSF. ZFEs with PSF and CC-ARQ achieves joint cooperative and receive diversity $2N = 4$, which verifies our Proposition 3. Also, the diversity of ZF-MLE with PSF and MLEs with PSF is $2N = 4$ as expected. However, though no CC-ARQ is required, the exponential complexity makes it infeasible for practical systems, especially when N and/or the constellation size is high.

Test case 4.2 (Asymmetric network topology): In this example, we test MIMO relay designs with ZFEs for asymmetric network topology where $\boldsymbol{H}_{\rm sr}$, $\boldsymbol{H}_{\rm rd}$ and $\boldsymbol{H}_{\rm sd}$ are the $N \times N$ random channel matrices with all entries being i.i.d. complex Gaussian variables with zero means and variance $\sigma^2_{\rm sr}$, $\sigma^2_{\rm rd}$ and $\sigma^2_{\rm sd}$, respectively. We compare three topologies with $(\sigma^2_{\rm sr}, \sigma^2_{\rm rd}, \sigma^2_{\rm sd}) = (2,1,1), (1,2,1), (1,1,2)$ in Figure 24. We can see that diversity order is not affected by network topology. Again, power-scaling

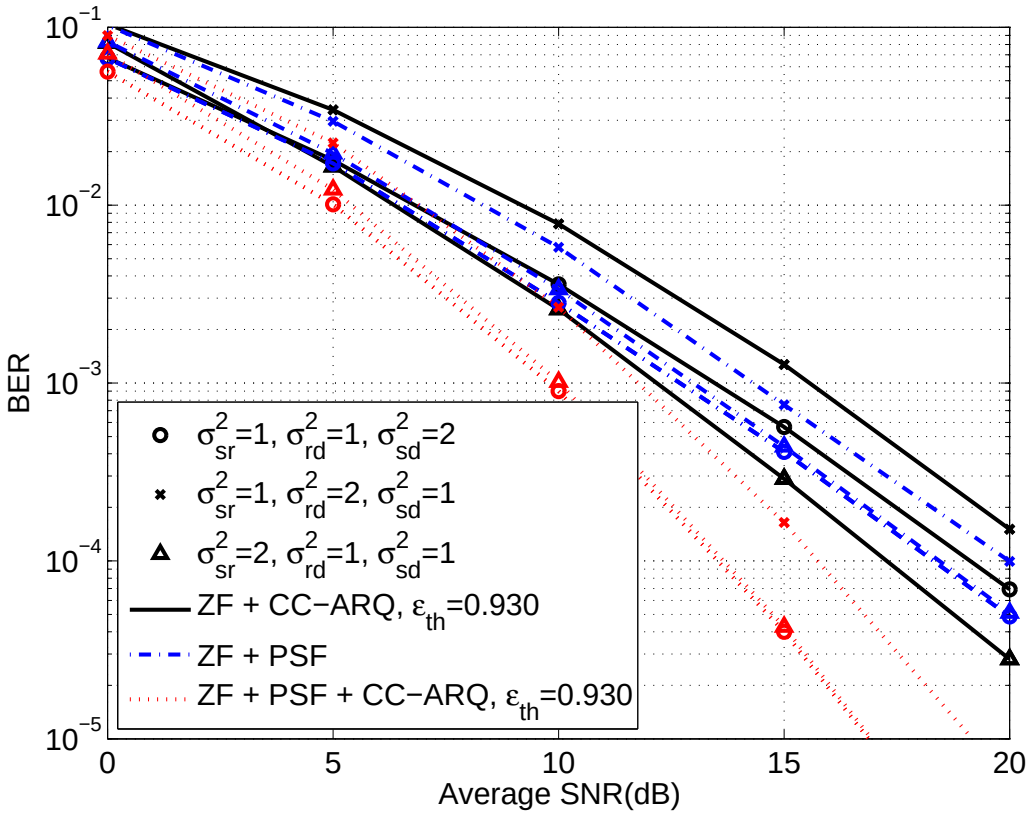

Figure 24: BER with asymmetric network topology, $N = 2$ and QPSK.

MIMO relay with CC-ARQ achieves joint diversity order of $2N = 4$, while power-scailng MIMO relay and MIMO relay with CC-ARQ achieve only cooperative diversity or receive diversity. For MIMO relay with CC-ARQ design, high $\sigma^2_{\rm sr}$ (or, when the relay is located close to the source) achieves better performance than other settings, while high $\sigma^2_{\rm sd}$ performs best in other designs where power scaling is adopted at the relay.

Test case 4.3 (BER comparison for different modulations): In this example, we test MIMO relay designs with ZFEs for various modulation schemes. We compare the average BER performance of QPSK, 16-QAM, and 64-QAM for power-scaling MIMO relay, MIMO relay with CC-ARQ, and power-scaling MIMO relay with CC-ARQ when the number of antennas at each node is $N = 2$. The CC-ARQ threshold $\epsilon_{\rm th} = 0.93$ is set at the relay and destination if CC-ARQ scheme is adopted. Figure 25

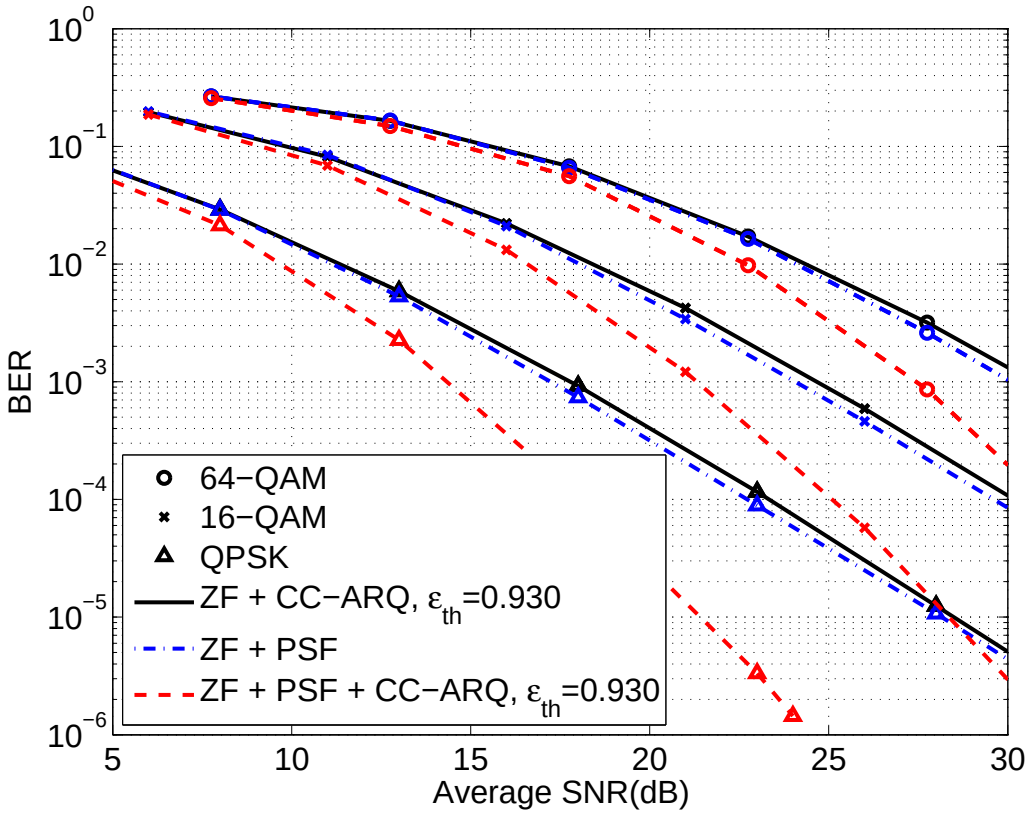

Figure 25: BER comparison for different constellations with $N = 2$.

verifies that each design achieves the same diversity for various modulation schemes. Also, while attaining the same diversity gain, higher-order constellation incurs loss in coding gain, as expected.

Test case 4.4 (The effect of the number of antennas): Next, we compare receive diversity collected at the destination for different number of antennas N when CC-ARQ scheme is adopted. The average BER for MIMO relay with CC-ARQ and power-scaling MIMO relay with CC-ARQ is plotted in Figure 26 with $N = 1$, 2 and 4. We use 16-QAM as the modulation scheme. The CC-ARQ threshold ϵ_{th} is set such that retransmission requirement rate is 20% for $N = 2$, 4. From the figure, we observe that the diversity order collected increases as N increases, showing the effect of multiple antennas on the receive diversity. The diversity of the latter scheme is higher, which is $2N$, because of the use of PSF $\boldsymbol{A}$ at the relay which also enables

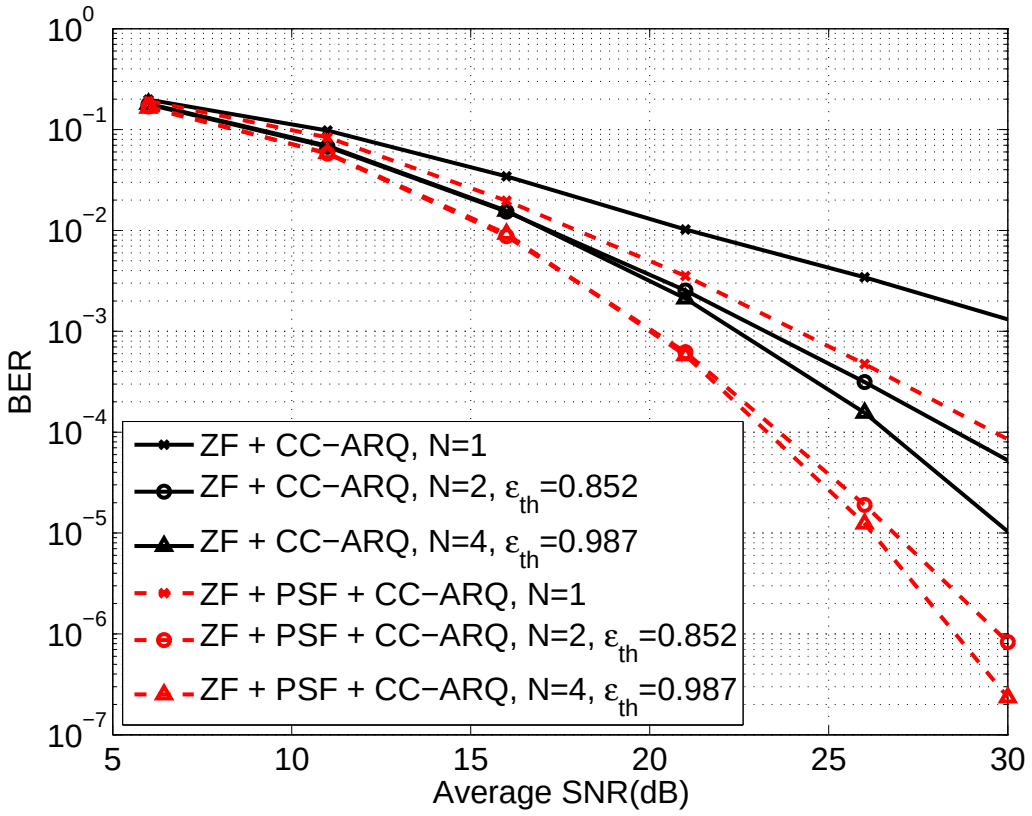

Figure 26: The effect of the number of antennas when $N = 1, 2, 4$ with 16-QAM.

cooperative diversity.

Test case 4.5 (The effect of CC-ARQ threshold ϵ_{th}): In this example, we illustrate the effect of ϵ_{th} on the BER performance of MIMO relay strategy that adopts the CC-ARQ scheme. In Figure 27, we plot the average BER of MIMO relay with CC-ARQ and power-scaling MIMO relay with CC-ARQ as $\epsilon_{\text{th}} = 0.987$, 0.974, and 0.951, for which the percentage of network realizations that require retransmissions are 20%, 33%, and 50%, respectively. The number of antennas is $N = 4$ and 64-QAM is used for modulation. It is shown in the figure that the slope decays faster, and thus, the BER performance is enhanced when ϵ_{th} is set small, which verifies that *od* of the received channel is a critical parameter that determines the performance of ZFE. However, a tradeoff emerges because smaller ϵ_{th} also means more retransmission requests which degrade the spectral efficiency.

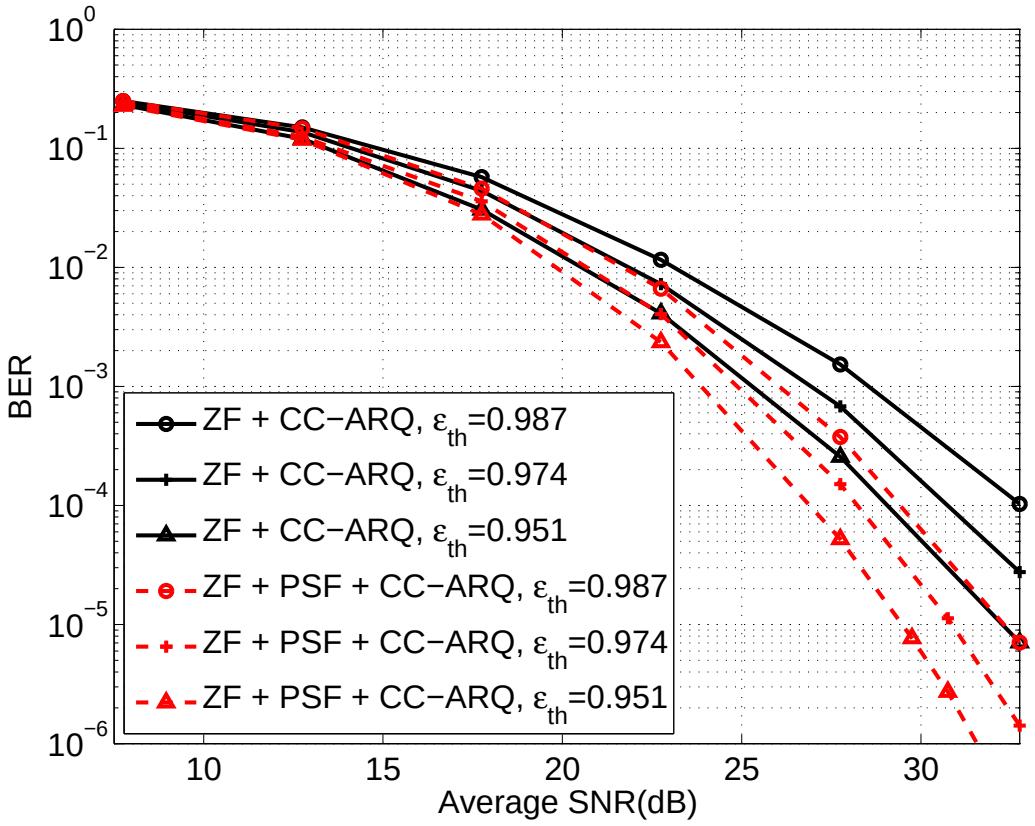

Figure 27: The effect of ϵ_{th} with $N = 4$ and 64-QAM.

Test case 4.6 (Comparisons with cooperative ARQ): We next compare our proposed designs with the cooperative ARQ design in [116] by extending the cooperative ARQ in [116] to MIMO relay networks and assuming ZFE is applied to obtain the estimate whenever decoding is required. For MIMO relay networks with $N = 4$ and 64-QAM modulation scheme, we plot the average BER of the cooperative ARQ, MIMO relay with CC-ARQ, and power-scaling MIMO relay with CC-ARQ with $\epsilon_{\text{th}} = 0.987$. As verified in Figure 28, the cooperative ARQ achieves cooperative diversity, while MIMO relay with CC-ARQ achieves receive diversity and power-scaling MIMO relay with CC-ARQ achieves joint diversity.

In Figure 29, we compare the average number of transmissions per packet for these ARQ designs, which is defined as the total number of transmissions from source over the number of packets received at destination. The cooperative ARQ design in [116] requires retransmissions depending on the correctness of received packets. Therefore, the average number of transmissions of cooperative ARQ decreases as SNR increases. Here we assume that cooperative ARQ can perfectly detect the error. However, due to the finite length of CRC, the performance of cooperative ARQ should be worse than what we present here. As shown in Figure 29, for practical SNR range (5 to 20 dB), proposed designs require much fewer number of retransmissions than the cooperative ARQ. Although the cooperative ARQ requires fewer retransmissions when SNR is high (> 20 dB), the improvement is marginal. Furthermore, cooperative ARQ requires higher encoding/decoding complexity because of CRC.

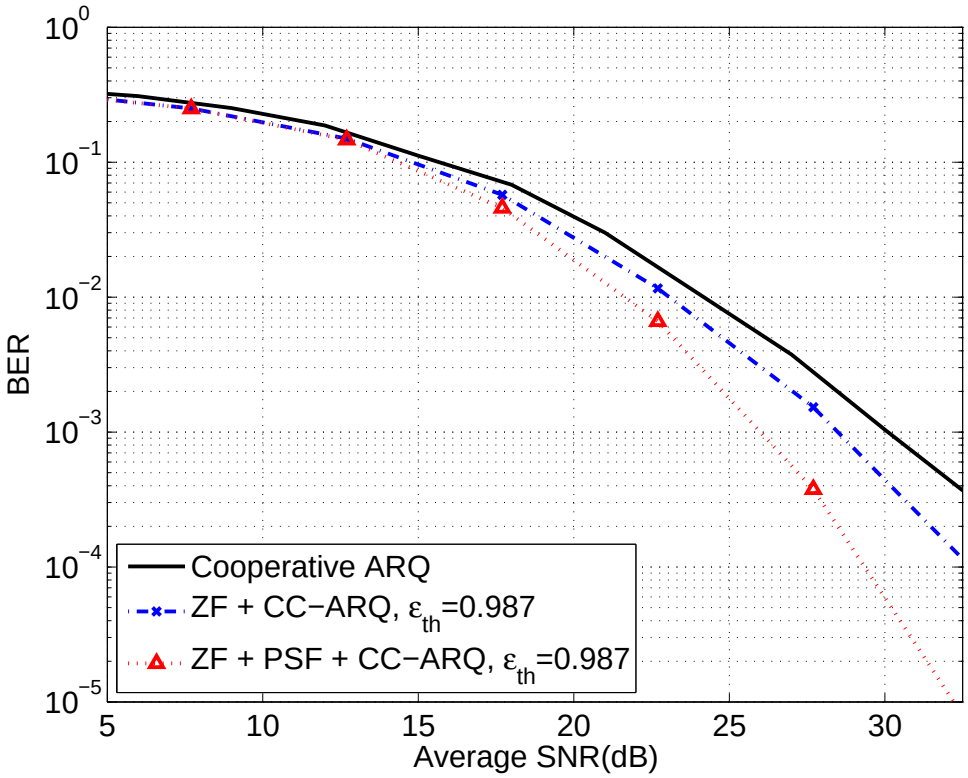

Figure 28: BER comparison with cooperative ARQ with $N = 4$ and 64-QAM.

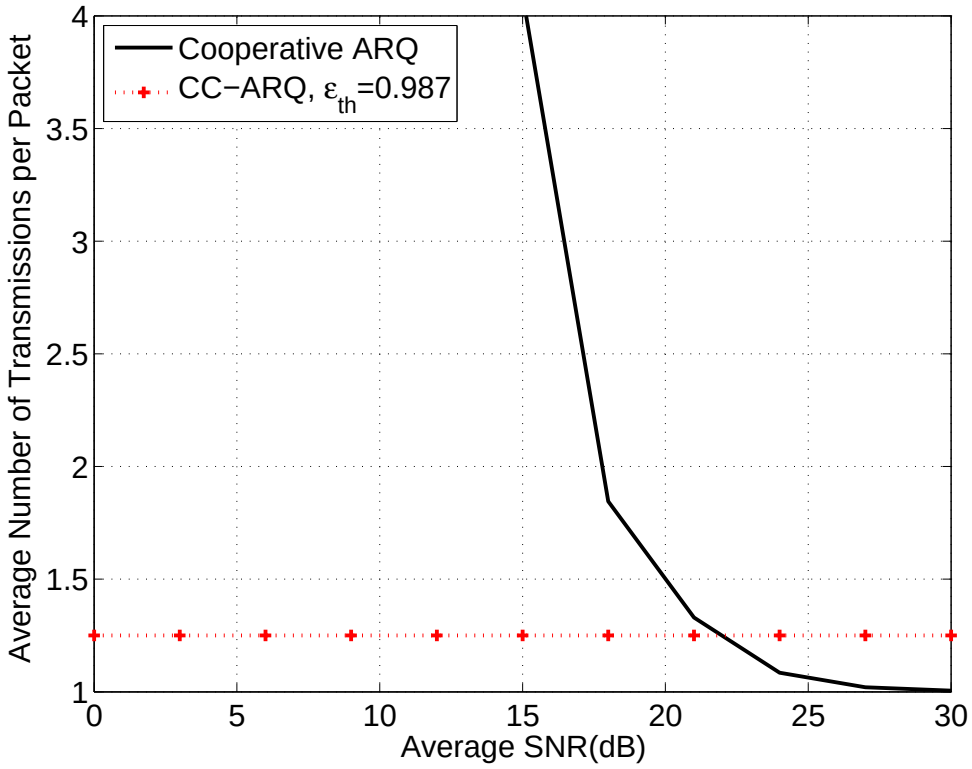

Figure 29: The average number of transmissions per packet.

4.6 Conclusions

In this chapter, we proposed several low-complexity DF MIMO relay designs that achieve diversity for i.i.d. complex Gaussian channels. We have analyzed the BER performance of each design in terms of diversity order. We have shown that the power-scaling design at the relay enables cooperative diversity at the destination. To exploit receive diversity, we propose a CC-ARQ scheme. Also, power scaling with the CC-ARQ scheme was proposed to achieve joint diversity enabled by the network. The proposed schemes exhibit low-complexity from the use of simple ZFE. Simulations show that the DF MIMO relay design with power scaling and CC-ARQ outperforms the existing design on both error performance and spectral efficiency in a practical SNR regime.

CHAPTER V

AMPLIFY-AND-FORWARD MIMO RELAY STRATEGY WITH PEAK-POWER CONSTRAINT

Along with the DF relay scheme, AF relay is another widely adopted relay strategy in the literature [31, 38, 48, 54, 59, 62, 100, 122]. In the AF strategy, the relay simply amplifies the received signal and forwards it to the destination. The destination combines received signals from the source and the relay using different techniques to collect the cooperative diversity [59, 62, 100]. However, one practical issue the AF relay strategy encounters is that many RF/analog components, e.g., power amplifiers (PAs), have a peak-power constraint [9, 29], while the amplifying gain and the output signal of the PAs at the relay may be unbounded. This may cause nonlinear distortion and/or clipping of the peaks in the output signal at the relay, which may result in a performance-error floor at the destination. Increasing back-off can avoid clipping at the relay, but the system becomes inefficient from the power resources point of view [85].

Several works have studied this issue in AF relay networks with single antenna setup [30, 63]. However, for the case when MIMO is used in AF relay networks, i.e., for AF MIMO relay networks, this issue has not been fully considered. In this chapter, we study AF MIMO relay networks with peak-power constraints at the relay when the direct link between source and destination is available. With the power-scaling strategy adopted at the relay, we give conditions for the power profile to enable joint cooperative and receive diversity at the destination while satisfying peak-power constraint conditions at the relay. The benefit of the proposed method is three-fold: (i) our proposed strategy avoids any saturation at peak-power constrained relays; (ii)

our strategy is able to collect joint cooperative and receive diversity without feedback information; and (iii) the proposed power profile is a simple and bounded scalar despite the MIMO structure.

5.1 System Model of AF MIMO Relay Networks

We consider a single-relay network consisting of a source (S), a relay (R), and a destination (D) with N antennas at each node. Each transmission period is divided into two time slots. In the first time slot, the source node transmits the $N \times 1$ information symbol vector $\boldsymbol{s}$ to the relay and destination node, while in the second one, the relay forwards the received symbol vector $\boldsymbol{y}_{\rm sr}$ to the destination after the amplification with power scaling factor (PSF) G. Note that we fully take multiple antennas for spatial multiplexity, i.e., no space-time coding. With subscripts signifying the corresponding link, e.g., the subscript $_{\rm sr}$ denotes the link from S to R, the mathematical formulation of the baseband equivalent model for AF MIMO relay system can be written as

$$\begin{aligned} \boldsymbol{y}_{\rm sr} &= \boldsymbol{H}_{\rm sr}\boldsymbol{s} + \boldsymbol{w}_{\rm sr}, \\ \boldsymbol{y}_{\rm sd} &= \boldsymbol{H}_{\rm sd}\boldsymbol{s} + \boldsymbol{w}_{\rm sd}, \\ \boldsymbol{y}_{\rm rd} &= \boldsymbol{H}_{\rm rd}\sqrt{G}\boldsymbol{y}_{\rm sr} + \boldsymbol{w}_{\rm rd}, \end{aligned} \tag{70}$$

where $\boldsymbol{y}$ is the $N \times 1$ received signal. G is a real-valued PSF at the relay. $\boldsymbol{H}_{\rm ij}$ is the $N \times N$ random channel with all entries being i.i.d. complex Gaussian variables with zero mean and variance $\sigma_{\rm ij}^2$ for i-j link. All the channels are considered to be flat and quasi-static. We assume all channel matrices are known at the corresponding receiver side. The $N \times 1$ noise vector $\boldsymbol{w}$ is i.i.d. complex Gaussian distributed with zero mean and variance N_0, i.e., $E[\boldsymbol{w}\boldsymbol{w}^{\mathcal{H}}] = N_0\boldsymbol{I}_{\rm N}$. The average symbol power $E[|s_{\rm i}|^2]$ is set to 1, and the average SNR is defined as $\bar{\rho} = 1/N_0$. The average transmit power at the relay is constrained to $E[\|\sqrt{G}\boldsymbol{y}_{\rm sr}\|^2] = N$.

Upon receipt of signals $\boldsymbol{y}_{\rm rd}$ and $\boldsymbol{y}_{\rm sd}$, the destination node stacks them to define an

extended system as follows:

$$\bar{\boldsymbol{y}} = \begin{bmatrix} \boldsymbol{y}_{\mathrm{rd}} \\ \boldsymbol{y}_{\mathrm{sd}} \end{bmatrix} = \underbrace{\begin{bmatrix} \boldsymbol{H}_{\mathrm{rd}}\sqrt{G}\boldsymbol{H}_{\mathrm{sr}} \\ \boldsymbol{H}_{\mathrm{sd}} \end{bmatrix}}_{\bar{\boldsymbol{H}}} \boldsymbol{s} + \underbrace{\begin{bmatrix} \boldsymbol{H}_{\mathrm{rd}}\sqrt{G} \\ \boldsymbol{0}_{\mathrm{N}\times\mathrm{N}} \end{bmatrix} \boldsymbol{w}_{\mathrm{sr}} + \begin{bmatrix} \boldsymbol{w}_{\mathrm{rd}} \\ \boldsymbol{w}_{\mathrm{sd}} \end{bmatrix}}_{\bar{\boldsymbol{w}}}, \tag{71}$$

where $\bar{\boldsymbol{H}}$ and $\bar{\boldsymbol{w}}$ are the effective channel matrix and the effective noise of the extended system, respectively.

The covariance matrix of the effective noise is not diagonal, i.e.,

$$\begin{aligned} E[\bar{\boldsymbol{w}}\bar{\boldsymbol{w}}^{\mathcal{H}}] &= E\left[\begin{bmatrix} \boldsymbol{H}_{\mathrm{rd}}\sqrt{G}\boldsymbol{w}_{\mathrm{sr}} + \boldsymbol{w}_{\mathrm{rd}} \\ \boldsymbol{w}_{\mathrm{sd}} \end{bmatrix} \begin{bmatrix} \boldsymbol{w}_{\mathrm{sr}}^{\mathcal{H}}\sqrt{G}\boldsymbol{H}_{\mathrm{rd}}^{\mathcal{H}} + \boldsymbol{w}_{\mathrm{rd}}^{\mathcal{H}} & \boldsymbol{w}_{\mathrm{sd}}^{\mathcal{H}} \end{bmatrix} \right] \\ &= \begin{bmatrix} N_0\boldsymbol{I}_{\mathrm{N}} + N_0 G\boldsymbol{H}_{\mathrm{rd}}\boldsymbol{H}_{\mathrm{rd}}^{\mathcal{H}} & \boldsymbol{0}_{\mathrm{N}\times\mathrm{N}} \\ \boldsymbol{0}_{\mathrm{N}\times\mathrm{N}} & N_0\boldsymbol{I}_{\mathrm{N}} \end{bmatrix} \\ &= N_0\boldsymbol{Q}, \end{aligned}$$

where $\boldsymbol{Q}$ and $\boldsymbol{Q}_1$ are defined as

$$\boldsymbol{Q} := \begin{bmatrix} \boldsymbol{Q}_1 & \boldsymbol{0}_{\mathrm{N}\times\mathrm{N}} \\ \boldsymbol{0}_{\mathrm{N}\times\mathrm{N}} & \boldsymbol{I}_{\mathrm{N}} \end{bmatrix},$$

and

$$\boldsymbol{Q}_1 := \boldsymbol{I}_{\mathrm{N}} + G\boldsymbol{H}_{\mathrm{rd}}\boldsymbol{H}_{\mathrm{rd}}^{\mathcal{H}}. \tag{72}$$

Thus, the effective noise vector $\bar{\boldsymbol{w}}$ is colored Gaussian noise and we need to normalize the covariance matrix in order to simplify the expressions in the white Gaussian noise case. The received signal vector $\bar{\boldsymbol{y}}$ Eq. (71) is first filtered by the noise whitening filter $\boldsymbol{Q}^{-\frac{1}{2}}$ as,

$$\begin{aligned} \bar{\boldsymbol{y}}_{\mathrm{w}} &= \boldsymbol{Q}^{-\frac{1}{2}}\bar{\boldsymbol{y}} \\ &= \boldsymbol{Q}^{-\frac{1}{2}}\bar{\boldsymbol{H}}\boldsymbol{s} + \bar{\boldsymbol{n}}, \end{aligned} \tag{73}$$

where now we have white Gaussian noise $\bar{\boldsymbol{n}} = \boldsymbol{Q}^{-\frac{1}{2}}\bar{\boldsymbol{w}}$ with $E[\bar{\boldsymbol{n}}\bar{\boldsymbol{n}}^{\mathcal{H}}] = N_0\boldsymbol{I}_{2\mathrm{N}}$.

After applying the whitening filter, the ML receiver detects the symbol vector $\boldsymbol{s}$ as

$$\hat{\boldsymbol{s}} = \arg \min_{s' \in \mathcal{S}^{\mathrm{N}}} \left\| \bar{\boldsymbol{y}}_{\mathrm{w}} - \boldsymbol{Q}^{-\frac{1}{2}} \bar{\boldsymbol{H}} \boldsymbol{s}' \right\|^2, \tag{74}$$

where $\mathcal{S}$ is the finite alphabet of the information symbols. Note, the ML receiver performs a minimization over all transmitted vector hypotheses.

In this chapter, we use diversity order, defined in Eq. (3), as a performance metric with peak-power constraints. It is well known that the diversity order depends on the degrees of freedom provided by the underlying fading channels. In AF MIMO relay networks adopting V-BLAST, the destination can collect two types of diversity: spatial diversity N due to multiple receive antennas and cooperative diversity 2 which comes from the additional $S - R - D$ path besides direct $S - D$ path. Accordingly, the appropriate design will collect a joint diversity order of $2N$.

One practical concern for AF relaying is that the output signal at the relay may be unbounded if the relay does not choose the amplifying gain carefully. Since many RF/analog components in the transmission chain, especially the PAs, are peak-power constrained devices, PAs should operate at low power efficiency by large back-off, or the output signal may suffer from nonlinear distortion and/or saturation at the relay, resulting in performance-error floor at the destination. Thus, in the next section, we study peak-power limited AF MIMO relay strategies which enable joint diversity order of $2N$.

5.2 Peak-Power Limited AF MIMO Relay Strategies

As discussed in the previous section, we consider practical situations where the peak power and relay gain G are constrained at the relay. In this section, we first find a sufficient condition on the PSF G to enable joint diversity $2N$ and we propose simple and practical peak-power limited PSF design examples that satisfy the condition.

5.2.1 Power Scaling at the Relay

Since PAs have a limited capability to amplify the received signal, we consider bounded PSF $G = \min(1, G')$ in this section. In the following proposition and proof, we show a sufficient condition on the PSF G such that the average error probability at the destination has diversity order of $2N$.

Proposition 4 *If the PSF G is designed such that*

$$G = \min(1, G'),$$

and G satisfies

$$E_{H_{\rm sr}}\left[G\boldsymbol{H}_{\rm sr}\boldsymbol{e}\boldsymbol{e}^{\mathcal{H}}\boldsymbol{H}_{\rm sr}^{\mathcal{H}}\right] = C_{\rm e}\boldsymbol{I}_{\rm N},$$

where $\boldsymbol{e} = \boldsymbol{s}_i - \boldsymbol{s}_j \neq \boldsymbol{0}$, $\forall \boldsymbol{s}_i, \boldsymbol{s}_j \in \mathcal{S}^{\rm N}$, and $C_{\rm e} > 0$ is a constant, then the ML detector in Eq. (74) at the destination achieves joint diversity order of $2N$.

Proof: Given the set of three channel matrices $\mathcal{H} = \{\boldsymbol{H}_{\rm sr}, \boldsymbol{H}_{\rm sd}, \boldsymbol{H}_{\rm rd}\}$, the instantaneous pairwise error probability of the ML receiver for an error pattern $\boldsymbol{e} = \boldsymbol{s} - \tilde{\boldsymbol{s}}$ is bounded above as

$$\begin{aligned} P_{\rm e}(\boldsymbol{s} \to \tilde{\boldsymbol{s}}|\mathcal{H}) &\leq \exp\left(-\frac{\|\boldsymbol{Q}^{-\frac{1}{2}}\bar{\boldsymbol{H}}\boldsymbol{e}\|^2}{4N_0}\right) \\ &= \exp\left(-\frac{\|\boldsymbol{Q}_1^{-\frac{1}{2}}\boldsymbol{H}_{\rm rd}\sqrt{G}\boldsymbol{H}_{\rm sr}\boldsymbol{e}\|^2\bar{\rho}}{4}\right)\exp\left(-\frac{\|\boldsymbol{H}_{\rm sd}\boldsymbol{e}\|^2\bar{\rho}}{4}\right). \end{aligned} \quad (75)$$

Using the method of calculating characteristic function of a random variable [101], we average Eq. (75) over $\boldsymbol{H}_{\rm sr}$ and $\boldsymbol{H}_{\rm sd}$ to further bound it above as

$$\begin{aligned}
& P_{\rm e}(\boldsymbol{s}\to\tilde{\boldsymbol{s}}|\boldsymbol{H}_{\rm rd}) \\
\leq\ & E_{H_{\rm sr}}\left[\exp\left(-\frac{\bar{\rho}}{4}\|\boldsymbol{Q}_1^{-\frac{1}{2}}\boldsymbol{H}_{\rm rd}\sqrt{G}\boldsymbol{H}_{\rm sr}\boldsymbol{e}\|^2\right)\right]\left(\frac{\sigma_{\rm sd}^2\|\boldsymbol{e}\|^2\bar{\rho}}{4}\right)^{-N} \\
\leq\ & \det\left(\boldsymbol{I}_N+\frac{\bar{\rho}}{4}E_{H_{\rm sr}}\left[\boldsymbol{Q}_1^{-\frac{1}{2}}\boldsymbol{H}_{\rm rd}\sqrt{G}\boldsymbol{H}_{\rm sr}\boldsymbol{e}\boldsymbol{e}^{\mathcal{H}}\boldsymbol{H}_{\rm sr}^{\mathcal{H}}\sqrt{G}\boldsymbol{H}_{\rm rd}^{\mathcal{H}}\boldsymbol{Q}_1^{-\frac{1}{2}}\right]\right)^{-1}\left(\frac{\sigma_{\rm sd}^2\|\boldsymbol{e}\|^2\bar{\rho}}{4}\right)^{-N} \\
\leq\ & \det\left(\boldsymbol{I}_N+\frac{\bar{\rho}}{4}E_{H_{\rm sr}}\left[\boldsymbol{Q}_2^{-\frac{1}{2}}\boldsymbol{H}_{\rm rd}\sqrt{G}\boldsymbol{H}_{\rm sr}\boldsymbol{e}\boldsymbol{e}^{\mathcal{H}}\boldsymbol{H}_{\rm sr}^{\mathcal{H}}\sqrt{G}\boldsymbol{H}_{\rm rd}^{\mathcal{H}}\boldsymbol{Q}_2^{-\frac{1}{2}}\right]\right)^{-1}\left(\frac{\sigma_{\rm sd}^2\|\boldsymbol{e}\|^2\bar{\rho}}{4}\right)^{-N} \\
\leq\ & \det\left(\boldsymbol{I}_N+\frac{\bar{\rho}}{4}\boldsymbol{Q}_2^{-\frac{1}{2}}\boldsymbol{H}_{\rm rd}E_{H_{\rm sr}}\left[G\boldsymbol{H}_{\rm sr}\boldsymbol{e}\boldsymbol{e}^{\mathcal{H}}\boldsymbol{H}_{\rm sr}^{\mathcal{H}}\right]\boldsymbol{H}_{\rm rd}^{\mathcal{H}}\boldsymbol{Q}_2^{-\frac{1}{2}}\right)^{-1}\left(\frac{\sigma_{\rm sd}^2\|\boldsymbol{e}\|^2\bar{\rho}}{4}\right)^{-N}, \quad (76)
\end{aligned}$$

where $\boldsymbol{Q}_2$ is defined as

$$\boldsymbol{Q}_2 := \boldsymbol{I}_{\rm N}+\boldsymbol{H}_{\rm rd}\boldsymbol{H}_{\rm rd}^{\mathcal{H}}.$$

Note we have used $\boldsymbol{Q}_1=\boldsymbol{I}_{\rm N}+G\boldsymbol{H}_{\rm rd}\boldsymbol{H}_{\rm rd}^{\mathcal{H}}$ from Eq. (72) and $G\leq 1$. If there exists $C_{\rm e}>0$, such that $E_{H_{\rm sr}}\left[G\boldsymbol{H}_{\rm sr}\boldsymbol{e}\boldsymbol{e}^{\mathcal{H}}\boldsymbol{H}_{\rm sr}^{\mathcal{H}}\right]=C_{\rm e}\boldsymbol{I}_{\rm N}$, then we have

$$P_{\rm e}(\boldsymbol{s}\to\tilde{\boldsymbol{s}}|\boldsymbol{H}_{\rm rd})\leq\det\left(\boldsymbol{I}_{\rm N}+\frac{C_{\rm e}\bar{\rho}}{4}\boldsymbol{Q}_2^{-\frac{1}{2}}\boldsymbol{H}_{\rm rd}\boldsymbol{H}_{\rm rd}^{\mathcal{H}}\boldsymbol{Q}_2^{-\frac{1}{2}}\right)^{-1}\left(\frac{\sigma_{\rm sd}^2\|\boldsymbol{e}\|^2\bar{\rho}}{4}\right)^{-N}. \quad (77)$$

We average Eq. (77) over $\boldsymbol{H}_{\rm rd}$ to get the upper bound of the average pairwise error probability as

$$\begin{aligned}
P_{\rm e}(\boldsymbol{s}\to\tilde{\boldsymbol{s}}) &\leq E_{H_{\rm rd}}\left[\det\left(\boldsymbol{I}_{\rm N}+\frac{C_{\rm e}\bar{\rho}}{4}\boldsymbol{Q}_2^{-\frac{1}{2}}\boldsymbol{H}_{\rm rd}\boldsymbol{H}_{\rm rd}^{\mathcal{H}}\boldsymbol{Q}_2^{-\frac{1}{2}}\right)^{-1}\right]\left(\frac{\sigma_{\rm sd}^2\|\boldsymbol{e}\|^2\bar{\rho}}{4}\right)^{-N} \\
&= E_{H_{\rm rd}}\left[\det\left(\boldsymbol{I}_{\rm N}+\frac{C_{\rm e}\bar{\rho}}{4}\boldsymbol{Q}_2^{-1}\boldsymbol{H}_{\rm rd}\boldsymbol{H}_{\rm rd}^{\mathcal{H}}\right)^{-1}\right]\left(\frac{\sigma_{\rm sd}^2\|\boldsymbol{e}\|^2\bar{\rho}}{4}\right)^{-N} \\
&= E_{W}\left[\det\left(\boldsymbol{I}_{\rm N}+\frac{C_{\rm e}\bar{\rho}}{4}(\boldsymbol{I}_{\rm N}+\sigma_{\rm rd}^2\boldsymbol{W})^{-1}\sigma_{\rm rd}^2\boldsymbol{W}\right)^{-1}\right]\left(\frac{\sigma_{\rm sd}^2\|\boldsymbol{e}\|^2\bar{\rho}}{4}\right)^{-N}, \quad (78)
\end{aligned}$$

where $\boldsymbol{W}=\frac{1}{\sigma_{\rm rd}^2}\boldsymbol{H}_{\rm rd}\boldsymbol{H}_{\rm rd}^{\mathcal{H}}$ is a complex central Wishart matrix $\boldsymbol{W}\sim\mathcal{W}\left(N,\boldsymbol{I}_{\rm N}\right)$ with N degrees of freedom and the scale matrix $\boldsymbol{I}_{\rm N}$. We use the result in [90, Lemma 1] with parameters $m=N$, $n=N$, and $p=1$, and we can claim the following:

$$E_W\left[\det\left(\boldsymbol{I}_{\rm N}+\frac{C_{\rm e}\bar{\rho}}{4}(\boldsymbol{I}_{\rm N}+\sigma_{\rm rd}^2\boldsymbol{W})^{-1}\sigma_{\rm rd}^2\boldsymbol{W}\right)^{-1}\right]\doteq\left(\frac{C_{\rm e}\bar{\rho}\sigma_{\rm rd}^2}{4}\right)^{-N}. \quad (79)$$

Hence, from Eqs. (78) and (79) we have shown that $P_{\mathrm{e}}(\boldsymbol{s} \to \tilde{\boldsymbol{s}}) \stackrel{\cdot}{\leq} \bar{\rho}^{-2N}$. Thus, the average pairwise error probability achieves diversity order of $2N$. ■

5.2.2 Practical Design Examples

Now, we propose simple and practical AF MIMO relay designs with bounded PSF G which satisfies the condition in Proposition 4 and compare them with the conventional fixed-gain AF strategy [48] extended to MIMO relay setup.

Fixed-gain AF [48]: *The PSF G_f is designed as*

$$G_{\mathrm{f}} = \lambda_{\mathrm{f}},$$

where λ_{f} is a power normalizer so that $E[\|\sqrt{G_{\mathrm{f}}}\boldsymbol{y}_{\mathrm{sr}}\|^2] = N$.

Design 1: *The PSF G_1 is designed as*

$$G_1 = \lambda_1 \min(1, G_1') \quad with \quad G_1' = \frac{1}{\|\boldsymbol{H}_{\mathrm{sr}}\|_{\mathrm{F}}^2},$$

where $\|\boldsymbol{H}_{\mathrm{sr}}\|_{\mathrm{F}}$ is the Frobenius norm of $\boldsymbol{H}_{\mathrm{sr}}$, i.e., $\|\boldsymbol{H}_{\mathrm{sr}}\|_{\mathrm{F}} = \sqrt{trace(\boldsymbol{H}_{\mathrm{sr}}^{\mathcal{H}}\boldsymbol{H}_{\mathrm{sr}})}$, and λ_1 is an average power normalizer.

Design 2: *The PSF G_2 is designed as*

$$G_2 = \lambda_2 \min(1, G_2') \quad with \quad G_2' = \frac{1}{\|\boldsymbol{y}_{\mathrm{sr}}\|^2},$$

and λ_2 is an average power normalizer.

In conventional fixed-gain strategy [48], the instantaneous output power at the relay is linearly proportional to the instantaneous received signal power, and thus the output signal waveform may suffer from large envelope variations. This leads to the power inefficiency [27] or the degradation of the performance if the output signal is saturated at the PA.

Design 1 considers the instantaneous $S - R$ channel state information to control the relay power. When the channel is strong, i.e., $\|\boldsymbol{H}_{\mathrm{sr}}\|_{\mathrm{F}}^2$ is high, the relay scales down the output power accordingly. On the other hand, when the channel is weak,

the relaying gain is increased. This is contrary to the PSF design for DF MIMO relay networks in Eq. (47), where the relay scales down the transmission power when the $S-R$ channel is weak. The maximum gain of G_1 is bounded since the gain of the power amplifier may be limited. In this way, the output peak power is also reduced compared to the conventional fixed gain strategy. However, the transmitted signal power is not strictly bounded because of random noises at the relay. Also, channel estimation is required at the relay for this design.

Design 2 uses the instantaneous received signal power $\|\boldsymbol{y}_{\rm sr}\|^2$ to determine the relay gain G_2. The peak power of the transmitted signal can be easily shown to be bounded by λ_2, and thus, Design 2 is suitable for peak-power constrained systems. In addition, channel estimation is not needed at the relay. Therefore, Design 2 is the most preferred design among these three in terms of the energy efficiency since the output signal power as well as the maximum gain of the PA at the relay are always bounded.

Next, we will prove that all three designs satisfy the condition in Proposition 4, so that all designs enable joint diversity $2N$ at the destination. We will first prove that G_1 (Design 1) enables diversity order of $2N$ by showing

$$E_{H_{\rm sr}}\left[G_1\boldsymbol{H}_{\rm sr}\boldsymbol{e}\boldsymbol{e}^{\mathcal{H}}\boldsymbol{H}_{\rm sr}^{\mathcal{H}}\right]=C_{1,\rm e}\boldsymbol{I}_{\rm N}, \tag{80}$$

where $C_{1,\rm e}>0$. Let $h_{\rm pq}$ be the $(p,q)^{th}$ element of $\boldsymbol{H}_{\rm sr}$ and $\boldsymbol{e}=[e_1\ \cdots\ e_N]^T$. Then, the $(p,q)^{th}$ element of the left-hand side of Eq. (80) is

$$E_{H_{\rm sr}}\left[G_1\sum_{\rm m=1}^{N}\sum_{\rm n=1}^{N}h_{\rm pm}h_{\rm qn}^{*}e_{\rm m}e_{\rm n}^{*}\right].$$

The off-diagonal entries ($p\neq q$) are all zeros, because $h_{\rm pm}$'s are i.i.d. with zero mean and $E_{H_{\rm sr}}\left[G_1h_{\rm pm}h_{\rm qn}^{*}e_{\rm m}e_{\rm n}^{*}\right]=0$ for $p\neq q$.

For the p^{th} diagonal entry, i.e., $p=q$, the left-hand side of Eq. (80) becomes

$$E_{H_{\rm sr}}\left[G_1\left|\sum_{m=1}^{N}h_{\rm pm}e_{\rm m}\right|^2\right]=E_{H_{\rm sr}}\left[G_1\sum_{m=1}^{N}|h_{\rm pm}|^2|e_{\rm m}|^2\right]=C_{1,\rm e}>0,$$

where the last equality comes from the assumption that h_{pm}'s are i.i.d. For non-i.i.d. channel matrices, $C_{1,e}$ can be selected as the minimum among all $C_{1,e}(p)$'s and the equal sign can be changed to "$\geq$", and Proposition 4 still holds true. Therefore, the relay gain G_1 enables joint diversity $2N$ by Proposition 4. The proof for G_{f} (fixed-gain design) is straightforward by following the same procedures as for G_1.

For G_2 (Design 2), $\frac{1}{\|\boldsymbol{y}_{\mathrm{sr}}\|^2}$ can be approximated at high SNR as,

$$\frac{1}{\|\boldsymbol{y}_{\mathrm{sr}}\|^2} \approx \frac{1}{\sum_{\mathrm{m}=1}^{N}\left|\sum_{\mathrm{n}=1}^{N} h_{\mathrm{mn}} s_{\mathrm{n}}\right|^2} \geq \frac{1}{\kappa \|\boldsymbol{H}_{\mathrm{sr}}\|_{\mathrm{F}}^2}, \tag{81}$$

where $\kappa = \max |s_{\mathrm{i}}|^2$. From Eq. (81), we have the inequality

$$E_{H_{\mathrm{sr}}}\left[\frac{\boldsymbol{H}_{\mathrm{sr}}\boldsymbol{e}\boldsymbol{e}^{\mathcal{H}}\boldsymbol{H}_{\mathrm{sr}}^{\mathcal{H}}}{\|\boldsymbol{y}_{\mathrm{sr}}\|^2}\right] \geq E_{H_{\mathrm{sr}}}\left[\frac{\boldsymbol{H}_{\mathrm{sr}}\boldsymbol{e}\boldsymbol{e}^{\mathcal{H}}\boldsymbol{H}_{\mathrm{sr}}^{\mathcal{H}}}{\kappa \|\boldsymbol{H}_{\mathrm{sr}}\|_{\mathrm{F}}^2}\right]. \tag{82}$$

Plugging Eq. (82) into Eq. (76) in the proof of Proposition 4, it shows that G_2 enables at least the same diversity as G_1 and we expect that Design 2 outperforms Design 1 at high SNR.

Note that, the diversity order at the destination is not affected by the underlying modulation scheme as shown in Chapters 3 and 4.

5.3 Simulation Results

In this section, we present some numerical examples to validate our designs for AF MIMO relay networks. The number of antennas at each node is N. For the fair comparisons among different designs, the PSF G is normalized to satisfy $E[\|\sqrt{G}\boldsymbol{y}_{\mathrm{sr}}\|^2] = N$. QPSK modulation is adopted unless otherwise mentioned.

Test case 5.1 (Peak-power at the relay): In Figure 30, we compare transmitted signal power distributions at the relay for fixed-gain AF, Design 1 and Design 2. We also plot the performance of joint MMSE (JMMSE) scheme [47] where the linear processing at the relay is designed based on the MMSE criterion. The average SNR is set to $\bar{\rho} = 15$dB. As shown in Figure 30, transmitted signal power distributions at

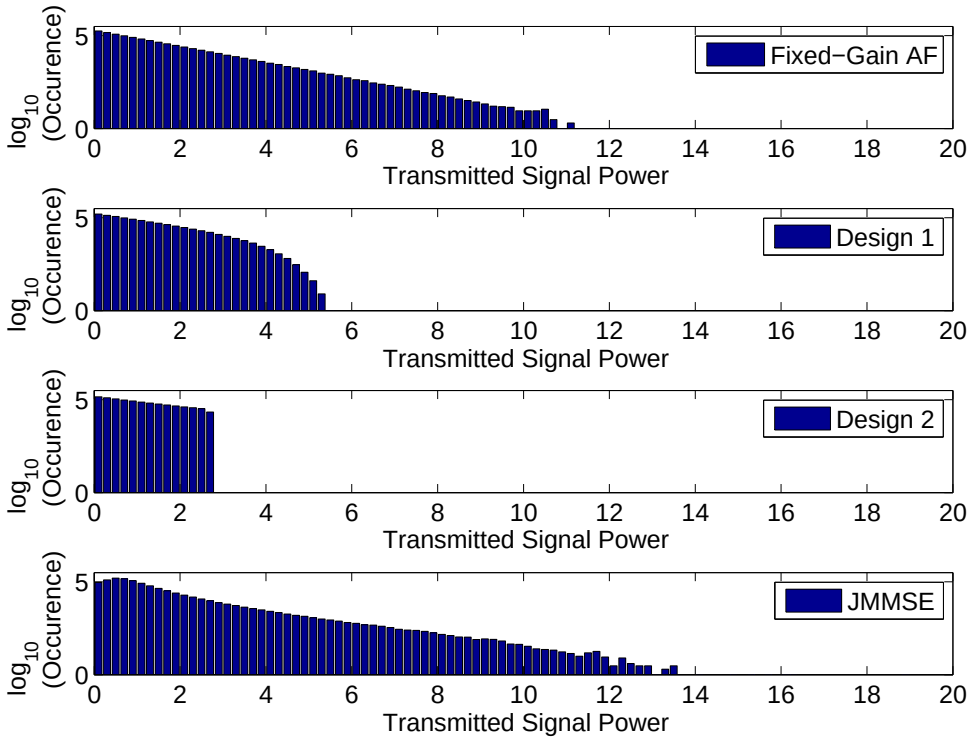

Figure 30: Transmitted signal power distribution per antenna at the relay with $\bar{\rho} = 15\text{dB}$.

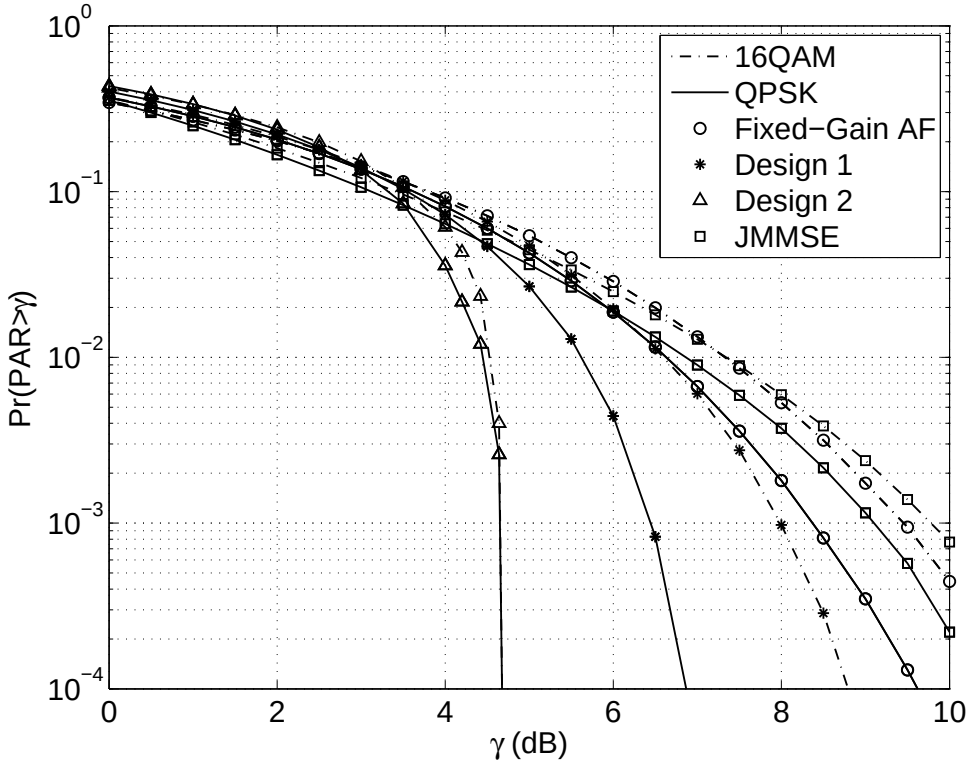

Figure 31: The comparison of CCDF curves of the PAR with $\bar{\rho} = 15$dB.

the relay for fixed-gain AF and JMMSE have much longer tails compared to Design 1 and Design 2, which means lower power efficiency and more saturation possibilities for fixed-gain AF and JMMSE. This is a consequence from the fact that the PSF G does not account for the instantaneous channel variations or the received signal power. The output peak powers for fixed-gain AF and JMMSE are around 11 and 14, while Design 1 and Design 2 have their peak power around 5.4 and 2.7, respectively.

In Figure 31, the complimentary cumulative distribution function (CCDF) curves for peak-to-average power ratio (PAR) are compared for four designs with QPSK and 16-QAM modulations. The boundedness of the peak power of Design 2 is demonstrated in the figure, which verifies that Design 2 is most suitable for peak-power constrained systems regardless of the underlying constellation.

Test case 5.2 (The effect of the number of antennas on the diversity order): In Figure 32, we plot the average BER curves versus the average SNR $\bar{\rho}$ for $N = 2$ and 4. We observe that the diversity order achieved increases as N increases, and all designs achieve the same diversity order of $2N$. We also observe that Design 1 and Design 2 perform slightly better than the fixed-gain AF. The performance of JMMSE scheme [47] is also plotted as a reference. Note that JMMSE scheme utilizes both $S - R$ and $R - D$ channel information at the relay while the other three use none of them or only $S - R$ channel information at the relay, which means they do not require any feedback information.

Test case 5.3 (Application of CC-ARQ): The ML receiver at the destination, presented in Eq. (74), provides the optimal error performance, but it comes with high decoding complexity for a large number of antennas and high-order constellations ($\mathcal{O}(|\mathcal{S}|^N)$). In Chapter 4, CC-ARQ was introduced for DF MIMO relay networks. Combined with the CC-ARQ at the receivers, low-complexity ZFEs enable the receive diversity for DF MIMO relay networks. Here, we can also apply CC-ARQ techniques to AF MIMO relay networks and use ZFE at the destination to reduce the decoding

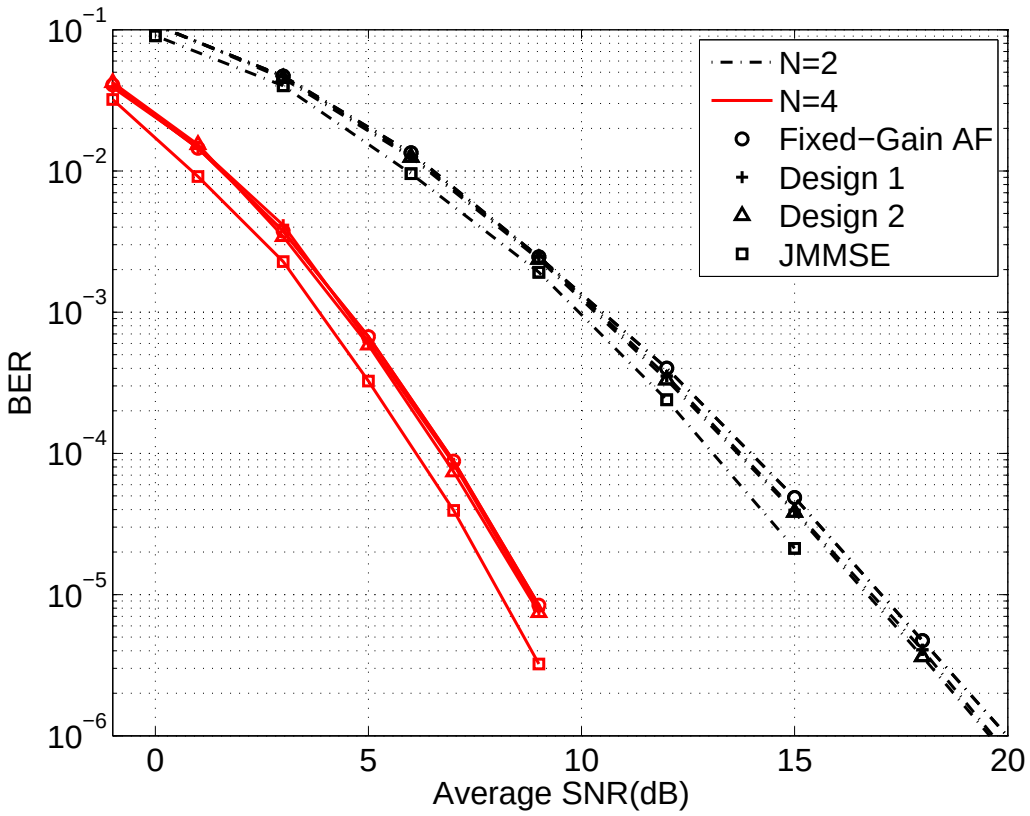

Figure 32: BER performance with $N = 2, 4$ and QPSK.

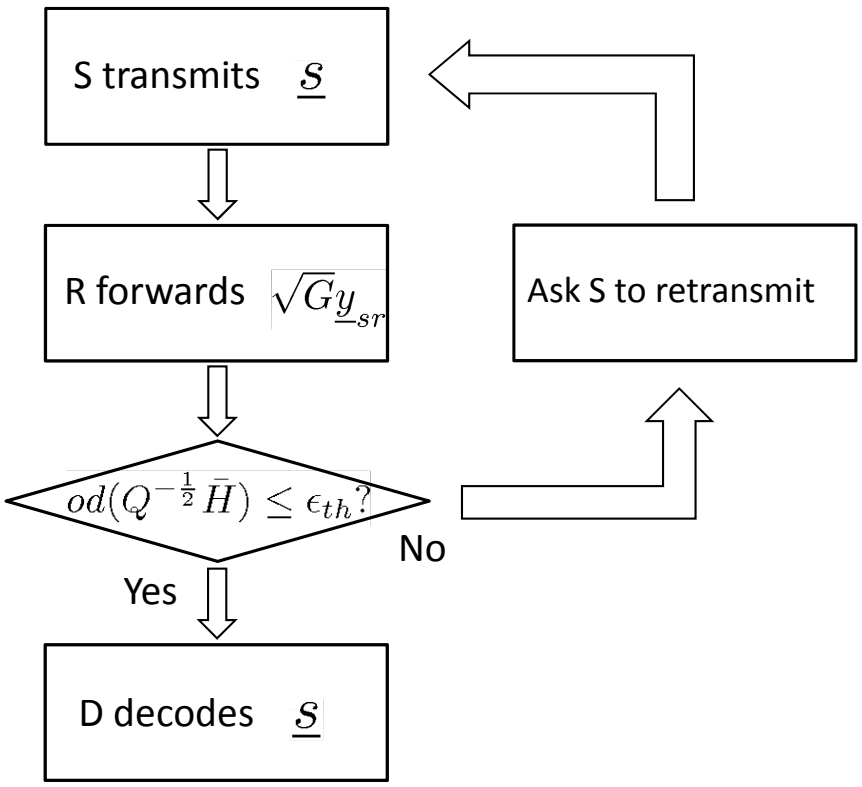

Figure 33: CC-ARQ protocol for AF MIMO relay networks.

complexity. The AF MIMO relay protocol with CC-ARQ is provided in Figure 33. After receiving signals from the source and the relay, the destination checks the *od* condition of $\boldsymbol{Q}^{-\frac{1}{2}}\bar{\boldsymbol{H}}$, and requests retransmission to the source if the *od* condition fails. In this way, $od(\boldsymbol{Q}^{-\frac{1}{2}}\bar{\boldsymbol{H}}) < \epsilon_{\text{th}} \in (0,1)$ is always guaranteed. According to [66], linear equalizers collect the same diversity as MLE does if $od(\boldsymbol{H}) \leq \epsilon$, $\forall \boldsymbol{H}$, and $\epsilon \in (0,1)$. For our ML detector in Eq. (74), we have $\boldsymbol{H} = \boldsymbol{Q}^{-\frac{1}{2}}\bar{\boldsymbol{H}}$. Thus, if $od(\boldsymbol{Q}^{-\frac{1}{2}}\bar{\boldsymbol{H}}) < \epsilon_{\text{th}}$ is guaranteed by the CC-ARQ protocol in Figure 33, the diversity order collected at the destination will be the same as that collected by ML receiver, which is $2N$. Note that, the retransmission is only requested from the destination, since the relay does not decode, but only amplifies and forwards the received signal.

Figure 34 shows the BER performance of proposed designs for AF MIMO relay networks when the destination adopts ZFE, ZFE combined with CC-ARQ (Figure

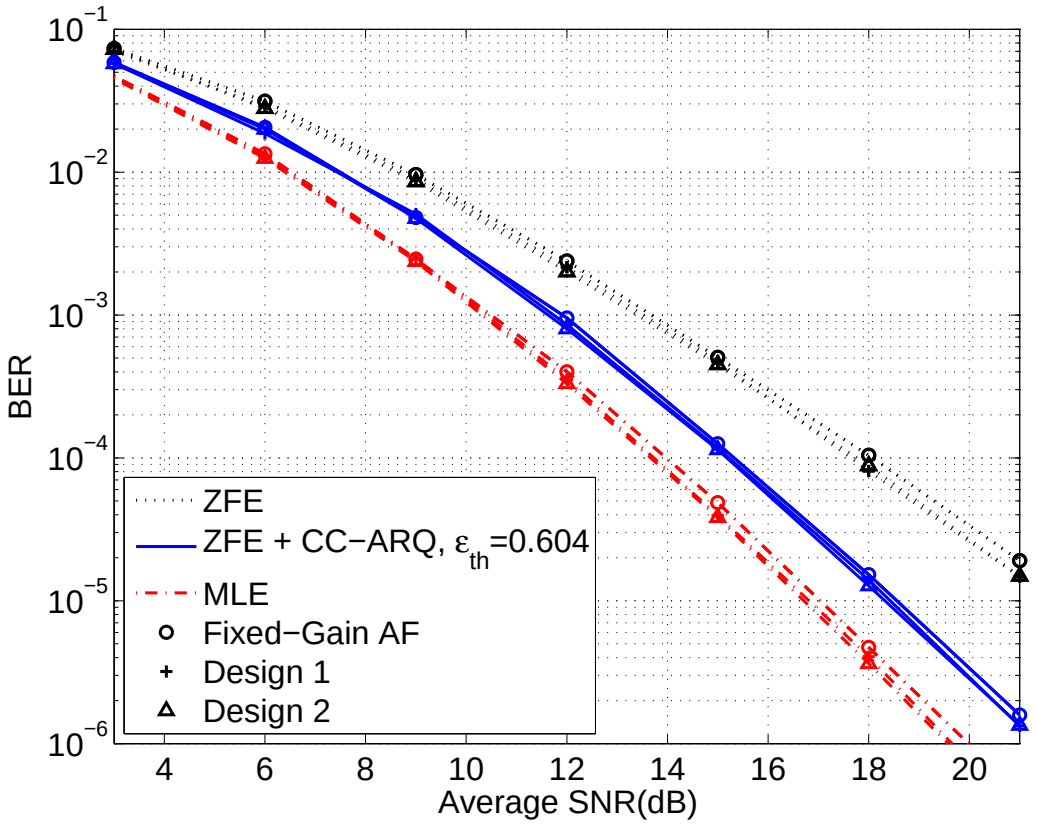

Figure 34: BER comparison for different receivers with $N = 2$ and QPSK.

33), and MLE (Eq. (74)). The CC-ARQ threshold $\epsilon_{\text{th}} = 0.604$ is set such that retransmission requirement rate is 10%. As verified in the figure, CC-ARQ scheme achieves the same diversity as MLE does at high SNR. At $BER = 10^{-4}$, the average SNR gap between ZFE and MLE is 4dB, but it is reduced to 1dB by using CC-ARQ with ZFE.

5.4 Conclusions

In this chapter, we presented AF MIMO relay strategies which guarantee bounded relay gain and bounded output power at the relay PA. We found sufficient conditions on gain-bounded PSF designs at the relay to achieve joint cooperative and receive diversity at the destination. Based on the conditions, we proposed a simple and practical yet diversity enabling relay design (Design 2) suitable for peak-power limited systems, while not requiring any channel state information at the relay.

CHAPTER VI

CONCLUSIONS

6.1 Contributions

In this dissertation, we have studied practical wireless cooperative relay designs that can achieve low error rate, low complexity, and high power efficiency. The main research results are summarized in the following list:

- General link-adaptive power-scaling relay strategy for DF cooperative relay networks was proposed;
- The diversity order enabled by general link-adaptive power-scaling relay strategy was studied and quantified;
- It was shown that the behavior of the power profile near its roots plays an important role in determining the diversity order at the destination;
- Necessary and sufficient conditions on the power profiles to guarantee full diversity for DF cooperative relay networks were provided;
- The diversity results for single-relay networks were extended to multi-relay networks;
- Low-complexity DF MIMO relay designs were proposed and the BER performance of each design was analyzed in terms of diversity order;
- General link-adaptive relay strategy was adopted to DF MIMO relay networks to enable cooperative diversity;
- CC-ARQ scheme with low-complexity LEs was developed to enable spatial diversity for DF MIMO relay networks;

- Power-scaling strategy combined with CC-ARQ is proposed to achieve joint cooperative and receive diversity for DF MIMO relay networks;
- Peak-power constrained AF MIMO relay was studied and sufficient conditions on the relay gain to achieve joint cooperative and receive diversity were found;
- Simple and practical yet diversity enabling relay design examples were provided suitable for peak-power limited systems;
- CC-ARQ is applied to AF MIMO relay networks to reduce the decoding complexity.

6.2 Suggestions for Future Research

The following is a list of interesting research topics that can be pursued as extensions of this dissertation:

- Spectral-efficient link-adaptive DF relay scheme to achieve diversity order of $N_R + 1$ for multi-relay networks, e.g., relay selection schemes;
- The impact of MIMO channel estimation errors on $od(\boldsymbol{H})$ and CC-ARQ;
- Peak-power constrained AF MIMO relay designs that do not require the destination to know two-hop CSI, i.e., the CSI of source-relay link.

REFERENCES

[1] 3GPP TS 36.300 V10.3.0, "3rd Generation Partnership Project; Technical Specification Group Radio Access Network; Evolved Universal Terrestrial Radio Access (E-UTRA) and Evolved Universal Terrestrial Radio Access Network (E-UTRAN); Overall description; Stage 2 (Release 10)."

[2] 3GPP TS 36.300 V8.7.0, "3rd Generation Partnership Project; Technical Specification Group Radio Access Network; Evolved Universal Terrestrial Radio Access (E-UTRA) and Evolved Universal Terrestrial Radio Access Network (E-UTRAN); Overall description; Stage 2 (Release 8)."

[3] 3GPP TS 36.814 V9.0.0, "3rd Generation Partnership Project; Technical Specification Group Radio Access Network; Evolved Universal Terrestrial Radio Access (E-UTRA); Further advancements for E-UTRA physical layer aspects (Release 9)."

[4] 3GPP2 C.S0024-0 v2.0, "CDMA2000 High Rate Packet Data Air Interface Specification," Oct. 2000.

[5] Abdaoui, A., Ikki, S. S., Ahmed, M. H., and Châtelet, E., "On the performance analysis of a MIMO-relaying scheme with space-time block codes," *IEEE Trans. Veh. Technol.*, vol. 59, pp. 3604–3609, Sept. 2010.

[6] Abramowitz, M. and Stegun, I. A., *Handbook of Mathematical Functions with Formulas, Graphs, and Mathematical Tables*. U.S. Department of Commerce, 1972.

[7] Adeane, J., Rodrigues, M. R. D., and Wassell, I. J., "Characterisation of the performance of cooperative networks in Ricean fading channels," in *Proc. International Conference on Telecommunications*, (Cape Town, South Africa), May 2005.

[8] Amarasuriya, G., Tellambura, C., and Ardakani, M., "Performance analysis framework for transmit antenna selection strategies of cooperative MIMO AF relay networks," *IEEE Trans. Veh. Technol.*, vol. 60, pp. 3030–3044, Sept. 2011.

[9] Andreoli, S., McClure, H., Banelli, P., and Cacopardi, S., "Digital linearizer for RF amplifiers," *IEEE Trans. Broadcast.*, vol. 43, pp. 12–19, Mar. 1997.

[10] Atapattu, S. and Rajatheva, N., "Exact SER of alamouti code transmission through amplify-forward cooperative relay over Nakagami-m fading channels," in *Proc. IEEE ISCIT*, (Sydney, Australia), pp. 1429–1433, Oct. 2007.

[11] Balaban, N. and Salz, J., "Dual diversity combining and equalization in digital cellular mobile radio," *IEEE Trans. Veh. Technol.*, vol. 40, pp. 342–354, May 1991.

[12] Barry, J. R., Lee, E. A., and Messerschmitt, D. G., *Digital Communication*. New York, NY: Springer, 2004.

[13] Bhatnagar, M. R. and Hjorungnes, A., "ML decoder for decode-and-forward based cooperative communication system," *IEEE Trans. Wireless Commun.*, vol. 10, pp. 4080–4090, Dec. 2011.

[14] Bölcskei, H., Nabar, R. U., Oyman, O., and Paulraj, A. J., "Capacity scaling laws in MIMO relay networks," *IEEE Trans. Wireless Commun.*, vol. 5, pp. 1433–1444, June 2006.

[15] Brueck, S., "Heterogeneous networks in LTE-Advanced," in *Proc. IEEE ISWCS*, (Aachen, Germany), pp. 171–175, Nov. 2011.

[16] Chae, C.-B., Tang, T., Heath, R. W., and Cho, S., "MIMO relaying with linear processing for multiuser transmission in fixed relay networks," *IEEE Trans. Signal Process.*, vol. 56, pp. 727–738, Feb. 2008.

[17] Chalise, B. K. and Vandendorpe, L., "Outage probability analysis of a MIMO relay channel with orthogonal space-time block codes," *IEEE Commun. Lett.*, vol. 12, pp. 280–282, Apr. 2008.

[18] Chandrasekhar, V., Andrews, J., and Gatherer, A., "Femtocell networks: a survey," *IEEE Commun. Mag.*, vol. 46, pp. 59–67, Sept. 2008.

[19] Chen, D. and Laneman, J. N., "Modulation and demodulation for cooperative diversity in wireless systems," *IEEE Trans. Wireless Commun.*, vol. 5, pp. 1785–1794, July 2006.

[20] Chen, S., Wang, W., Zhang, X., and Zhao, D., "Performance of amplify-and-forward MIMO relay channels with transmit antenna selection and maximal-ratio combining," in *Proc. IEEE WCNC*, (Budapest, Hungary), pp. 1–6, Apr. 2009.

[21] Chiani, M., Dardari, D., and Simon, M. K., "New exponential bounds and approximations for the computation of error probability in fading channels," *IEEE Trans. Wireless Commun.*, vol. 2, pp. 840–845, July 2003.

[22] Choi, G., Ma, X., and Zhang, W., "Designing diversity-enabled power profiles for decode-and-forward wireless relay networks," *IEEE Trans. Wireless Commun.*, vol. 10, pp. 2124–2134, July 2011.

[23] Choi, G., Zhang, W., and Ma, X., "Achieving joint diversity in decode-and-forward MIMO relay networks with zero-forcing equalizers," *IEEE Trans. Commun.*, vol. 60, pp. 1545–1554, June 2012.

[24] Choi, G., Zhang, W., and Ma, X., "Diversity-enabled power profile design for relay networks," in *Proc. IEEE MILCOM*, (San Diego, CA), pp. 1–7, Nov. 2008.

[25] Choi, G., Zhang, W., and Ma, X., "Achieving joint diversity in MIMO relay networks with low-complexity equalizers," in *Proc. IEEE ASILOMAR*, (Pacific Grove, CA), pp. 1869–1873, Nov. 2010.

[26] Cover, T. and Gamal, A. E., "Capacity theorems for the relay channel," *IEEE Trans. Inf. Theory*, vol. 25, pp. 572–584, Sept. 1979.

[27] Cripps, S. C., *RF Power Amplifiers for Wireless Communications*. Norwood, MA: Artech House Publishers, 1999.

[28] Damnjanovic, A., Montojo, J., Cho, J., Ji, H., Yang, J., and Zong, P., "UE's role in LTE advanced heterogeneous networks," *IEEE Commun. Mag.*, vol. 50, pp. 164–176, Feb. 2012.

[29] D'Andrea, A. N., Lottici, V., and Reggiannini, R., "RF power amplifier linearization through amplitude and phase predistortion," *IEEE Trans. Commun.*, vol. 44, pp. 1477–1484, Nov. 1996.

[30] del Razo, V., Rihonen, T., Gregorio, F., Werner, S., and Wichman, R., "Nonlinear amplifier distortion in cooperative amplify-and-forward OFDM systems," in *Proc. IEEE WCNC*, (Budapest, Hungary), pp. 1–5, Apr. 2009.

[31] Deng, X. and Haimovich, A. M., "Power allocation for cooperative relaying in wireless networks," *IEEE Commun. Lett.*, vol. 9, pp. 994–996, Nov. 2005.

[32] Ding, L., Zhou, G. T., Morgan, D. R., Ma, Z., Kenney, J. S., Kim, J., and Giardina, C. R., "A robust digital baseband predistorter constructed using memory polynomials," *IEEE Trans. Commun.*, vol. 52, pp. 159–165, Jan. 2004.

[33] Ding, M., Liu, S., Luo, H., and Chen, W., "MMSE based greedy antenna selection scheme for AF MIMO relay systems," *IEEE Signal Process. Lett.*, vol. 17, pp. 433–436, May 2010.

[34] El-Moutaouakkil, Z., Ait-Idir, T., Yanikomeroglu, H., and Saoudi, S., "Relay ARQ strategies for single carrier MIMO broadband amplify-and-forward cooperative transmission," in *Proc. IEEE PIMRC*, (Istanbul, Turkey), pp. 713–717, Sept. 2010.

[35] Ezri, J. and Gastpar, M., "On the performance of independently designed LDPC codes for the relay channel," in *Proc. IEEE ISIT*, (Seattle, WA), pp. 977–981, July 2006.

[36] Falahati, A. and Samadi, Z., "MIMO relaying for multi-user transmission using a two stage transmit and relay pre-processing technique," in *Proc. IEEE APCC*, (Auckland, New Zealand), pp. 520–525, Nov. 2010.

[37] Fan, Y. and Thompson, J., "MIMO configurations for relay channels: theory and practice," *IEEE Trans. Wireless Commun.*, vol. 6, pp. 1774–1786, May 2007.

[38] Farhadi, G. and Beaulieu, N. C., "On the performance of amplify-and-forward cooperative links with fixed gain relays," *IEEE Trans. Wireless Commun.*, vol. 7, pp. 1851–1856, May 2008.

[39] Firag, A., Suraweera, H. A., Smith, P. J., and Yuen, C., "Dual-hop MIMO amplify-and-forward relay channel capacity with keyhole effect," *IEEE Commun. Lett.*, vol. 15, pp. 1050–1052, Nov. 2011.

[40] Foschini, G. J. and Gans, M. J., "On limits of wireless communications in a fading environment when using multiple antennas," *Wireless Personal Commun.*, vol. 6, pp. 311–335, Mar. 1998.

[41] Gamal, H. E., Caire, G., and Damen, M. O., "The MIMO ARQ channel: diversity-multiplexing-delay tradeoff," *IEEE Trans. Inf. Theory*, vol. 52, pp. 3601–3621, Aug. 2006.

[42] Gao, Y. and Ge, J., "Outage probability analysis of transmit antenna selection in amplify-and-forward MIMO relaying over Nakagami-m fading channels," *Electron. Lett.*, vol. 46, pp. 1090–1092, July 2010.

[43] Gastpar, M. and Vetterli, M., "On the capacity of wireless networks: the relay case," in *Proc. IEEE INFOCOM*, (New York, NY), pp. 1577–1586, June 2002.

[44] Ghosh, A., Ratasuk, R., Mondal, B., Mangalvedhe, N., and Thomas, T., "LTE-advanced: next-generation wireless broadband technology," *IEEE Wireless Commun.*, vol. 17, pp. 10–22, June 2010.

[45] Ghosh, A., Zhang, J., Andrews, J. G., and Muhamed, R., *Fundamentals of LTE*. Upper Saddle River, NJ: Prentice Hall, 2010.

[46] Golden, G. D., Foschini, G. J., Valenzuela, R. A., and Wolniansky, P. W., "Detection algorithm and initial laboratory results using V-BLAST space-time communication architecture," *Electron. Lett.*, vol. 35, pp. 14–16, Jan. 1999.

[47] Guan, W. and Luo, H., "Joint MMSE transceiver design in non-regenerative MIMO relay systems," *IEEE Commun. Lett.*, vol. 12, pp. 517–519, July 2008.

[48] Hasna, M. O. and Alouini, M. S., "A performance study of dual-hop transmission with fixed gain relays," *IEEE Trans. Wireless Commun.*, vol. 3, pp. 1963–1968, Nov. 2004.

[49] Hassibi, B. and Vikalo, H., "On the sphere-decoding algorithm I. Expected complexity," *IEEE Trans. Signal Process.*, vol. 53, pp. 2806–2818, Aug. 2005.

[50] Haykin, S. and Moher, M., *Modern Wireless Communications*. Saddle River, NJ: Pearson Education Inc., 2005.

[51] Hiroike, A., Adachi, F., and Nakajima, N., "Combined effects of phase sweeping transmitter diversity and channel coding," *IEEE Trans. Veh. Technol.*, vol. 41, pp. 170–176, May 1992.

[52] Hunter, T. E. and Nosratinia, A., "Diversity through coded cooperation," *IEEE Trans. Wireless Commun.*, vol. 5, pp. 283–289, Feb. 2006.

[53] IEEE P802.16j/D9, "Draft Amendment to IEEE Standard for Local and Metropolitan Area Networks Part 16: Air Interface for Fixed and Mobile Broadband Wireless Access Systems: Multihop Relay Specification."

[54] Ikki, S. S. and Ahmed, M. H., "Performance of multiple-relay cooperative diversity systems with best relay selection over Rayleigh fading channels," *EURASIP J. Adv. Signal Process*, vol. 2008, pp. 145:1–145:7, Jan. 2008.

[55] Jing, Y. and Hassibi, B., "Cooperative diversity in wireless relay networks with multiple-antenna nodes," in *Proc. IEEE ISIT*, (Adelaide, SA), pp. 815–819, Sept. 2005.

[56] Ju, M. and Kim, I.-M., "ML performance analysis of the decode-and-forward protocol in cooperative diversity networks," *IEEE Trans. Wireless Commun.*, vol. 8, pp. 3855–3867, July 2009.

[57] Karmakar, S. and Varanasi, M. K., "Diversity-multiplexing-delay tradeoff of a DDF protocol on a half-duplex ARQ relay channel," in *Proc. IEEE ASILOMAR*, (Pacific Grove, CA), pp. 1729–1733, Nov. 2009.

[58] Keisler, H. J., *Elementary calculus: An infinitesimal approach*. Boston, MA: Prindle, Weber & Schmidt, 1986.

[59] Laneman, J. N., Tse, D. N. C., and Wornell, G. W., "Cooperative diversity in wireless networks: efficient protocols and outage behavior," *IEEE Trans. Inf. Theory*, vol. 50, pp. 3062–3080, Dec. 2004.

[60] Laneman, J. N., Wornell, G. W., and Tse, D. N. C., "An efficient protocol for realizing cooperative diversity in wireless networks," in *Proc. IEEE ISIT*, (Washington, D.C.), p. 294, June 2001.

[61] Lawton, G., "What lies ahead for cellular technology?," *IEEE Computer*, vol. 38, pp. 14–17, June 2005.

[62] Li, H. and Zhao, Q., "Distributed modulation for cooperative wireless communications," *IEEE Signal Process. Mag.*, vol. 23, pp. 30–36, Sept. 2006.

[63] Liu, Q., Zhang, W., Ma, X., and Zhou, G. T., "A practical amplify-and-forward relaying strategy with an intentional peak power limit," in *Proc. IEEE ICASSP*, (Dallas, TX), pp. 2518–2521, Mar. 2010.

[64] Luo, J., Blum, R. S., Cimini, L. J., Greenstein, L. J., and Haimovich, A. M., "Decode-and-forward cooperative diversity with power allocation in wireless networks," *IEEE Trans. Wireless Commun.*, vol. 6, pp. 793–799, Mar. 2007.

[65] Ma, X. and Giannakis, G. B., "Complex field coded MIMO systems: performance, rate, and tradeoffs," *Wireless Communications and Mobile Computing*, pp. 693–717, Nov. 2002.

[66] Ma, X. and Zhang, W., "Fundamental limits of linear equalizers: diversity, capacity and complexity," *IEEE Trans. Inf. Theory*, vol. 54, pp. 3442–3456, Aug. 2008.

[67] Ma, X. and Zhang, W., "Performance analysis for MIMO systems with lattice-reduction aided linear equalization," *IEEE Trans. Commun.*, vol. 56, pp. 309–318, Feb. 2008.

[68] Mo, R. and Chew, Y., "MMSE-based joint source and relay precoding design for amplify-and-forward MIMO relay networks," *IEEE Trans. Wireless Commun.*, vol. 8, pp. 4668–4676, Sept. 2009.

[69] Mo, R. and Chew, Y., "Precoder design for non-regenerative MIMO relay systems," *IEEE Trans. Wireless Commun.*, vol. 8, pp. 5041–5049, Oct. 2009.

[70] Mouly, M. and Pautet, M. B., "Current evolution of the GSM systems," *IEEE Personal Commun. Mag.*, vol. 2, pp. 9–19, Oct. 1995.

[71] Munoz-Medina, O., Vidal, J., and Agustin, A., "Linear transceiver design in nonregenerative relays with channel state information," *IEEE Trans. Signal Process.*, vol. 55, pp. 2593–2604, June 2007.

[72] Ojanpera, T. and Prasad, R., *Wideband CDMA for Third Generation Mobile Communications*. Norwood, MA: Artech House Publishers, 1998.

[73] Onat, F., Fan, Y., Yanikomeroglu, H., and Thompson, J., "Asymptotic BER analysis of threshold digital relaying schemes in cooperative wireless systems," *IEEE Trans. Wireless Commun.*, vol. 7, pp. 4938–4947, Dec. 2008.

[74] Pabst, R., Walke, B. H., Schultz, D. C., Herhold, P., Yanikomeroglu, H., Mukherjee, S., Viswanathan, H., Lott, M., Zirwas, W., Dohler, M., Aghvami, H., Falconer, D. D., and Fettweis, G. P., "Relay-based deployment concepts for wireless and mobile broadband radio," *IEEE Commun. Mag.*, vol. 42, pp. 80–89, Sept. 2004.

[75] Papoulis, A. and Pillai, S. U., *Probability, Random Variables and Stochastic Processes*. New York, NY: McGraw-Hill, 2002.

[76] Proakis, J. G., *Digital Communications*. New York, NY: McGraw-Hill, 2001.

[77] Raich, R., Qian, H., and Zhou, G. T., "Optimization of SNDR for amplitude-limited nonlinearities," *IEEE Trans. Commun.*, vol. 53, pp. 1964–1972, Nov. 2005.

[78] Raleigh, G. and Cioffi, J. M., "Spatio-temporal coding for wireless communications," in *Proc. IEEE GLOBECOM*, (London, England), pp. 1809–1814, Nov. 1996.

[79] Rappaport, T. S., *Wireless Communications: Principles and Practice*. Upper Saddle River, NJ: Prentice Hall, 2002.

[80] Ribeiro, A., Cai, X., and Giannakis, G. B., "Symbol error probabilitiesfor general cooperative links," *IEEE Trans. Wireless Commun.*, vol. 4, pp. 1264–1273, May 2005.

[81] Rong, Y., "Optimal linear non-regenerative multi-hop MIMO relays with MMSE-DFE receiver at the destination," *IEEE Trans. Wireless Commun.*, vol. 9, pp. 2268–2279, July 2010.

[82] Schiller, J., *Mobile Communications*. Boston, MA: Addison-Wesley, 2003.

[83] Sendonaris, A., Erkip, E., and Aazhang, B., "User cooperation diversity - Part I: System description," *IEEE Trans. Commun.*, vol. 51, pp. 1927–1938, Nov. 2003.

[84] Sendonaris, A., Erkip, E., and Aazhang, B., "User cooperation diversity - Part II: Implementaion aspects and performance analysis," *IEEE Trans. Commun.*, vol. 51, pp. 1939–1948, Nov. 2003.

[85] Senst, M. and Ascheid, G., "Optimal output back-off in OFDM systems with nonlinear power amplifiers," in *Proc. IEEE ICC*, (Dresden, Germany), pp. 1–6, June 2009.

[86] Simoens, S., Munoz, O., Vidal, J., and Coso, A. D., "Capacity bounds for Gaussian MIMO relay channel with channel state information," in *Proc. IEEE SPAWC*, (Recife, Brazil), pp. 441–445, July 2008.

[87] Simon, M. K. and Alouini, M. S., *Digital Communication over Fading Channels*. New York, NY: Wiley, 2005.

[88] Siriwongpairat, W. P., Himsoon, T., Su, W., and Liu, K. J. R., "Optimum threshold-selection relaying for decode-and-forward cooperation protocol," in *Proc. IEEE WCNC*, (Las Vegas, NV), pp. 1015–1020, Apr. 2006.

[89] Song, C., Lee, K. J., and Lee, I., "MMSE based transceiver designs in closed-loop non-regenerative MIMO relaying systems," *IEEE Trans. Wireless Commun.*, vol. 9, pp. 2310–2319, July 2010.

[90] Song, Y., Shin, H., and Hong, E. K., "MIMO cooperative diversity with scalar-gain amplify-and-forward relaying," *IEEE Trans. Commun.*, vol. 57, pp. 1932–1938, July 2009.

[91] Stefanov, A. and Erkip, E., "Cooperative coding for wireless networks," *IEEE Trans. Commun.*, vol. 52, pp. 1470–1476, Sept. 2004.

[92] Stuber, G. L., *Principles of Mobile Communications*. Norwell, MA: Kluwer Academic Publishers, 1996.

[93] Tabet, T., Dusad, S., and Knopp, R., "Diversity-multiplexing-delay tradeoff in half-duplex ARQ relay channels," *IEEE Trans. Inf. Theory*, vol. 53, pp. 3797–3805, Oct. 2007.

[94] Taherzadeh, M., Mobasher, A., and Khandani, A. K., "LLL reduction achieves the receive diversity in MIMO decoding," *IEEE Trans. Inf. Theory*, vol. 53, pp. 4801–4805, Dec. 2007.

[95] Tang, X. and Hua, Y., "Optimal design of non-regenerative MIMO wireless relays," *IEEE Trans. Wireless Commun.*, vol. 6, pp. 1398–1407, Apr. 2007.

[96] Tarokh, V., Jafarkhani, H., and Calderbank, A. R., "Space-time block coding for wireless communications: performance results," *IEEE J. Sel. Areas Commun.*, vol. 17, pp. 451–460, Mar. 1999.

[97] TIA/EIA IS-95, "Mobile Station-Base Station Compatibility Standard for Dual-Mode Wideband Spread Spectrum Cellular System," July 1993.

[98] Tse, D. and Viswanath, P., *Fundamentals of Wireless Communication*. Cambridge, UK: Cambridge University Press, 2005.

[99] Tseng, F.-S., Chang, M.-Y., and Wu, W.-R., "Joint Tomlinson-Harashima source and linear relay precoder design in amplify-and-forward MIMO relay systems via MMSE criterion," *IEEE Trans. Veh. Technol.*, vol. 60, pp. 1687–1698, May 2011.

[100] Tsiftsis, T. A., Karagiannidis, G. K., Mathiopoulos, P. T., and Kotsopoulos, S. A., "Nonregenerative dual-hop cooperative links with selection diversity," *EURASIP J. Wirel. Commun. Netw.*, vol. 2006, pp. 34–34, Apr. 2006.

[101] Turin, G., "The characteristic function of hermitian quadratic forms in complex normal variables," *Biometrika*, vol. 47, pp. 199–201, 1960.

[102] van der Meulen, E. C., "Three-terminal communication channels," *Adv. Appl. Prob.*, vol. 3, pp. 120–154, 1971.

[103] van Nee, R., van Zelst, A., and Awater, G., "Maximum likelihood decoding in a space division multiplexing system," in *Proc. IEEE VTC*, (Tokyo, Japan), pp. 6–10, May 2000.

[104] Vaze, R. and Heath, R. W., "On the capacity and diversity-multiplexing tradeoff of the two-way relay channel," *IEEE Trans. Inf. Theory*, vol. 57, pp. 4219–4234, July 2011.

[105] Wang, B., Zhang, J., and Host-Madsen, A., "On the capacity of MIMO relay channels," *IEEE Trans. Inf. Theory*, vol. 51, pp. 29–43, Jan. 2005.

[106] Wang, T., Cano, A., Giannakis, G., and Laneman, J., "High-performance cooperative demodulation with decode-and-forward relays," *IEEE Trans. Commun.*, vol. 55, pp. 1427–1438, July 2007.

[107] Wang, T. and Giannakis, G. B., "Complex field network coding for multiuser cooperative communications," *IEEE J. Sel. Areas Commun.*, vol. 26, pp. 561–571, Apr. 2008.

[108] Wang, T., Giannakis, G. B., and Wang, R., "Smart regenerative relays for link-adaptive cooperative communications," *IEEE Trans. Commun.*, vol. 56, pp. 1950–1960, Nov. 2008.

[109] Wang, Z. and Giannakis, G. B., "A simple and general parameterization quantifying performance in fading channels," *IEEE Trans. Commun.*, vol. 51, pp. 1389–1398, Aug. 2003.

[110] Weisstein, E. W., "Erfc," *From MathWorld - A Wolfram Web Resource. http://mathworld.wolfram.com/Erfc.html*.

[111] Winters, J., Salz, J., and Gitlin, R. D., "The impact of antenna diversity on the capacity of wireless communication systems," *IEEE Trans. Commun.*, vol. 42, no. 2/3/4, pp. 1740–1751, 1994.

[112] Xia, X., Wu, G., and Li, S., "A novel method to estimate the end to multi-end capacity bounds in MU-MIMO-relay broadcast channel," in *Proc. IEEE WiCom*, (Chengdu, China), pp. 1–4, Sept. 2010.

[113] Xie, Y., Gunduz, D., and Goldsmith, A., "Multihop MIMO relay networks with ARQ," in *Proc. IEEE GLOBECOM*, (Honolulu, HI), pp. 1–6, Nov. 2009.

[114] Yanikomeroglu, H., "Cellular multihop communications: Infrastructure-based relay network architecture for 4G wireless systems," in *Proc. 22nd Queen's Biennial Symp. Comm.*, (Kingston, ON, Canada), pp. 76–78, June 2004.

[115] Yiu, S., Schober, R., and Lampe, L., "Distributed space-time block coding for cooperative networks with multiple-antenna nodes," in *Proc. IEEE CAMSAP*, (Puerto Vallarta, Mexico), pp. 52–55, Dec. 2005.

[116] Yu, G., Zhang, Z., and Qiu, P., "Cooperative ARQ in wireless networks: protocols description and performance analysis," in *Proc. IEEE ICC*, (Istanbul, Turkey), pp. 3608–3614, June 2006.

[117] Yu, J., Liu, D., Yin, C., and Yue, G., "Relay-assisted MIMO multiuser precoding in fixed relay networks," in *Proc. IEEE WiCom*, (Shanghai, China), pp. 881–884, Sept. 2007.

[118] Zhang, R., Chai, C. C., and Liang, Y. C., "Joint beamforming and power control for multiantenna relay broadcast channel with QoS constraints," *IEEE Trans. Signal Process.*, vol. 57, pp. 726–737, Feb. 2009.

[119] Zhang, W., Ma, X., Gestner, B., and Anderson, D. V., "Designing low-complexity equalizers for wireless systems," *IEEE Commun. Mag.*, vol. 47, pp. 56–62, Jan. 2009.

[120] Zhao, B. and Valenti, M. C., "Distributed turbo coded diversity for relay channel," *Electron. Lett.*, vol. 39, pp. 786–787, May 2003.

[121] Zheng, L. and Tse, D. N. C., "Diversity and multiplexing: a fundamental tradeoff in multiple-antenna channels," *IEEE Trans. Inf. Theory*, vol. 49, pp. 1073–1096, May 2003.

[122] Zimmermann, E., Herhold, P., and Fettweis, G., "On the performance of cooperative diversity protocols in practical wireless systems," in *Proc. IEEE VTC*, (Orlando, FL), pp. 2212–2216, Oct. 2003.

VITA

Gi Wan Choi was born in Incheon, Republic of Korea on October 9, 1983. He received the B.S. degree in electrical engineering from Korea Advanced Institute of Science and Technology (KAIST), Daejeon, Republic of Korea, in 2006 and the M.S. degree in electrical and computer engineering from the Georgia Institute of Technology, Atlanta, Georgia, USA in 2008, where he is now working towards the Ph.D. degree in electrical and computer engineering.